# Flow Through an Abrupt Constriction
# –
# 2D Hydrodynamic Model Performance and Influence of Spatial Resolution

**Cathie Louise Barton**
**BE (Civil)**

**School of Environmental Engineering**
**Faculty of Environmental Sciences**
**Griffith University**

Submitted in partial fulfillment of the requirements of the Master of Engineering Science in Environmental Engineering Degree

**July 2001**

# SUMMARY

This study documents work undertaken to investigate the ability of 2D hydrodynamic models to adequately predict energy losses through an abrupt constriction. In particular, the investigation focuses on the impact that model spatial resolution has on the ability of the model to predict expansion and contraction losses due to the abrupt constriction.

The work outlined in this report began as a result of a perceived lack of understanding in the ability of 2D models to portray the energy losses associated with the turbulent nature of water flow. As flow through an abrupt constriction has been the subject of many investigations throughout the last 50 years, it was decided that such flow would provide a suitable test case for the 2D model assessments.

It was initially decided that a goal standard was needed against which the 2D model predictions could be compared to determine the accuracy of such predictions. Two manual methods using a combination of theoretical and empirical techniques were utilised in the hope that they would provide such a goal standard. In addition, two 1D models were utilised to provide support to the goal standard selected. A suitable goal standard was not found. Ranges of expansion and contraction losses across these four methods were too extreme to allow their use as a standard.

However, the impact of 2D model spatial resolution was still able to be assessed. Two 2D models (TUFLOW and RMA2) were investigated using five spatial resolutions varying from coarse to fine. Flow rates and constriction widths were also varied to provide a comprehensive data set.

Principal outcomes of the study are:

- an improved understanding of different numerical solution schemes;
- an improved understanding of the nature of contracting and expanding flow;
- the confirmation that the spatial resolution of 2D models does have an impact on the ability of these models to predict energy losses due to turbulent effects;
- an understanding of the importance of the eddy viscosity formulation technique on the predictive ability of 2D models;
- a preliminary assessment of the impact of varying the eddy viscosity formulation technique.

# CONTENTS

# LIST OF FIGURES

# LIST OF TABLES

# LIST OF SYMBOLS

| Symbol | Description |
|---|---|
| a | Bottom elevation (m) |
| $A_{ds}$ | Cross-sectional area in channel downstream of constriction ($m^2$) |
| $A_{us}$ | Cross-sectional area in channel upstream of constriction ($m^2$) |
| $A_c$ | Cross-sectional area in constriction ($m^2$) |
| D | Water depth (m) |
| $C_c$ | Coefficient of Contraction (HEC-RAS) |
| $C_e$ | Coefficient of Expansion (HEC-RAS) |
| g | Acceleration due to gravity ($m/s^2$) |
| h | Water surface elevation = a + D (m) |
| $L_c$ | Length of Expansion Reach (HEC-RAS) |
| $L_e$ | Length of Contraction Reach (HEC-RAS) |
| $q_s$ | Tributary inflow into system |
| t | Time (usually s) |
| $\Delta t$ | Timestep (s) |
| u | Velocity in the x-direction (m/s) |
| v | Velocity in the y-direction (m/s) |
| $v_c$ | Average velocity in constriction (m/s) |
| $v_{us}$ | Velocity in the uniform flow area of channel upstream of the constriction (m/s) |
| $v_{ds}$ | Velocity in the channel downstream of the constriction where uniform flow has re-established (m/s) |
| V | Total velocity (m/s) |
| $\Delta x$, $\Delta y$ | Length of model element in the x and y directions (m) |
| $\varepsilon_{yy}, \varepsilon_{xy}, \varepsilon_{yx}, \varepsilon_{xx}$ | Turbulent eddy coefficients |
| $\Omega_{vh}, \Omega_{uh}$ | Coriolis forcing in the x and y directions |
| $\rho$ | Kinematic viscosity ($kg/m^3$) |

# STUDY TERMINOLOGY

| Term | Units | Description |
|---|---|---|
| Total Head Loss | m | Total energy loss across the full length of the study test channel. This includes the expansion loss, the contraction loss and the loss due to friction. |
| Total Energy Loss | m | See Total Head Loss |
| Expansion Loss | m | Energy loss due to expansion of flow downstream of the constriction. |
| Contraction Loss | m | Energy loss due to contraction of flow upstream of the constriction. |
| Total Friction Loss | m | Energy loss due to frictional effects of the channel bottom across the full length of the study test channel. This is calculated in Appendix A. In this study, the total friction loss is often removed from the total head loss results so that the focus is restricted to expansion and contraction losses (see "Constriction Loss"). |
| Constriction Loss | m | Energy loss due to losses associated with the contraction and expansion of flow through the constriction alone. This is equivalent to the total head loss minus the total friction loss. |
| Dynamic Head | m | $v_c^2/2g$ |
| Dynamic Head Loss Coefficient | - | The dynamic head loss coefficient is the sum of the expansion and contraction losses expressed in relation to the dynamic head through the constriction ($v_c^2/2g$). That is, a dynamic head loss coefficient of 1.5 is equivalent to a loss of 1.5 x ($v_c^2/2g$); a dynamic head loss coefficient of 0.5 is equivalent to a loss of 0.5 x ($v_c^2/2g$). The dynamic head loss coefficient is dimensionless. |
| 1D | | Usually referring to a one-dimensional (1D) numerical model. |
| 2D | | Usually referring to a two-dimensional (2D) numerical model. |
| 3D | | Usually referring to a three-dimensional (3D) numerical model. |
| Mesh | | Network of elements and nodes created when developing a 2D finite element model. The term 'mesh' is also sometimes used in this study to refer to the grid of the finite difference model. See also 'grid'. |
| Grid | | Grid of elements and nodes created when developing a 2D finite difference model. For the purposes of this study report, the term 'grid' is used solely when referring to a 2D finite difference model network as this network must be uniform throughout. See also 'mesh'. |
| Spatial Resolution | | The spatial resolution of the model is determined by the density of the model network (ie the mesh). The higher the spatial resolution (or 'mesh resolution' or 'grid resolution'), the greater the number of nodes and elements within a defined area. The higher the spatial resolution, the smaller the average element size. |

# STATEMENT

This work has not previously been submitted for a degree or diploma in any university. To the best of my knowledge and belief, the study report contains no material previously published or written by another person except where due reference is made in the report itself.

Cathie Barton BE (Civil)

# ACKNOWLEDGEMENTS

The author would like to acknowledge the following people who have provided support and advice throughout this study.

- Chris Nielsen and Mark Jempson for their patience and advice on many occasions;
- Bofu Yu for his support;
- Don Muir for his enthusiasm and help;
- Greg Barton for things to numerous to list.

# 1 INTRODUCTION

## 1.1 General

Understanding the behaviour of water bodies that surround us is becoming increasingly important as we place more pressure on these natural resources. It is beneficial to be able to quantify the behaviour of water bodies in terms of hydraulics, water quality and other processes in order to predict the impacts of changes to the natural or existing system. Numerical models are often used for this purpose.

The effectiveness of these models in replicating the natural system is dependent upon a variety of factors. These include the quality of physical data used to establish the model, the ability of the modeller to develop a model that is representative of the system, and the numerical capability of the actual model itself in replicating certain aspects of system behaviour. It is on the latter two issues that this study concentrates.

A significant amount of the variability in water quality and other environmental water systems is controlled by the fundamental mechanism of water flow (McCutcheon, 1989). Knowledge of the pathway, volume and velocity of water (hydraulic behaviour) is needed to undertake any fundamental study of water quality or other water process, including modelling investigations (Martin and McCutcheon, 1999). A numerical model used to represent the natural system in a water body must be able to accurately replicate the hydraulic behaviour as well as any other system behaviour, such as water quality. This study focuses on the ability of numerical models to reproduce hydraulic behaviour, specifically the hydraulic behaviour of flow through a constriction. It may be argued that the ability of modelling hydraulic behaviour is critical to the success or otherwise of any numerical modelling of water bodies.

A numerical model which is used to represent the hydraulic behaviour of a water body is called a hydraulic model. Hydraulic models may be broadly categorised into one-dimensional (1D), two-dimensional (2D) and three-dimensional (3D) schemes. This study utilises both 1D and 2D numerical models to simulate the flow of water through a constriction. Fully 2D depth averaged solution schemes have been widely used for modelling river and coastal hydraulics and, more recently, have become a practical option for floodplain modelling (Syme et al, 1998). A number of different types of solution schemes are available and are based on the finite difference and finite element methods.

Impacts on hydraulic and water quality behaviour due to such things as developments, point and non-point source discharges, upgrading of road and rail services may be predicted using 1D and 2D numerical models. Results from these assessments often form the critical decision basis upon which design and placement of these works is made. This makes numerical models an integral component of the planning and decision-making process. Thus, the ability of modellers and the models themselves to produce accurate results is important.

This study aims to provide an understanding of the abilities of selected 1D and 2D models to predict flow through a constriction. The focus is on the impact of model spatial resolution on model predictions. A comparison of two 2D schemes (RMA-2 and TUFLOW), two 1D schemes (HEC-

RAS and MIKE-11) and some manual calculations aid in providing an understanding of the behaviour of the different schemes.

## 1.2 Study Objectives

The study objectives are as follows:

1. To provide a summary of the numerical solution schemes utilised in this study;
2. To assess the ability of 2D models in predicting energy losses through an abrupt constriction;
3. To assess the impact that the spatial resolution of the 2D models has on prediction of energy losses through an abrupt constriction.

During the course of the study, with particular regard to Objective 3, it became apparent that further research into the impact of eddy viscosity on model behaviour was needed. This lead to the development of the additional objective:

4. To provide a preliminary assessment and understanding of the impact of eddy viscosity on 2D model results.

## 1.3 Background

### 1.3.1 Numerical Models

Numerical models are developed to represent a natural or existing system. Due to the complexity of the natural environment, numerical models rely on certain simplifying assumptions and theories. The simplification of the complex process creates an uncertainty that is important to recognise and understand.

Hydraulic models specifically, represent hydraulic behaviour of water bodies using a numerical approximation of fluid flow. Due to the complexity of the equations of motion, analytical solutions are not possible. Instead, numerical techniques are used to convert differential equations into algebraic difference forms that can be solved for unknown values at incremental, finite points in space and time. The early models used finite difference numerical techniques. Numerical techniques in use today include finite difference, finite element, finite volume and Langrangian techniques.

The accuracy of the model is related to the degree of complexity represented by the model. Thus, 1D models provide a simpler and less descriptive representation of the real world than 3D models. However, a more complex model is not necessarily a more suitable one, nor does it provide more reliable results. Suitability of a model is determined by the nature of the particular situation being replicated and the accuracy of the output required. For example, assessment of in-bank river flow behaviour may be suitably modelled in 1D and not require a higher dimension model. Alternatively, as discussed by Crowder and Diplas (2000), assessment of suitable fish habitat within a pool and riffle stream may require a 2D or 3D model to reproduce the meso-scale hydraulic behaviour in the downstream shadow of boulders that a 1D model is simply incapable of simulating. In addition, there is a direct relationship between the level of complexity of a model and the amount of data required. If data requirements exceed the data available, the model, despite being complex, cannot reproduce the complexity reliably.

The most common examples of unsteady free surface flow requiring assessment are flows in rivers and tidal flows in estuaries, bays and oceans. 1D schemes are usually used for situations where the flow is channelised or in one direction such as for rivers and estuaries. As truly 1D flow does not occur in nature, the basic assumption involved in undertaking this type of modelling is that channel velocity is uniform over the cross-section and water level across the channel is horizontal. Assumptions such as these date back to the principles proposed by de Saint Venant in 1871 (Cunge et al., 1980). Extensive use of both steady state (flow constant) and hydrodynamic (flow varies with time) 1D models based on these principles has confirmed that the assumptions are adequate for hydraulic modelling in rivers and estuaries.

2D numerical hydrodynamic modelling has its origins in the work of Hansen (1956). Again, truly 2D behaviour does not occur in nature and simplifying assumptions are made. These schemes are normally in plan view with velocities averaged over the depth of the water column.

### 1.3.2 Numerical Techniques

One of the most common numerical methods is the **finite difference** method in which time and space are divided into discrete (finite) intervals. Solutions are determined using an explicit or implicit scheme. An explicit scheme expresses one unknown value in terms of several known values. At each time step, a new value can be determined directly (explicitly) using known values from the previous time step. An implicit scheme expresses one unknown value in terms of other unknown values in addition to known values from the previous time step. An implicit scheme requires a matrix solution which means that these schemes require greater computational effort per timestep than explicit schemes.

Explicit schemes are conditionally stable while implicit schemes are unconditionally stable. Stability may be expressed by the Courant number (Abbot, 1979; Syme, 1991, Hardy et al., 1999), which is directly proportional to the timestep. An explicit scheme is only stable for a Courant number of less than or equal to 1. Implicit schemes generally use a Courant number of between 2 and 15 (Syme, 1991) although some studies utilising implicit models (for example, Hardy *et al*., 1999) use Courant numbers of less than 1 to ensure that the simulation quality due to timestep is not an issue when assessing other factors.

**Finite element** methods assume that the solution has a simple form over small regions (elements). Error-minimising criteria is used to assemble and adjust the individual pieces of the solution so that the best solution over the entire domain is obtained (Martin and McCutcheon, 1999). A system of simultaneous equations is assembled from coefficient matrices for each element. To obtain a solution, these equations are solved simultaneously. The finite element solution technique is often used to represent the water bodies of more-complex shape as the component elements can be assembled in any number of ways.

Finite element models are typically run at much larger timesteps than the finite difference models but require more computational effort per timestep.

# 1.4 Flow through an Abrupt Constriction

## 1.4.1 General

A constriction in the flow width results in energy dissipation due to turbulence. The dissipation of energy is physically evident by a drop in water level through the constriction. This is usually termed "head loss" and is due primarily to turbulent effects in the contraction of the flow and subsequent expansion of the flow. Constriction types may be of a gradual (tapering) nature or an abrupt nature. Tapered constrictions typically result in lower head losses while abrupt constrictions typically produce larger head losses. Within this study consideration is given only to abrupt constrictions.

Theoretical flow lines for an abrupt constriction are shown in Figure 1-1. As flow progresses downstream toward a constriction, flow lines converge in the **contraction reach** to allow flow to pass through the constriction. Within the constriction, the continued convergence of the flow lines can produce a **vena contracta**, where the active flow width is reduced to less than the constriction width. Divergence of flow occurs downstream of the constriction in the **expansion reach** where turbulence causes eddies to form.

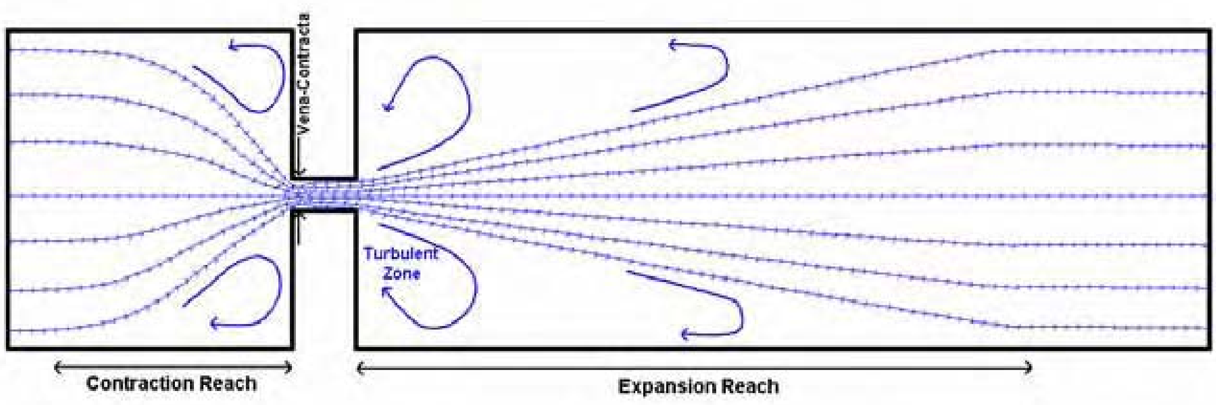


**Figure 1-1 Theoretical Flow Lines Through an Abrupt Constriction**

## 1.4.2 Losses

Studies of turbulent flows through abrupt constrictions using Laser Doppler Velocimetry (El-Sherwey *et al.*, 1996) show that turbulence intensities increase in the contraction reach and increase further within the constriction. However, the highest turbulence intensities occur within the expansion reach. These observations verify the consistent advice given throughout the literature that expansion losses exceed contraction losses for an abrupt constriction (for example, Henderson, 1966; Chow, 1959; Martin and McCutcheon, 1999; HEC, 1998; Formica, 1955)

Total energy loss through a constriction may be divided into three sources: contraction loss, expansion loss and friction loss. It is with the initial two sources that this study is predominately concerned and these have collectively been termed "constriction losses" for the purpose of this study. Terminology used frequently throughout this study report is aimed at distinguishing between these sources. The reader is referred to the Study Terminology summary at the front of this report for clarification on specific terms used.

A simplifying representation of constriction losses may be found in several hydraulics texts (for example, Henderson (1966)), as

$$\begin{aligned} \text{Constriction Loss} &= \text{Contraction Loss} + \text{Expansion Loss} \\ &= \frac{C_c v_c^2}{2g} + \frac{(v_c - v_{ds})^2}{2g} \end{aligned}$$

Where $C_c$ is a function of the contraction ratio, $v_c$ is the average velocity in the constriction (downstream of the vena contracta), $v_{ds}$ is the velocity downstream of the constriction and g is the acceleration due to gravity. This equation is developed using a combination of empirical and theoretical methods. Within this study, manual calculations such as this are used to provide an indication of the head loss through a constriction for comparison with those constriction losses predicted by numerical modelling. It was intended that these manual calculations, in conjunction with the 1D model results, would provide a goal standard against which the 2D model results could be compared. However, the manual calculations undertaken did not perform as expected. This is discussed in Section 8 and Section 9.

### 1.4.3 Flow Regime

All calculations undertaken in this study were based on the assumption that the flow regime through the constriction is subcritical. That is, the Froude number $\left( v / \sqrt{gy} \right)$ is at all times less than 1. As discussed in Section 2.1, this is one of the reasons for limiting the results presented to average constriction velocities of 4m/s and lower.

Supercritical flow occurs when the Froude number exceeds 1. At a velocity of 4m/s and a depth of 2m, the Froude number is around 0.9. An increase in velocity or a decrease in depth will cause the Froude number to increase and may result in the flow regime becoming supercritical. It is important to be mindful of the potential for supercritical flow when assessing model results for the highest average constriction velocities as the numerical models considered are not capable of reliably replicating this flow regime.

### 1.4.4 Numerical Modelling

1D models, such as HEC-RAS and MIKE 11, use the basic principles in the equation presented above to determine constriction losses. The 1D models use the theoretical/empirical solution method as they are unable to numerically represent the contraction and expansion of flow that causes the energy losses.

2D models may be capable of adequately reproducing these complex flows in a vertically averaged sense. Thus, 2D models do not use the theoretical/empirical solution method of the previous equation but rather rely on the ability of the 2D model to sufficiently represent the flow characteristics that cause energy losses (that is, the contraction and expansion). 2D models may require the use of a combination of theoretical/empirical methods and model equations if the micro complex flow patterns, such as the vena-contracta, are not reproduced.

A comparison of flow behaviour through a constriction for some of the common 2D models currently in use was undertaken by Syme *et al.* (1998). A list of these models and their solution scheme is given in Table 1–1. Syme *et al.* (1998) compared constriction loss results due to flow through an abrupt constriction for each of the models listed to theoretical/empirical calculations and 1D solution scheme results (refer to Table 1–2). Conclusions reached from these comparisons were that a) 2D schemes were able to adequately predict head loss across both a vertical and, possibly a horizontal flow constriction; b) increases in eddy viscosity lead to increases in head losses, and c) time-step variations yielded different results in the MIKE21 model.

**Table 1–1 2D Models Used by Syme *et al.* (1998)**

| Model Name | Solution Technique | Solution Scheme | Reference |
|---|---|---|---|
| FESWMS | Finite Element | - | FHA |
| MIKE21 | Finite Difference | Implicit (some terms are explicit) | DHI (1998) |
| RMA2 | Finite Element | - | King (1998) |
| TUFLOW | Finite Difference | Implicit | Syme (1991) |

**Table 1–2 1D Models Used for Comparison by Syme *et al.* (1998)**

| Model Name | Flow Regime | Solution Technique | Solution Scheme | Reference |
|---|---|---|---|---|
| MIKE11 | Unsteady | Finite Difference | Implicit | DHI (1999) |
| ESTRY | Unsteady | Finite Difference | Explicit | WBM (1996) |
| HEC-RAS | Steady | - | - | USACE (1998) |

## 1.5 Spatial Resolution of 2D Models

### 1.5.1 General

2D models rely on the development of a mesh or grid system to define the model variables such as topography and roughness and to provide a framework upon which the solution schemes operate. In finite element models the typical name for the network defining the model is the **mesh**, while in finite difference models the typical name used is **grid**. These naming conventions stem from the fact that a finite difference grid must be a uniform grid of square elements while a finite element mesh can comprise a non-uniform mesh of rectangular and triangular elements with the element size able to change over the model domain. However, this is a typical naming convention rather than standard and the two terms are sometimes used interchangeably. This study uses 'mesh' when referring to the finite element model and also when referring to both the finite element and finite difference model, and 'grid' is used solely when referring to the finite difference model.

Spatial resolution in 2D models refers to the density, or resolution, of the mesh developed. Selection of the spatial resolution of the model is typically based on a number of factors:

- *Resolution and importance of certain features within the topography.* For example, modelling a 10m wide creek entirely within a 2D system requires a mesh resolution of less than 10m. This constraint is particularly applicable to finite difference models which must maintain the same element dimension across the model domain.
- *Minimum mesh resolution at which numerical convergence could be achieved.* (Lardner and Song, 1992)
- *Maximum mesh resolution that allows a simulation to be completed within a reasonable and practical time frame.* For example, a simulation time of 2 weeks is not practical in a real world of budgets and deadlines.
- *Experience and knowledge of the modeller.*

A factor not usually included in the selection of a suitable spatial resolution is the effect of model resolution on the solution of the equations. The problems associated with failing to consider this effect are highlighted by many authors who confirm that the spatial resolution of the mesh alone will have an impact on model predictions (Farajalla and Vieux, 1995; Hardy et al., 1999; Crowder and Diplas, 2000, Syme and King (pers. comm. 2000)). Farajalla and Vieux (1995) acknowledge that there is a tendency to assume that an increase in spatial resolution of a model will improve the realism of the model's predictive ability. Hardy *et al.* (1999) also recognises the trend among many modellers to increase the spatial resolution in a model in the expectation of improved insights into temporal and spatial processes. The following three avenues of thought are responsible for this trend:

- Expected improvements in solution stability as the mesh resolution tends toward the true continuum level;
- The ability of high resolution models to facilitate complex, and thereby more realistic representation of the parameters of the code;
- A closer correspondence between field measurement and model scales.

Hardy *et al.* (1999) believed that mesh resolution is the only unbounded parameter value as there are no accepted standards for mesh construction. This is in contrast to calibration parameters, such as bed roughness, which are bounded and documented in physically realistic ranges (eg Chow, 1959; Henderson, 1966).

The central aim of the study by Hardy *et al.* (1999) was to present an assessment of the impact of spatial resolution on a typical non-linear numerical scheme. The scheme selected was the 2D, implicit, finite element hydraulic model, TELEMAC-2D. Hardy *et al.* (1999) found that mesh resolution effects were at least as important as the Manning's roughness. Details of these assessments and results are discussed throughout this study report.

### 1.5.2 Eddy Viscosity

The use of eddy viscosity in 2D numerical modelling provides an approximate representation of the energy losses due to **turbulent effects at sub-grid scale** (Nielsen, 2000; Rodi, 1980). In assessing the impact of spatial resolution, the current study found that the energy loss results were sensitive to the formulation used to provide the eddy viscosity values. While other studies (eg. Hardy *et al.*, 1999; Crowder and Diplas, 2000) have investigated the impact of varying spatial resolution in 2D models, none of these, with the exception of Nielsen (2000), have investigated the evaluation of the eddy viscosity and the associated impacts.

Although not initially featured as a focus of the current study, the significant impact of the eddy viscosity formulation has meant that it has received considerable attention in these assessments. Appendix B contains a full description of eddy viscosity, evaluation methods and sensitivity assessments.

# 2 METHODOLOGY

## 2.1 General

Details of the test channel used for all calculation methods throughout this study are presented in Section 2.2. In all methods the test channel is considered to have a constant downstream head level of 2m. The upstream boundary is a discharge boundary and five discharges were used varying from $30m^3/s$ to $480m^3/s$. Three constriction widths were used: 15m, 30m and 60m. The combination of these variables produced average velocities in the constriction ($v_c$) varying from 0.25m/s to 16m/s. Supercritical flow is expected to occur within the test channel when average constriction velocities ($v_c$) exceed 4m/s. Supercritical flow may also occur with a $v_c$ of 4m/s. As models are typically incapable of reliably simulating supercritical flow, results from simulations where average constriction velocities exceeded 4m/s were ignored. In addition, although results from simulations where $v_c$ is equal to 4m/s have been included, these results should be treated with caution as supercritical flow may occur and results may not be stable or realistic. Highlighting this is the fact that some methods did not complete simulations at the 4m/s limit due to instabilities. Instabilities at the higher constriction velocities are discussed further throughout this report.

Two 2D hydrodynamic models have been developed to represent the test channel. The 2D models used in this study are RMA2 and TUFLOW. Details are provided in Table 2–2. In order to assess the ability of the 2D models to accurately predict head loss across a constriction in the flow width, other computation techniques are used to compare head loss results. These include development of two 1D models and the use of two theoretical/empirical manual calculation methods. The 1D models used are MIKE11 and HEC-RAS and further details are provided in Table 2–2. Details of the manual calculation methods used are provided in Table 2–3.

Models are used to calculate the total energy loss across the model length. The total energy loss comprises the contraction loss, the expansion loss and the frictional loss. As this study is primarily concerned with expansion and contraction losses through the constriction, frictional losses are calculated manually in Appendix A and are subtracted from the total energy loss to give 'constriction losses' (expansion plus contraction losses). A Manning's 'n' of 0.025 has been used to represent the bed roughness in this study. The low value has been chosen to minimise the bed friction effects and ensure that impacts of other parameters, such as the eddy viscosity, are evident.

Constriction losses may be expressed in terms of head with units of metres or as a dimensionless dynamic head loss coefficient (in terms of the dynamic head, $v_c^2/2g$). Expressing losses in terms of the dynamic head allows comparison of constriction losses across all velocities and for this reason this approach has been adopted in this study.

## 2.2 Test Channel Specifications

All methods used to calculate head loss in this study use the test channel specifications detailed in Table 2–1 unless otherwise stated.

**Table 2–1 Test Channel Specifications**

| Description | Symbol | Value |
|---|---|---|
| Total length of channel in the downstream direction | $L_{ch}$ | 1140m |
| Length of channel from the upstream boundary to the constriction: | $L_{us}$ | 270m |
| Length of channel from the constriction to the downstream boundary: | $L_{ds}$ | 810m |
| Length of constriction in the downstream direction | L | 60m |
| Width of channel | B | 300m |
| Width of constriction | b | 15m, 30m & 60m |
| Elevation of channel bottom | - | 0m |
| Downstream water surface elevation | $h_{ds}$ | 2m |
| Channel slope | S | 0 |
| Manning's n | n | 0.025 |

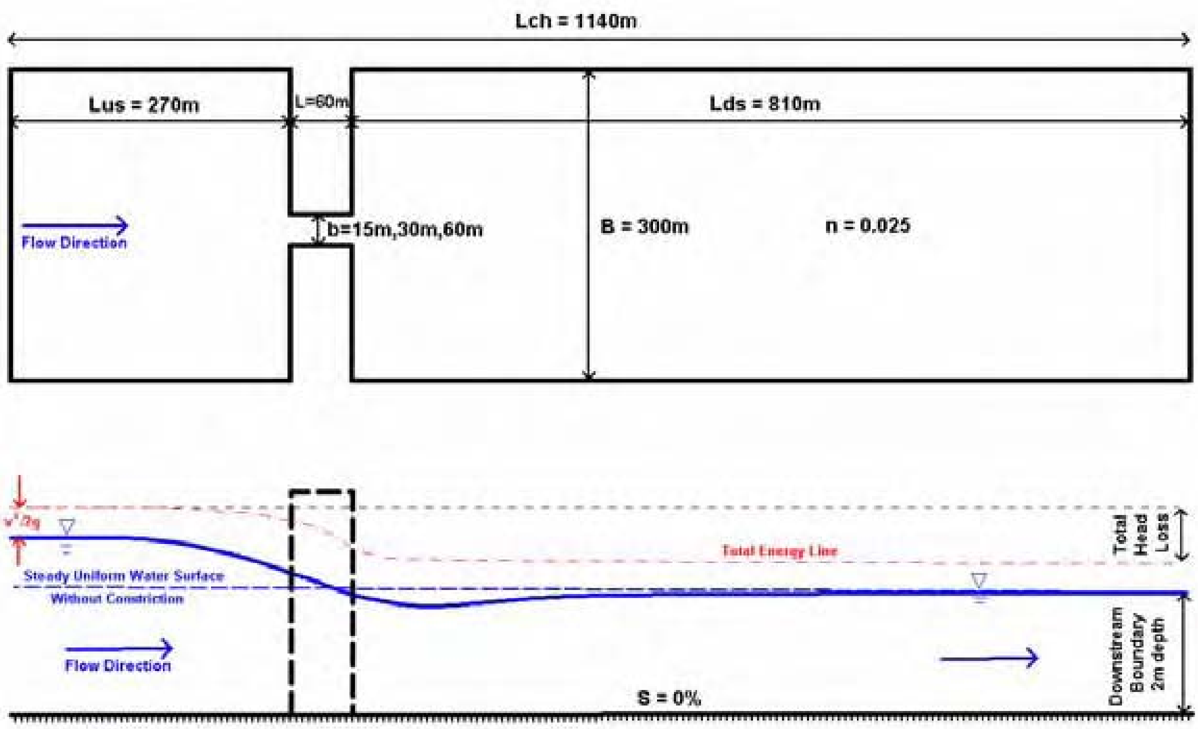


**Figure 2-1 Test Channel Specifications**

# 2.3 Calculation Methods Used

## 2.3.1 Numerical Models

Details of the models used to determine the total head loss across the model domain are provided in Table 2–2.

**Table 2–2 Details of Models Used**

| Model Name | Version | Model Type | Solution Technique | Solution Scheme | Reference |
|---|---|---|---|---|---|
| RMA2 | 6.5 | 2D | Finite Element | Implicit | King (1998) |
| TUFLOW | 3.0 | 2D | Finite Difference | Implicit | WBM (2000) |
| MIKE11 | 1999b | 1D Unsteady | Finite Difference | Implicit | DHI (1992,2000) |
| HEC-RAS | 2.2 | 1D Steady | Standard Step Backwater | - | HEC (1998) |

## 2.3.2 Manual Methods

A summary of the manual theoretical/empirical methods used to provide a total head loss comparison tool is provided in Table 2–3. Other manual methods were considered for use and are discussed in Section 8.4.

**Table 2–3 Manual Methods Used**

| Method Name | Reference | Description |
|---|---|---|
| "Henderson" | Henderson (1966) | Provides a summary of past research into expansion and contraction losses. Combines both empirical and theoretical methods to estimate expected losses. |
| Waterway Design | AUSTROADS (1994) | Reproduction of Bradley (1978) for Australian bridge design. Method based on empirical studies involving both laboratory models and field measurements. |

# 2.4 2D Model Development

## 2.4.1 Spatial Resolution

For each 2D model, five mesh resolutions were developed in order to assess the impact of mesh resolution on constriction loss results. These models were developed according to the test channel specification in Table 2–1 for each width of constriction tested. In conducting these assessments it was found that the eddy viscosity formulation used within the models has a significant impact on the model's ability to define flow behaviour. Hence, the impact of the eddy viscosity is a major secondary assessment component of this study. Two different eddy viscosity formulations were tested in each of the 2D models and results are compared. The formulations used are the constant eddy approach and the Smagorinsky formulation. This additional work is presented as Appendix B.

#### *2.4.1.1 TUFLOW*

TUFLOW itself was used in conjunction with MapInfo, a GIS based mapping package, to develop the grids that varied in 5 stages of density from coarse (15m Grid) to fine (1m Grid). The differences in grid resolution are demonstrated from Figure 2-2 through Figure 2-6 for the 30m width of constriction subset. In some cases the TUFLOW grid was not able to provide a centred constriction. A summary of constriction placement is provided in Table 2–4. In addition, the 10m grid size was not able to represent the 15m constriction. However, TUFLOW does have the capacity to incorporate a width contraction factor over a number of grid cells (termed the "Flow Constriction" feature in WBM, 2000). By utilising this feature, the 15m width of constriction was modelled as 2 x 10m grid cells with a constriction factor of 0.75.

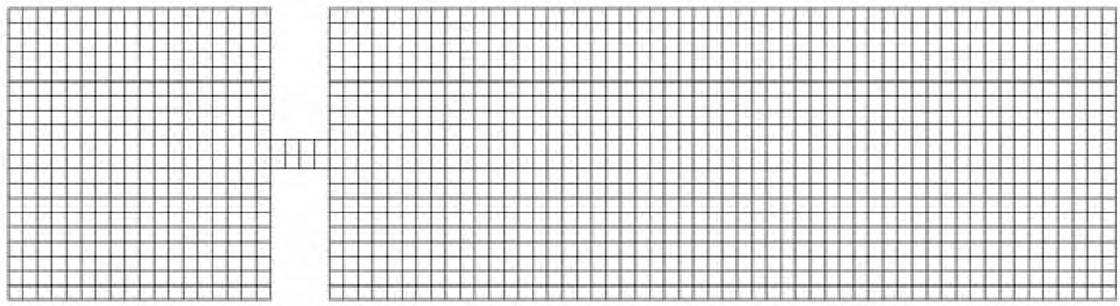

**Figure 2-2 TUFLOW 15m Grid**

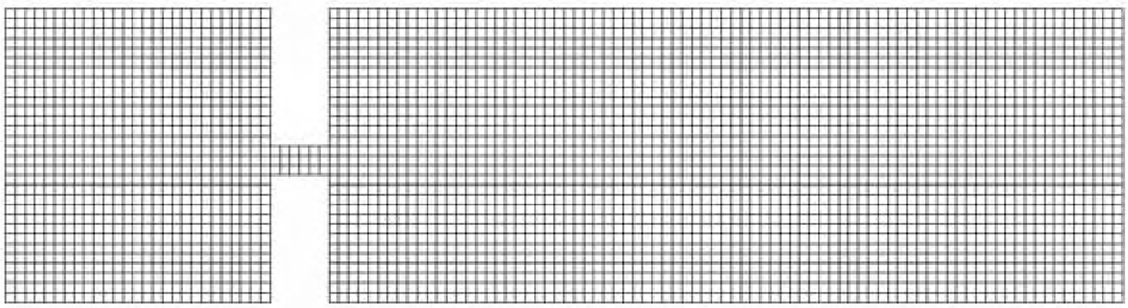

**Figure 2-3 TUFLOW 10m Grid**

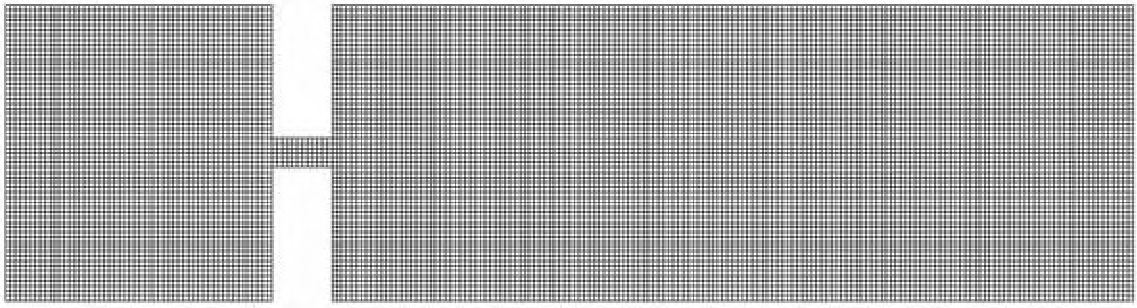

Figure 2-4 TUFLOW 5m Grid

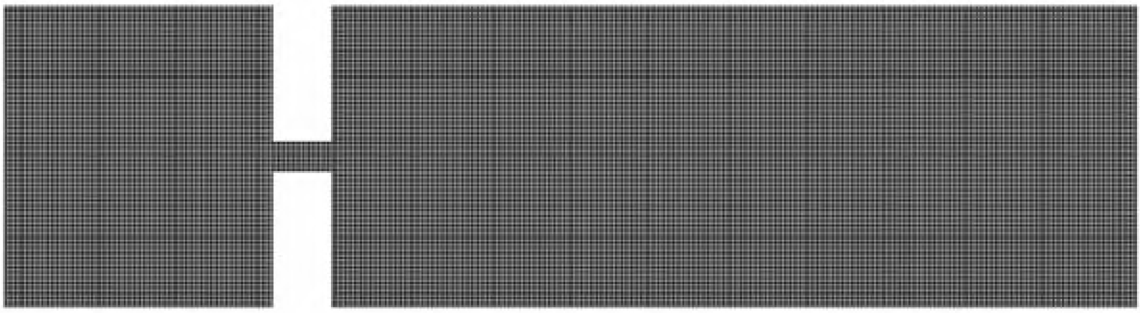

Figure 2-5 TUFLOW 2.5m Grid

Figure 2-6 TUFLOW 1m Grid

**Table 2–4 TUFLOW – Location of Constriction**

| Width of Constriction (m) | Grid Dimension (m) | Constriction Centred? |
|---|---|---|
| 15 | 1 | × |
| | 2.5 | × |
| | 5 | × |
| | 10 | ✓⌘ |
| | 15 | × |
| 30 | 1 | ✓ |
| | 2.5 | ✓ |
| | 5 | ✓ |
| | 10 | × |
| | 15 | ✓ |
| 60 | 1 | ✓ |
| | 2.5 | ✓ |
| | 5 | ✓ |
| | 10 | ✓ |
| | 15 | ✓ |

⌘ Flow Constriction Feature used to represent 15m constriction width

✓ Constriction Centred in Channel

× Constriction Not Centred in Channel

### 2.4.1.2 RMA2

The software package SMS 6.0 was used to establish the meshes that varied in density from coarse (Mesh 1) to fine (Mesh 5). The differences in mesh density are demonstrated from Figure 2-7 through Figure 2-11 for the 30m width of constriction subset.

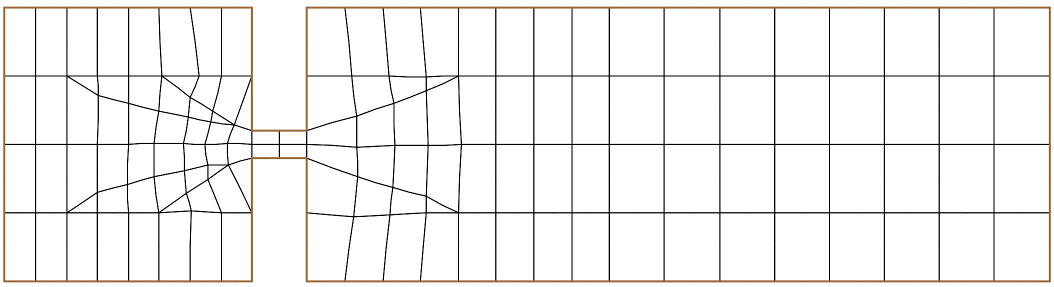

**Figure 2-7 RMA Mesh 1 – Coarsest Mesh**

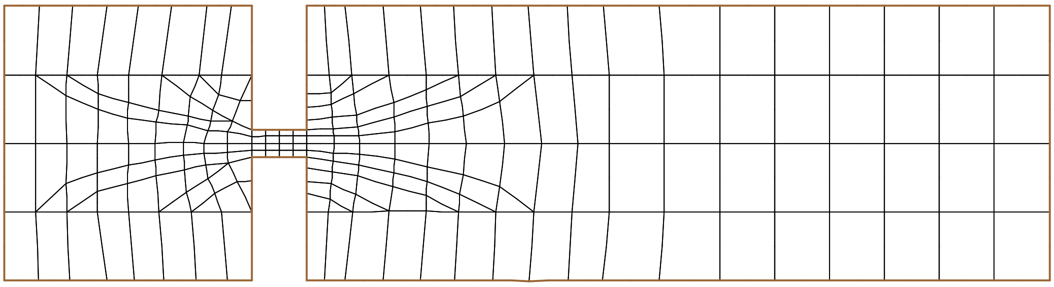

**Figure 2-8 RMA Mesh 2 – Coarse Mesh**

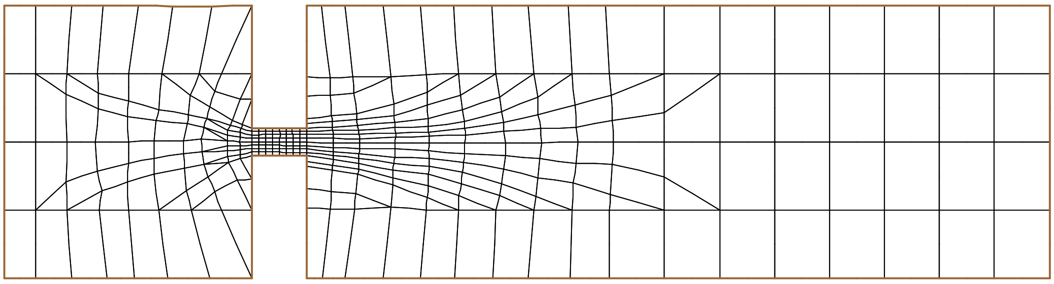

**Figure 2-9 RMA Mesh 3 – Medium Mesh**

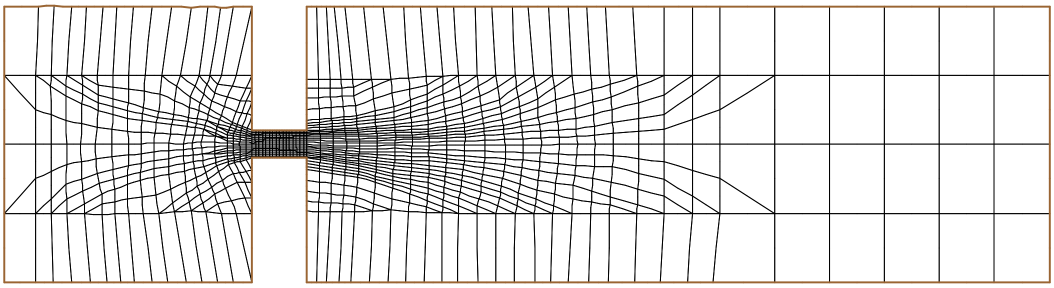

**Figure 2-10 RMA Mesh 4 – Fine Mesh**

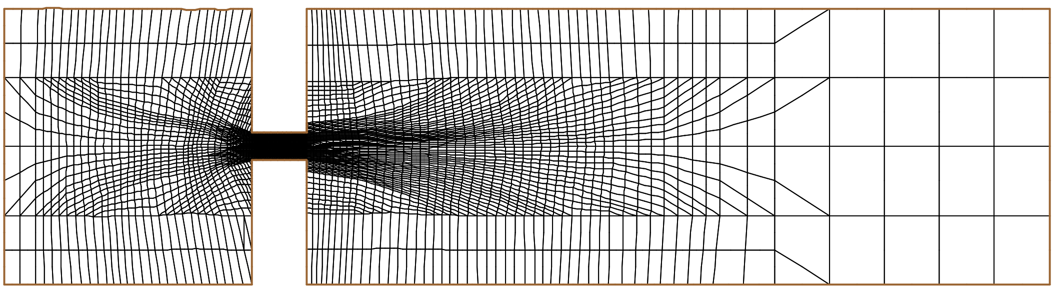

**Figure 2-11 RMA Mesh 5 – Finest Mesh**

Difficulties were experienced in developing and assessing these varying mesh densities. The initial approach in developing the mesh was to attempt to automate the mesh generation process as much as possible as this would remove any potential bias in results according to the experience of the modeller. However, meshes generated in this way proved to be extremely unstable and runs could not be completed. A complete series of new meshes were then created, accounting for the way in which water was expected to flow with increasing localised mesh density in areas where instabilities were believed to be generated. The new series of meshes, which are those shown in the previous figures, were created as they would be by an experienced modeller (advice and guidance received from Nielsen). This changing process was time-consuming but several important conclusions were drawn from the experience and these are detailed in Section 5.

### 2.4.2 Flows

Flows at the upstream boundary over the simulation period were varied from 0m$^3$/s to 480m$^3$/s. Figure 2-12 and Figure 2-13 show the ramping of flows for TUFLOW and RMA2 respectively. The flows at which output is taken are 30m$^3$/s, 60m$^3$/s, 120m$^3$/s, 240m$^3$/s and 480m$^3$/s.

At 4m/s, the flow rate in TUFLOW had to be held constant for an extended period so that the model provided non-fluctuating results (that is, head losses did not fluctuate by more than 2mm). This was particularly relevant for the constriction width of 15m. Thus, all TUFLOW model simulations were run for 8 hours even though some of them required a smaller range of flow rates.

RMA2 simulations were initially ramped to each of the flows for which output was required and then the simulation run at steady state (timestep=0) at each flow to produce a stable result. To increase flows from 240m$^3$/s to 480m$^3$/s it was necessary to ramp the flows through the intermediate flow rates shown in Figure 2-13. Results were not extracted for these intermediate flow rates.

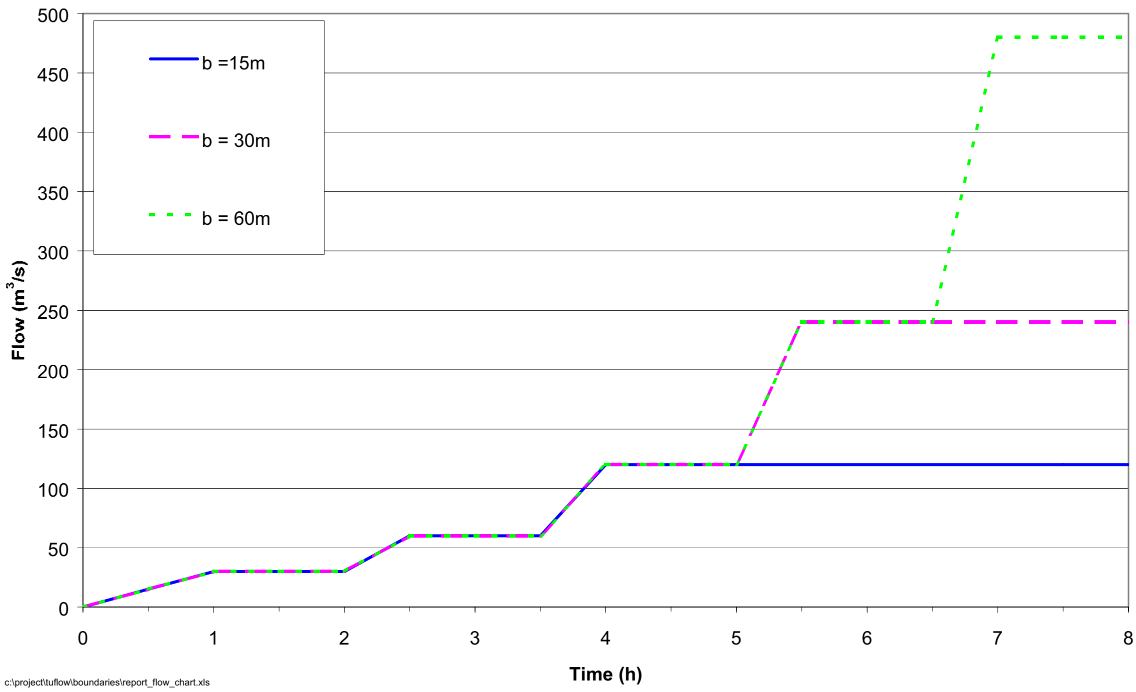


**Figure 2-12 TUFLOW - Variation of Flows at the Upstream Boundary**

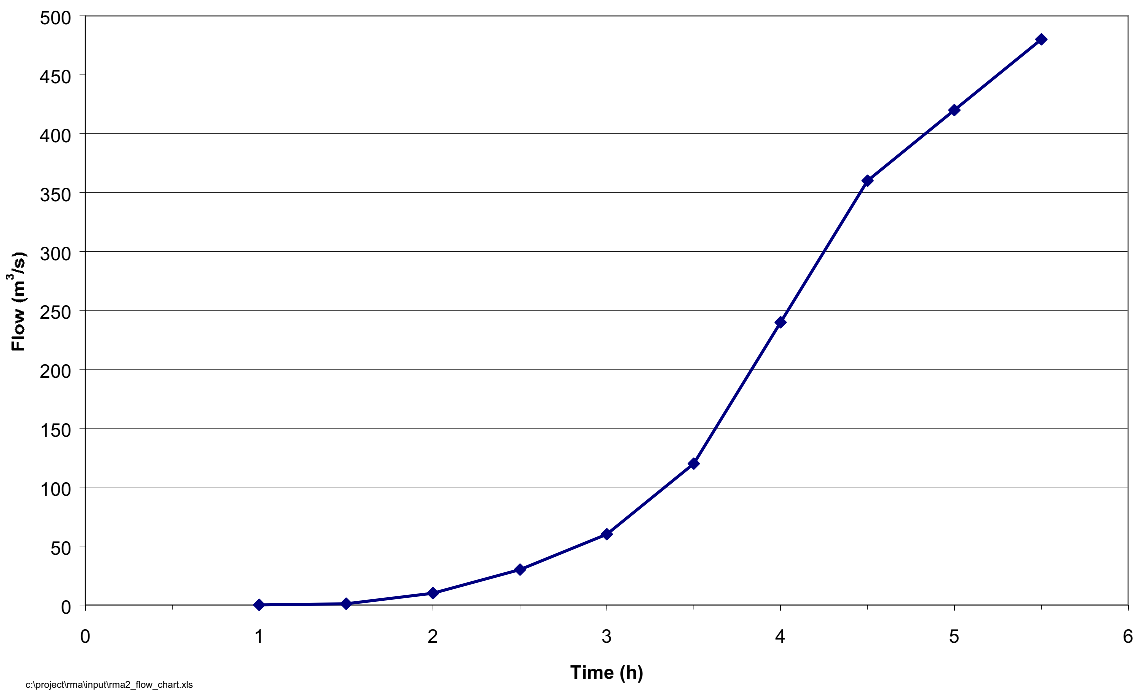


**Figure 2-13 RMA2 – Variation in Flows at the Upstream Boundary**

### 2.4.3 Courant Number / Peclet Number

The Courant Number, $C_r$, extends from the 'Courant-Friedrichs-Lewy (CFL) condition' (Abbot, 1979). The $C_r$ is used for determining a suitable computation timestep for a model simulation. For a 1D scheme the following equation is used to calculate the Courant Number, $C_r$:

$$C_r = \frac{\Delta_t \sqrt{gD}}{\Delta_x}$$

For a 2D scheme the following equation applies:

$$C_r = \Delta_t \sqrt{gD\left(\frac{1}{\Delta_x{}^2} + \frac{1}{\Delta_y{}^2}\right)}$$

And for a 2D square grid scheme the above equation reduces to:

$$C_r = \frac{\Delta_t \sqrt{2gD}}{\Delta_x}$$

Where: $\Delta t$ = timestep in seconds

$\Delta x$, $\Delta y$ = length of model element in x and y direction

g = acceleration due to gravity ($m/s^2$)

D = depth of water

An implication of the CFL condition is that the stability of an **explicit** solution scheme is conditional on $C_r$ being less than 1. Both TUFLOW and RMA2 are **implicit** schemes. Implicit schemes are generally not conditional on $C_r$ being less than 1 and are referred to as unconditionally stable.

However, the inaccuracy (phase error) of an implicit scheme increases with increasing $C_r$. It is difficult to determine the magnitude of the inaccuracy except by comparing one simulation with another that used a lower value of $C_r$. Syme (1991) notes that for most implicit schemes a Courant Number of between 2 and 15 is typically used.

The value of $C_r$ varies over the model domain as either the element lengths and/or depths vary. The Courant Number quoted for a particular model is usually the largest over the model domain and is referred to as the critical Courant Number. Courant Numbers for the TUFLOW simulations are presented in Table 2–5. The numbers contained in this table were calculated using the maximum depth predicted by the model for the maximum flow rate (ie 480m$^3$/s) and are thus the critical Courant Numbers. For the majority of the simulation the Courant Numbers will be less than this value. The timesteps were chosen so as to minimise the critical Courant Number.

**Table 2–5 TUFLOW Critical Courant Numbers**

| Grid Size (m) | Simulation Timestep (s) | Courant Number, $C_r$ |
|---|---|---|
| 15 | 7.5 | 4.0 |
| 10 | 5 | 6.3 |
| 5 | 4 | 6.3 |
| 2.5 | 2 | 4.0 |
| 1 | 0.5 | 4.0 |

Sensitivity simulations were undertaken on a subset of the TUFLOW simulation set to determine the impact of a lower simulation timestep (and therefore a lower Courant Number) on results. The differences in total head loss due to timestep reduction were less than 3% of the total head loss. Thus, it may be assumed that the timesteps used in this study provide accurate results.

Hardy *et al.* (1999) removes the need for sensitivity checks of model stability by maintaining a critical Courant Number of less than 1 for all simulations despite TELEMAC-2D being an implicit model. Maintaining a Courant Number of less than 1 across all TUFLOW simulations was not practical as simulation times would have increased by a factor of 4, meaning that the longest simulation would take 16 days to complete (refer to Table 5–2). However, as explained above, sensitivity simulations have confirmed that stability has been achieved with Courant Numbers greater than the limit of 1 used by Hardy *et al.* (1999).

King (1998) recommends consideration of the Peclet number in developing a stable RMA2 simulation. The Peclet number may be used as a guide to mesh density and coefficient selection:

$$P = \frac{\rho_V \Delta_x}{\varepsilon}$$

Where: $\rho$ = kinematic viscosity (kg/m$^3$)

$\Delta$x = mesh spacing (m)

V = velocity along a particular streamline (m/s)

$\varepsilon$ = eddy viscosity (Pa.s)

In order for the solution to be stable, the Peclet number should be less than 50. The Peclet number will vary from point to point in a mesh depending on the flow velocity, mesh density and eddy viscosity. The Peclet number can be reduced by increasing the mesh density or increasing the eddy viscosity. (It is interesting to note that when using the Smagorinsky formulation to calculate eddy viscosity (refer to Section 1.5.2 and Appendix B), mesh density is an important variable in the calculation and thus eddy viscosity and mesh density are not able to be independently varied).

The Peclet number has not been calculated in this study as RMA2 does not output the eddy viscosity calculated according to Smagorinsky (refer to Appendix B). Thus, evaluation of the Peclet number is not possible. However, future investigations should consider a means to extract the eddy viscosity from RMA2 to enable calculation of the Peclet number.

### 2.4.4 Eddy Viscosity Formulation

The use of eddy viscosity in 2D numerical modelling provides an approximate representation of the energy losses due to **turbulent effects at sub-grid scale**. As this study has found the eddy viscosity to have a significant impact on results, a detailed description and analysis of eddy viscosity is provided in Appendix B. A brief summary is given in this section.

#### *2.4.4.1 TUFLOW*

TUFLOW has three methods of determining the eddy viscosity:

- Fixed constant;
- Empirical scaling; and
- Smagorinsky turbulence closure.

WBM (2000) recommends the use of the fixed constant approach when grid size is much greater than the depth. As this was not the case in this study (grid size varies from 1m to 15m and depth varies from 2m to 4m), the Smagorinsky turbulence closure formulation is used. This formulation calculates eddy viscosity values on an element by element basis based primarily on the velocity gradient across the grid, the grid size and an input factor. The factor used in this case is 0.2 which is the same as that used in the RMA2 simulations. There is no minimum limit for the eddy viscosity (that is, the minimum eddy viscosity may be 0).

#### *2.4.4.2 RMA2*

RMA2 has three methods of determining the eddy viscosity:

- Fixed constant;
- Scale factor based on size and shape of elements; and
- Smagorinsky turbulence closure.

As the element size typically varies throughout the RMA2 model domain, the standard recommended approach is to utilise the Smagorinksy formulation (King, 1998). This formulation calculates eddy viscosity values on an element by element basis based primarily on the velocity gradient across the grid, the grid size and an input factor. The factor used in this case is the default value of 0.2. In

RMA2, the user has the option of setting a minimum limit to the eddy viscosity. However, in order to remain consistent with TUFLOW, this has been set to 0.

Sensitivity simulations are undertaken for both TUFLOW and RMA2 using the constant eddy viscosity approach with a value of $1m^2/s$ used across the model domain. Substantial differences in results are evident. These are presented and discussed in Appendix B.

### 2.4.5 Processing Results

TUFLOW and RMA2 provide output in a form able to be imported into the SMS[1] package. This allows velocity, head and eddy viscosity results, amongst other output variables, to be contoured and vectored. However, in order to produce the contoured figures contained in this study, a suite of Fortran programs developed by WBM Oceanics Australia were made available to post-process the output data into triangular format. The data for each simulation is then triangulated using the Vertical Mapper (version 2.5) package. Vertical Mapper, in conjunction with MapInfo, is then used to contour and present the data in the desired format.

[1]SMS is a pre- and post-processor for surface water modelling, analysis, and design developed by Brigham Young University. While it includes two-dimensional finite element, two-dimensional finite difference, three-dimensional finite element and one-dimensional backwater modelling tools, it has been used in the current study to prepare RMA2 grids and post-process 2D model results only.

## 2.5 1D Model Development

The 1D MIKE 11 and HEC-RAS models are used to calculate losses through the abrupt constriction for comparison with the two-dimensional model computations.

### 2.5.1 MIKE 11

In MIKE 11 the constriction is modelled as one rectangular culvert of open section type with a length in the flow direction of 60m. The top of the culvert is set at a height above the maximum water level and does not influence computations. All coefficients used are the MIKE 11 default coefficients (DHI, 2000). Dx-max (the maximum distance between cross-sections before automatic interpolation of a h-point occurs) has been set at a value greater than the overall channel length. This was done to ensure that the results were produced with the exact model layout shown in Figure 2-14.

The Courant number is given by the following equation:

$$C_r = \frac{\Delta_t \left(v + \sqrt{gD}\right)}{\Delta_x}$$

| | | |
|---|---|---|
| Where: | $\Delta t$ | = timestep in seconds |
| | $\Delta x$ | = minimum distance between cross-sections |
| | g | = acceleration due to gravity ($m/s^2$) |
| | D | = depth of water |
| | v | = velocity |

A timestep of 2 minutes has been used for all MIKE 11 simulations. This gives a critical Courant number of 0.3 which is much less than the maximum of 10 specified by DHI (2000) and thus the model simulations satisfy the Courant stability criteria.

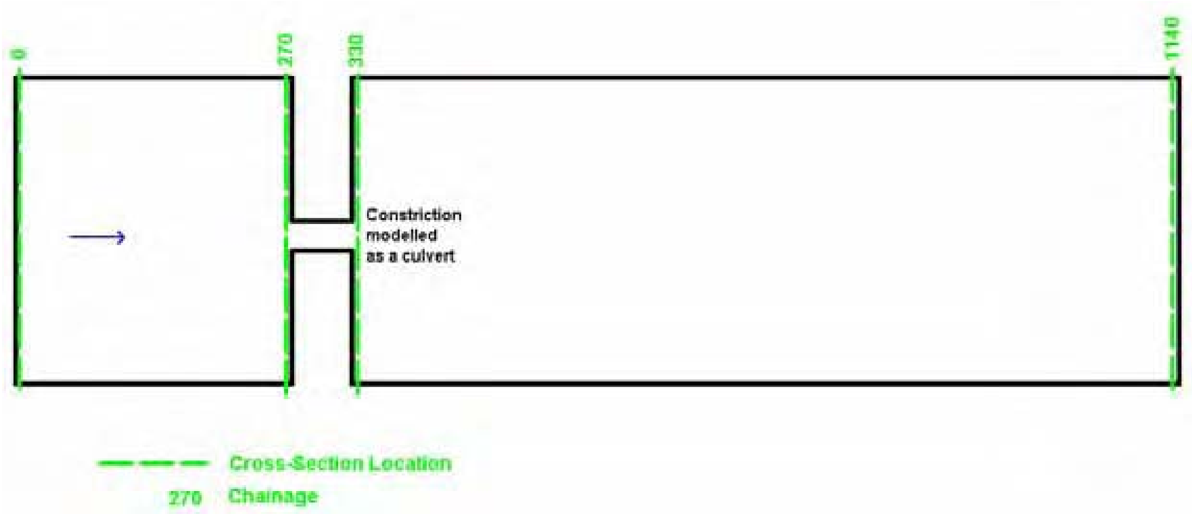


**Figure 2-14 Layout of the MIKE 11 Model**

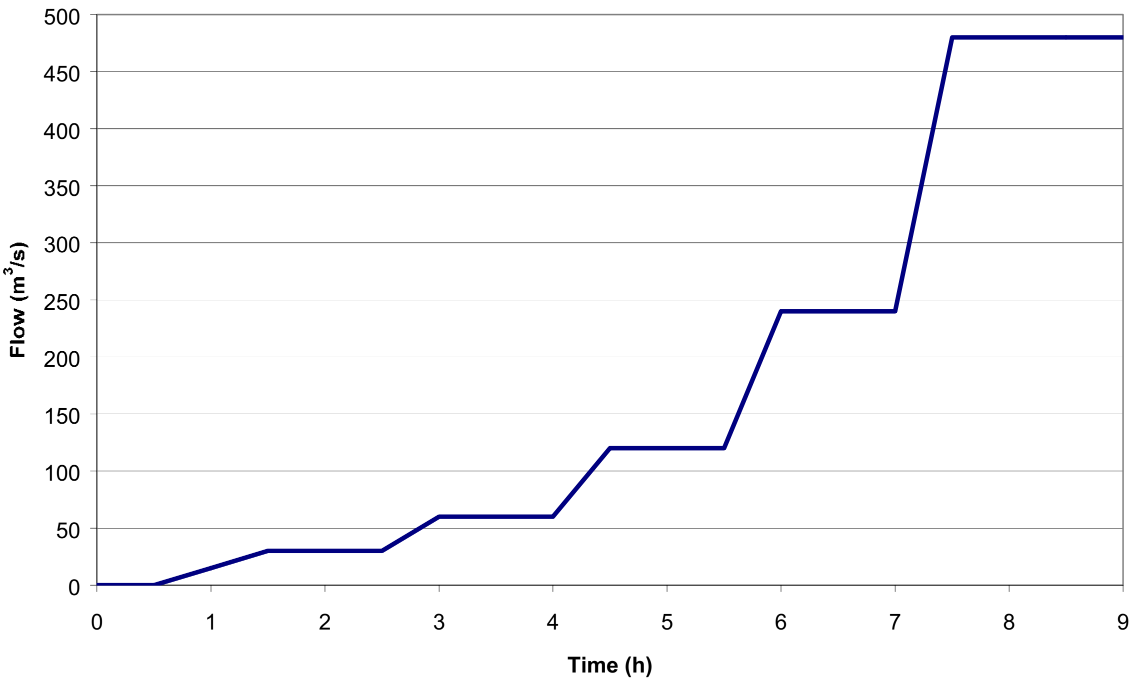


**Figure 2-15 MIKE 11 – Variation of Flows at the Upstream Boundary**

### 2.5.2 HEC-RAS

In HEC-RAS the abrupt constriction is modelled as a bridge opening with no piers. The deck is set at a level above the maximum water surface elevation so that it does not influence computations. Ineffective flow areas are defined according to the manual (HEC, 1998). The method of calculating friction slope is the default method using the average conveyance equation. Physical characteristics of the channel are as specified in Table 2–1. The model layout is shown schematically in Figure 2-16.

Key issues associated with the development of the HEC-RAS model for this study are as follows:

- Selection of expansion and contraction coefficients, and
- Selection of the expansion and contraction reach lengths.

The methods and calculations used in these selection processes are covered in detail in Appendix C. A summary of the values selected for each of the key parameters is provided in Table 2–6.

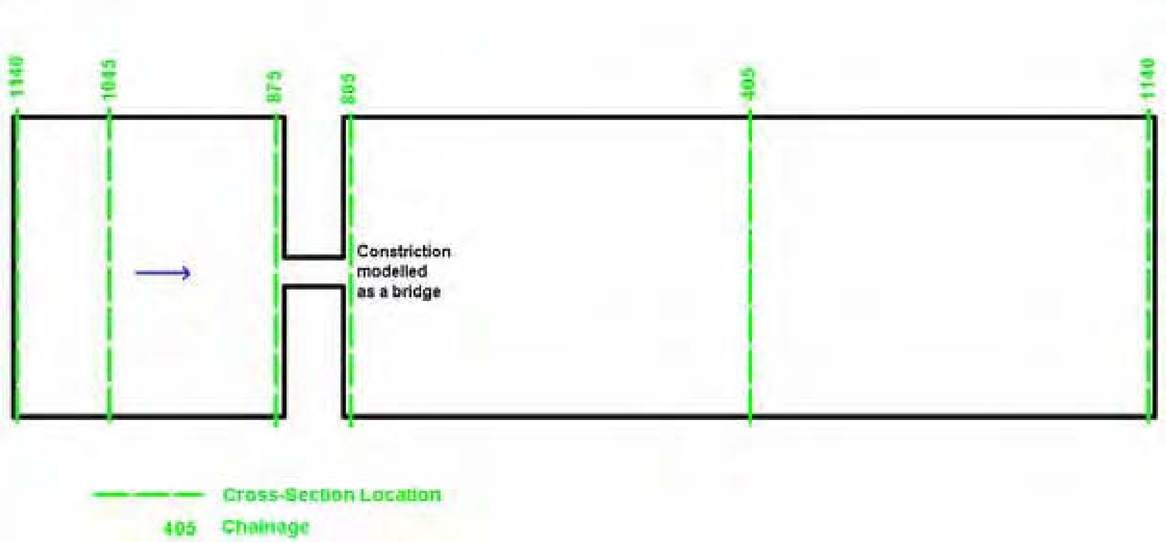


**Figure 2-16 Layout of the HEC-RAS Model**

**Table 2–6 Summary of Key HEC-RAS Parameters**

| b (m) | Q ($m^3/s$) | Expansion Reach $L_e$ | Expansion Reach $C_e$ | Contraction Reach $L_c$ | Contraction Reach $C_c$ |
|---|---|---|---|---|---|
| 15 | 30 | 570 | 0.8 | 330 | 0.5 |
| | 60 | 570 | 0.8 | 330 | 0.5 |
| | 120 | 570 | 0.8 | 330 | 0.5 |
| 30 | 30 | 540 | 0.7 | 310 | 0.5 |
| | 60 | 540 | 0.7 | 310 | 0.5 |
| | 120 | 540 | 0.7 | 310 | 0.5 |
| | 240 | 540 | 0.7 | 310 | 0.5 |
| 60 | 30 | 360 | 0.4 | 170 | 0.4 |
| | 60 | 360 | 0.4 | 170 | 0.4 |
| | 120 | 360 | 0.4 | 170 | 0.4 |
| | 240 | 360 | 0.4 | 170 | 0.4 |
| | 480 | 360 | 0.4 | 170 | 0.4 |

## 2.6 Presentation of Results

For each calculation method, total head loss results are presented in units of millimetres. Constriction losses (total head loss minus friction loss) are then presented as a dynamic head loss coefficient. As explained in the study terminology section, a dynamic head loss coefficient of 1.5 is equivalent to a constriction loss of 1.5 x ($v_c^2/2g$) where $v_c$ is the average velocity through the constriction. It is important to note that there are advantages and disadvantages in using $v_c$ as the basis for the dynamic head:

Advantages:

- $v_c$ is simple to calculate. $v_c = Q/A_c$ where $A_c$ is the average constriction area.
- $v_c$ remains constant regardless of model spatial resolution or method of calculation used.

Disadvantages:

- $v_c$ does not account for the presence or otherwise of the vena contracta.
- $v_c$ is neither the maximum or minimum velocity through the constriction.
- At low values of $v_c$, total head loss is also low and dynamic head loss coefficients are very sensitive to the dynamic head ($v_c^2/2g$). The accuracy of the dynamic head calculated using $v_c$ at these low velocities may introduce sensitivity errors into the coefficients. This is discussed further throughout the report.

## 2.7 Methodology Comparison with Previous Studies

This current study provides some extension of the previous work by Syme *et al.* (1998) described in Section 1.3.2. Head losses for varying widths of constriction for varying flows are calculated using two 2D models, two 1D models and theoretical/empirical manual calculations. However, the specific focus of this study is the impact that varying the spatial resolution of the 2D models has on flow behaviour. Five sets of meshes were developed for each 2D model ranging from coarse to fine resolution. It is similar to the work undertaken by Hardy *et al.* (1999) who investigated the impact of mesh resolution across 7 different mesh resolutions for one 2D model. However, there are several significant differences between this current study and that undertaken by Hardy *et al.* (1999) that are important to note:

- Hardy *et al.* (1999) investigated a compound meandering channel rather than a simple rectangular channel.
- Increasing the model spatial resolution by Hardy *et al.* (1999), resulted in a change to the channel dimensions due to the means employed to define the topography. Therefore, prior to any impact that may have been generated by the difference in the solution of equations due to the changing resolution, the actual channel volume and conveyance was different. No scaling corrections were made as Hardy *et al.* (1999) believes that the differences in the filtering of data is one of the first effects of spatial resolution. While this is true, the resolution of important topographical features is one of the key factors in selecting an appropriate mesh resolution. Therefore, if the modeller believes that this factor is satisfied by the mesh resolution chosen, it is necessary to investigate the impacts that occur beyond this resolution if the mesh is further refined. The current study avoids this complication as all meshes developed define the same simple,

rectangular channel geometry so the actual channel volume and conveyance are the same regardless of spatial resolution.

- Hardy *et al.* (1999) investigated the effect of model resolution on total flow, inundation extent, velocity and depth values at specific points within the model domain and the relative sensitivity of spatial resolution versus roughness. The current study focuses on the effect of model resolution predominately on contraction and expansion losses, although velocities, eddy formation and depths throughout the model domain are also considered.
- Hardy *et al.* (1999) makes no attempt to compare model results against field data or theoretical/empirical calculations as there was 'no wish to analyse the model's predictive ability for a particular reach'. Comparisons are limited to the results achieved within the one model used for that study. The current study compares results from different models and methods as, in this study, the predictive ability of the 2D models is also important. The current study has the advantages that a) modelling is of a relatively simple channel, and b) contraction and expansion losses have been the subject of previous research and thus were hoped to be more readily quantifiable by other methods. As explained by Hardy *et al.* (1999), the field data required for comparison with the compound meandering channel mode results is unlikely to exist.
- One issue that the current study found to be of great importance in assessing the impact of mesh resolution is the choice of eddy viscosity formulation used in the 2D model. Hardy *et al.* (1999) acknowledges that eddy viscosity is one of the two parameters able to be varied in the investigation. However, the author makes no further mention of the formulation technique employed within TELEMAC-2D nor the value/s of the eddy viscosity parameter.

# 3 TUFLOW COMPUTATIONS

## 3.1 Introduction

TUFLOW is a two dimensional, implicit finite difference model (Syme, 1991 and WBM, 2000) and is used for the solution of the two-dimensional depth averaged shallow water flow equations. TUFLOW uses a regular grid of square elements to represent the modelled area. Variation of the mesh resolution within the model domain is not possible at this stage.

## 3.2 Computational Procedure

TUFLOW is specifically oriented toward establishing flow patterns in coastal waters, estuaries and rivers where flow patterns are essentially 2D in nature. The solution algorithm is based on Stelling (1984).

**Continuity Equation**

$$\frac{\partial(D u)}{\partial_x} + v\frac{\partial(D v)}{\partial_y} + \frac{\partial_h}{\partial_t} = 0$$

**Momentum Equation X-Direction**

$$\frac{\partial_u}{\partial_t} + u\frac{\partial_u}{\partial_x} + v\frac{\partial_u}{\partial_y} + g\frac{\partial_h}{\partial_x} + \frac{gn^2 u|V|}{D} - \Omega_{vh} - \mu\left(\frac{\partial^2 u}{\partial_x{}^2} + \frac{\partial^2 u}{\partial_y{}^2}\right) = F_x$$

**Momentum Equation Y-Direction**

$$\frac{\partial_v}{\partial_t} + u\frac{\partial_v}{\partial_x} + v\frac{\partial_v}{\partial_y} + g\frac{\partial_h}{\partial_y} + \frac{gn^2 v|V|}{D} - \Omega_{uh} - \mu\left(\frac{\partial^2 v}{\partial_x{}^2} + \frac{\partial^2 v}{\partial_y{}^2}\right) = F_y$$

| | | |
|---|---|---|
| Where: | x,y | = horizontal cartesian coordinates |
| | t | = time |
| | u,v | = horizontal velocity components in the x and y directions |
| | D | = depth of water |
| | h | = water elevation |
| | V | = total water velocity |
| | g | = gravitational acceleration |
| | n | = Mannings ‘n’ |
| | $\Omega_{vh}, \Omega_{uh}$ | = coriolis forcing in the x and y directions |
| | $F_x$, $F_y$ | = sum of components of external forces in the x and y directions (including wave and wind forces) |

## 3.3 Results

A summary of the simulations undertaken is provided in Table 3–1 with an indication of success of the simulation. As explained in Section 2.1, simulations where the average velocity in the constriction is greater than 4m/s are not included due to stability problems associated with supercritical flow regimes.

**Table 3–1 Summary of TUFLOW Simulations Undertaken**

| Width of Constriction (m) | Grid Dimension (m) | Flow | | | | |
|---|---|---|---|---|---|---|
| | | $30m^3/s$ | $60m^3/s$ | $120m^3/s$ | $240m^3/s$ | $480m^3/s$ |
| 15 | 1 | ✓ | ✓ | ✓ | - | - |
| | 2.5 | ✓ | ✓ | ✓ | - | - |
| | 5 | ✓ | ✓ | ✓ | - | - |
| | 10 | ✓ | ✓ | ✓ | - | - |
| | 15 | ✓ | ✓ | ✓ | - | - |
| 30 | 1 | ✓ | ✓ | ✓ | ✓ | - |
| | 2.5 | ✓ | ✓ | ✓ | ✓ | - |
| | 5 | ✓ | ✓ | ✓ | ✓ | - |
| | 10 | ✓ | ✓ | ✓ | ✓ | - |
| | 15 | ✓ | ✓ | ✓ | ✓ | - |
| 60 | 1 | ✓ | ✓ | ✓ | ✓ | ✓ |
| | 2.5 | ✓ | ✓ | ✓ | ✓ | ✓ |
| | 5 | ✓ | ✓ | ✓ | ✓ | ✓ |
| | 10 | ✓ | ✓ | ✓ | ✓ | ✓ |
| | 15 | ✓ | ✓ | ✓ | ✓ | ✓ |

- Simulation not included due to fluctuations in results requiring excessive (>8hours model time) simulation times

✓ Simulation ran to completion

Average Velocity in Constriction

| 0.25m/s | 0.5m/s | 1m/s | 2m/s | 4m/s | 8m/s | 16m/s |
|---|---|---|---|---|---|---|

### 3.3.1 Flow Characteristics

Velocities within the vena contracta for the 60m width of constriction subset are shown in Figure 3-1 and are grouped according to *average* velocity through the constriction, $v_c$. The velocity within the vena contracta has been extracted from the same location for all simulations. This location is within the full contraction region of the vena contracta at the centre of the constriction.

Flow patterns for all grids are shown for the 60m width of constriction subset of the TUFLOW simulations in Figure 3-2 to Figure 3-6. These are grouped according to average velocity through the constriction, $v_c$. The figures show the relative size and direction of the velocity vectors overlain on the colours representing the velocity magnitude as indicated in the legend.

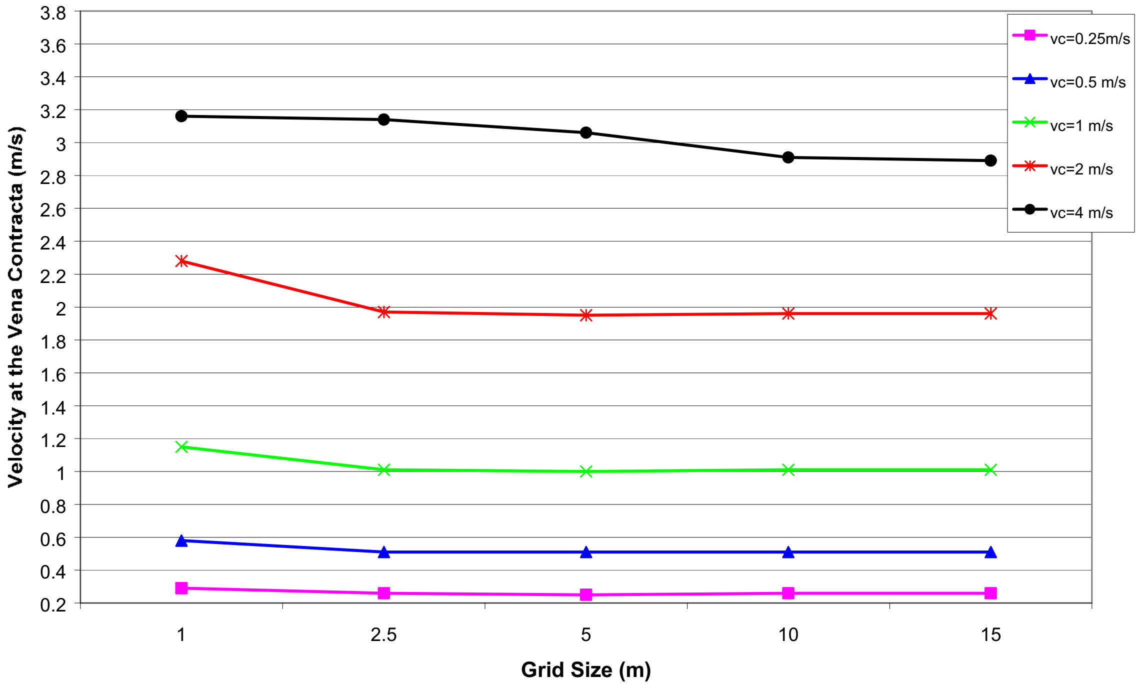


**Figure 3-1 TUFLOW – Velocities Within the Vena Contracta: b=60m**

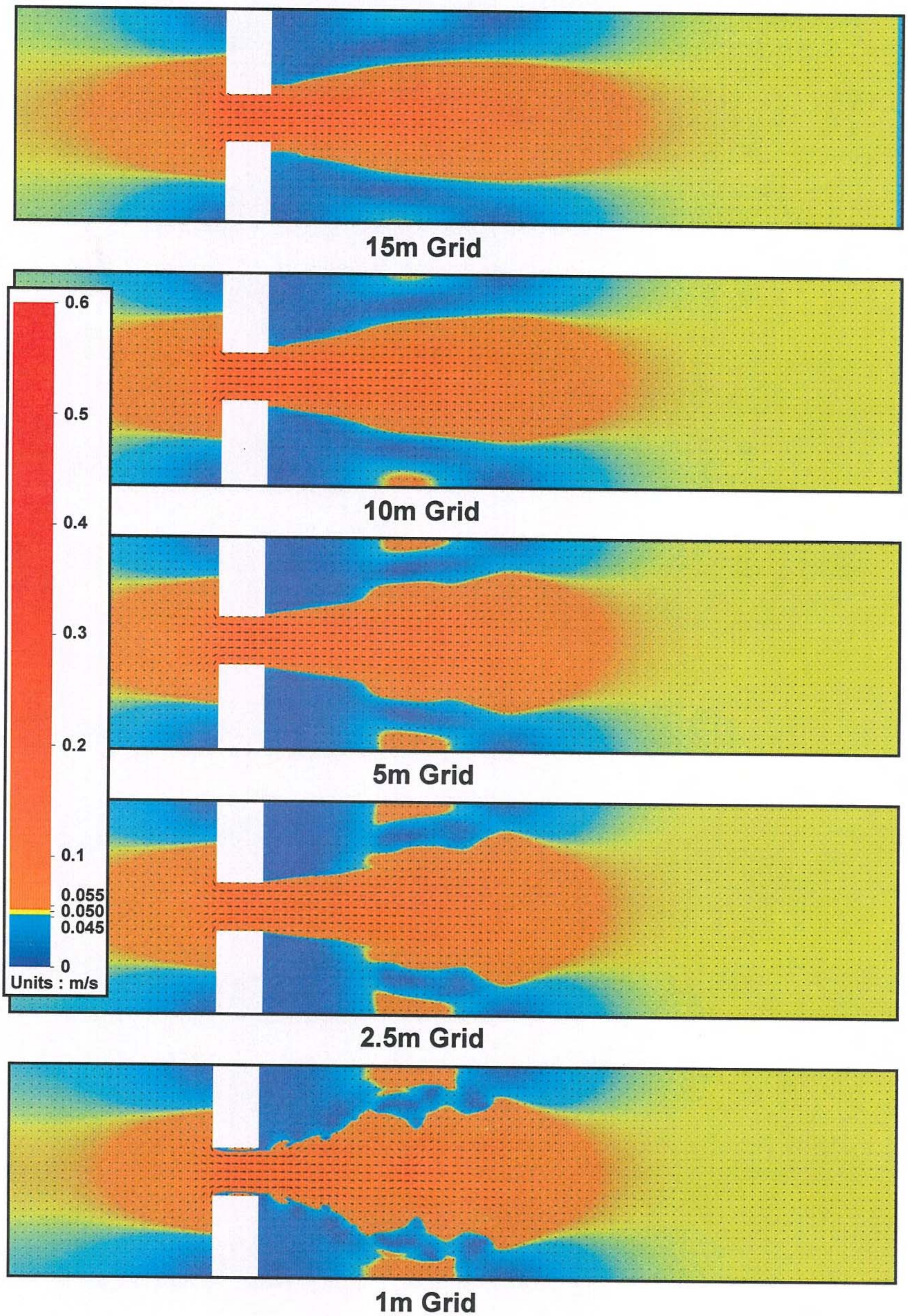


**TUFLOW - Flow Patterns :**
**Vc = 0.25m/s (Q=30m$^3$/s & b=60m)**

**Figure 3-2**

TUFLOW 025_b60.wor

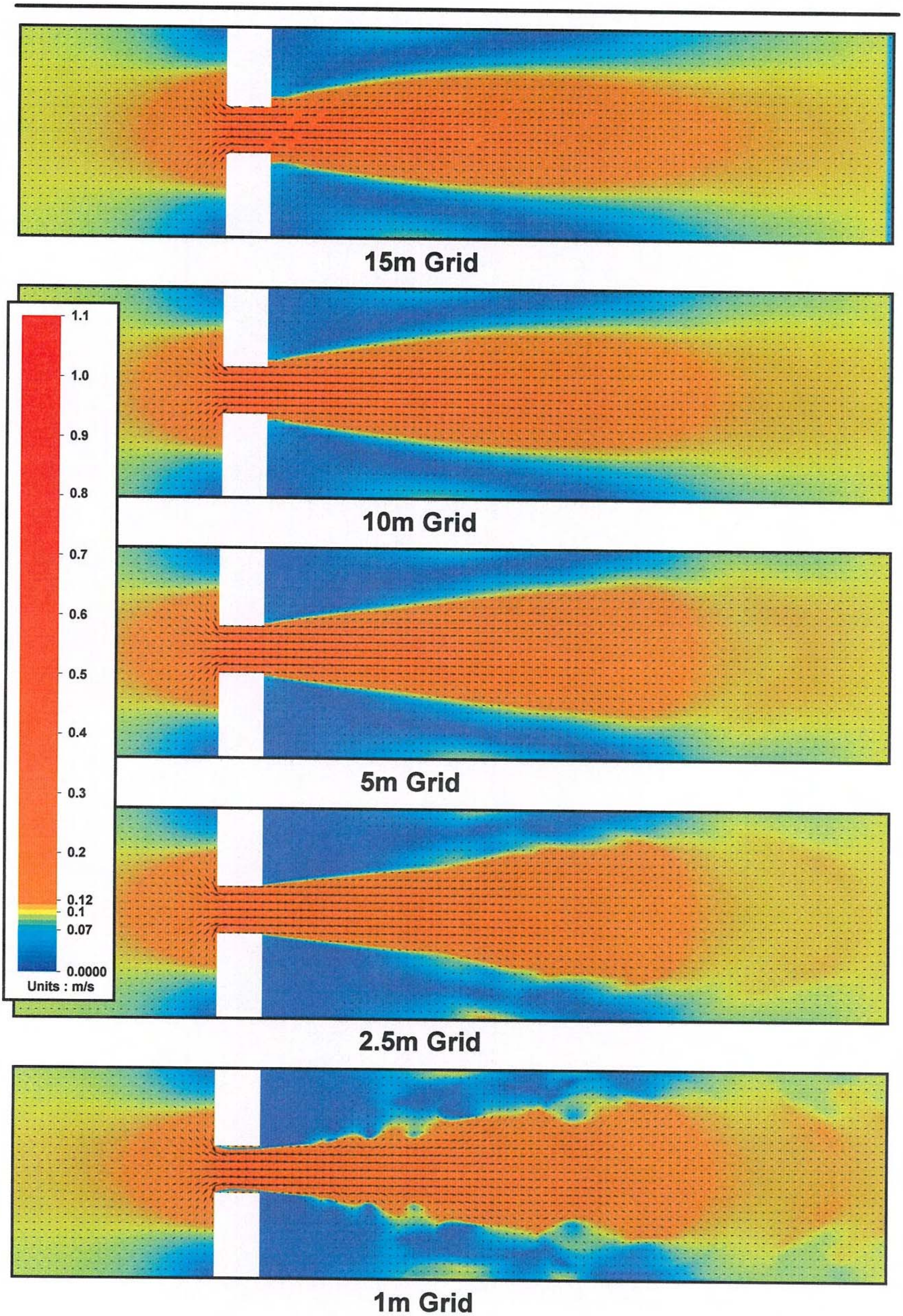


**TUFLOW - Flow Patterns :**
**Vc = 0.5m/s (Q=60m$^3$/s & b=60m)**

**Figure 3-3**

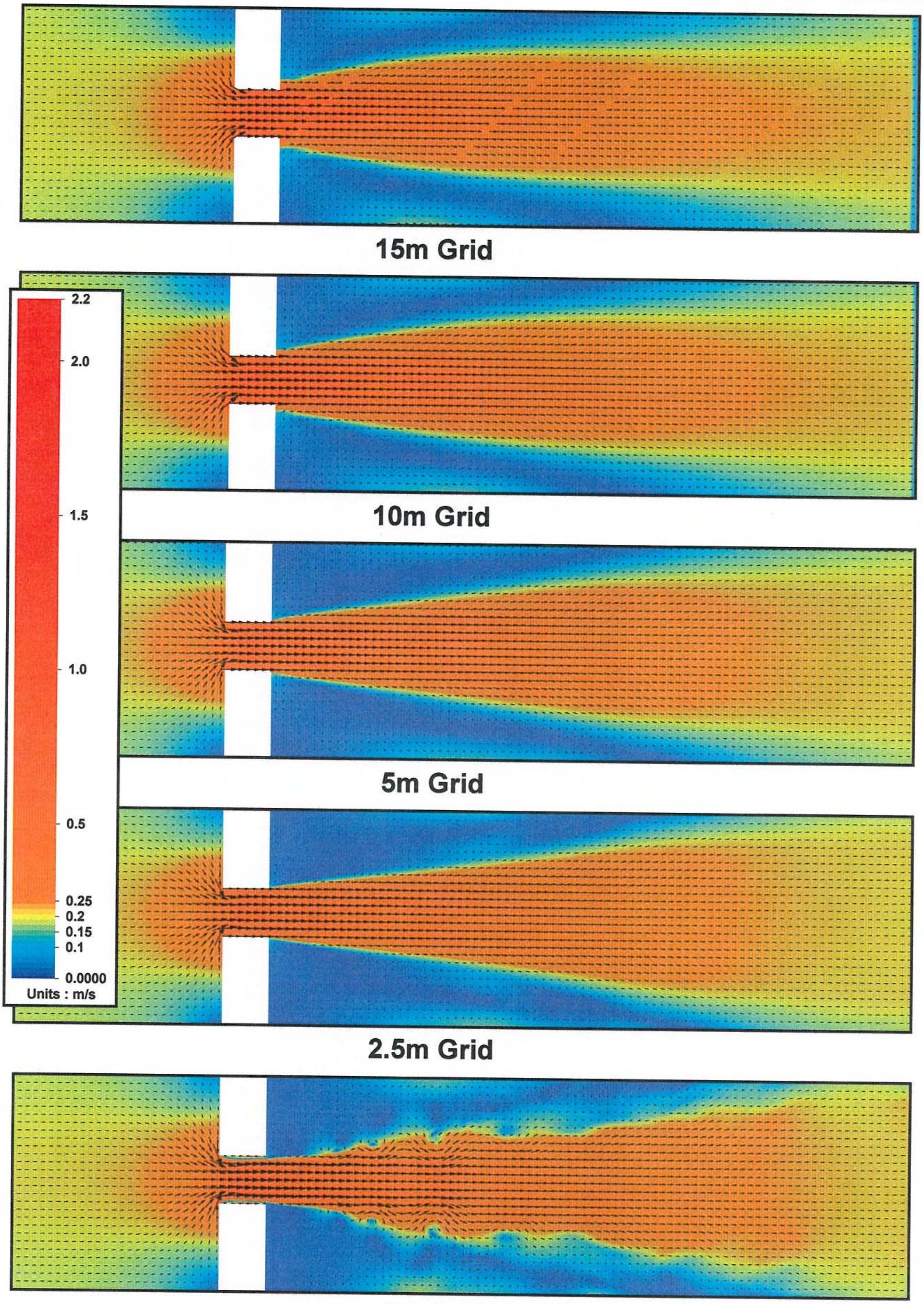


**TUFLOW - Flow Patterns :**
**Vc = 1m/s (Q=120m³/s & b=60m)**

**Figure 3-4**

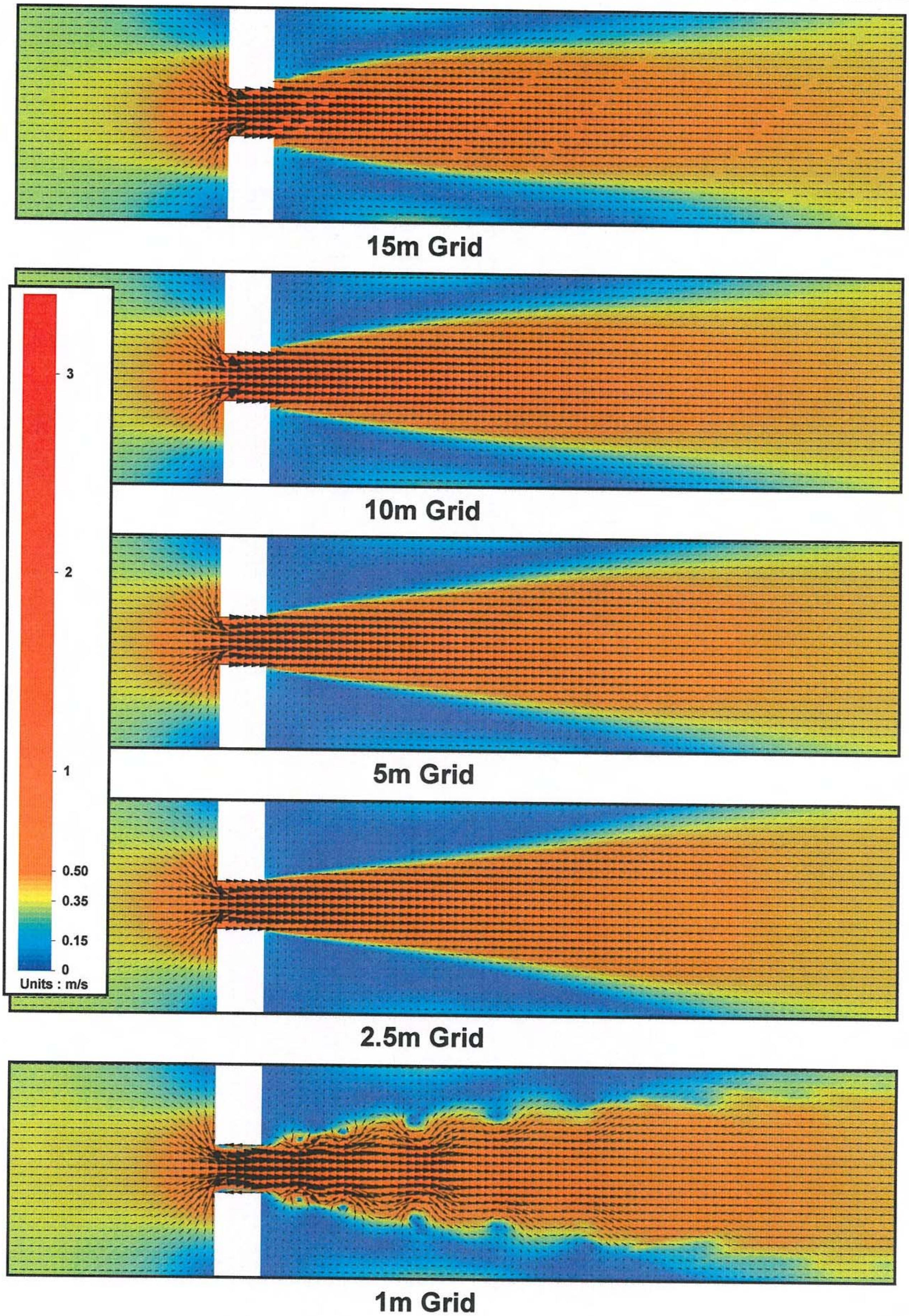


TUFLOW - Flow Patterns :
Vc = 2m/s (Q=240m$^3$/s & b=60m)

Figure 3-5

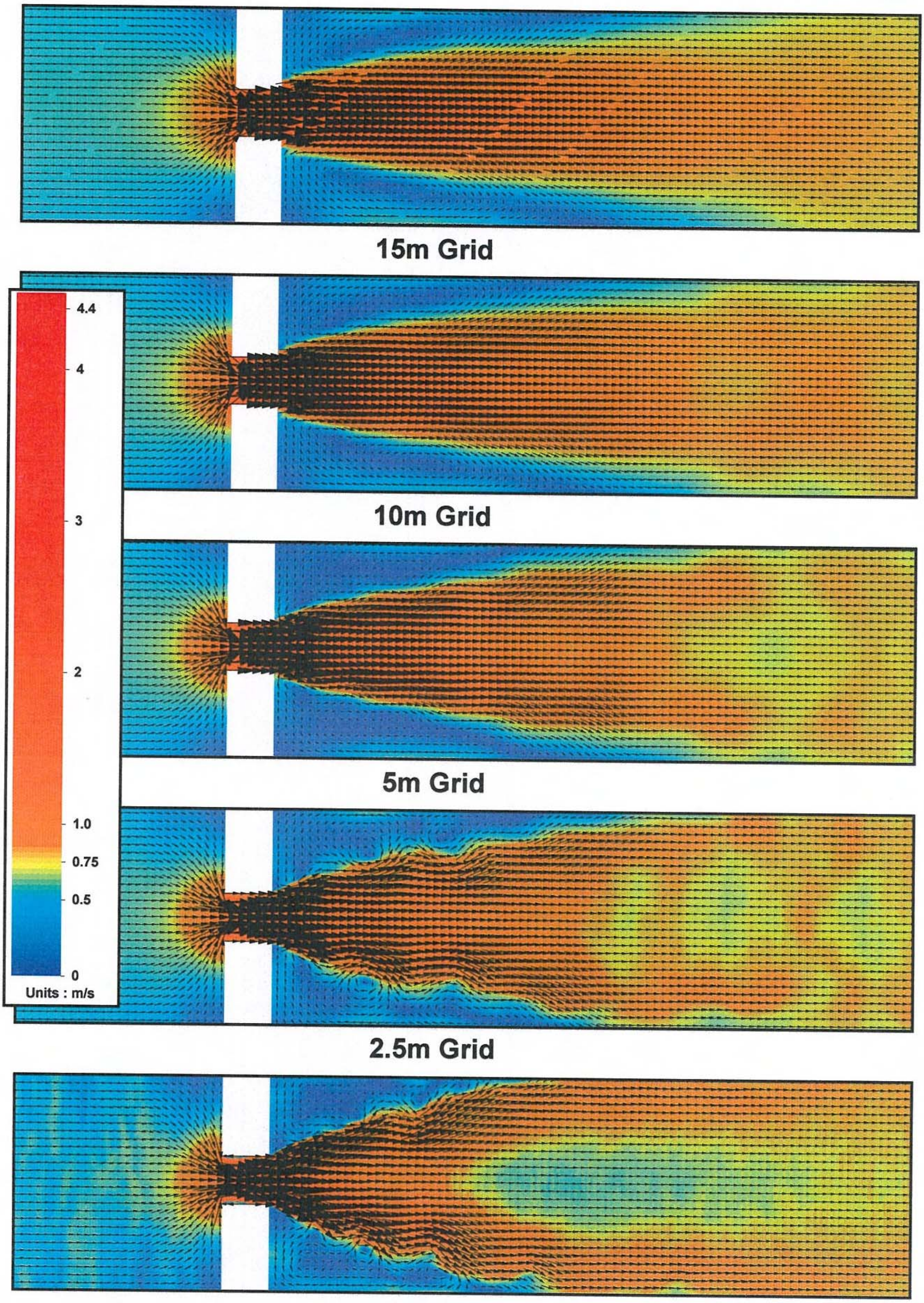


TUFLOW - Flow Patterns :
Vc = 4m/s (Q=480m$^3$/s & b=60m)

Figure 3-6

TUFLOW 4_b60.wor

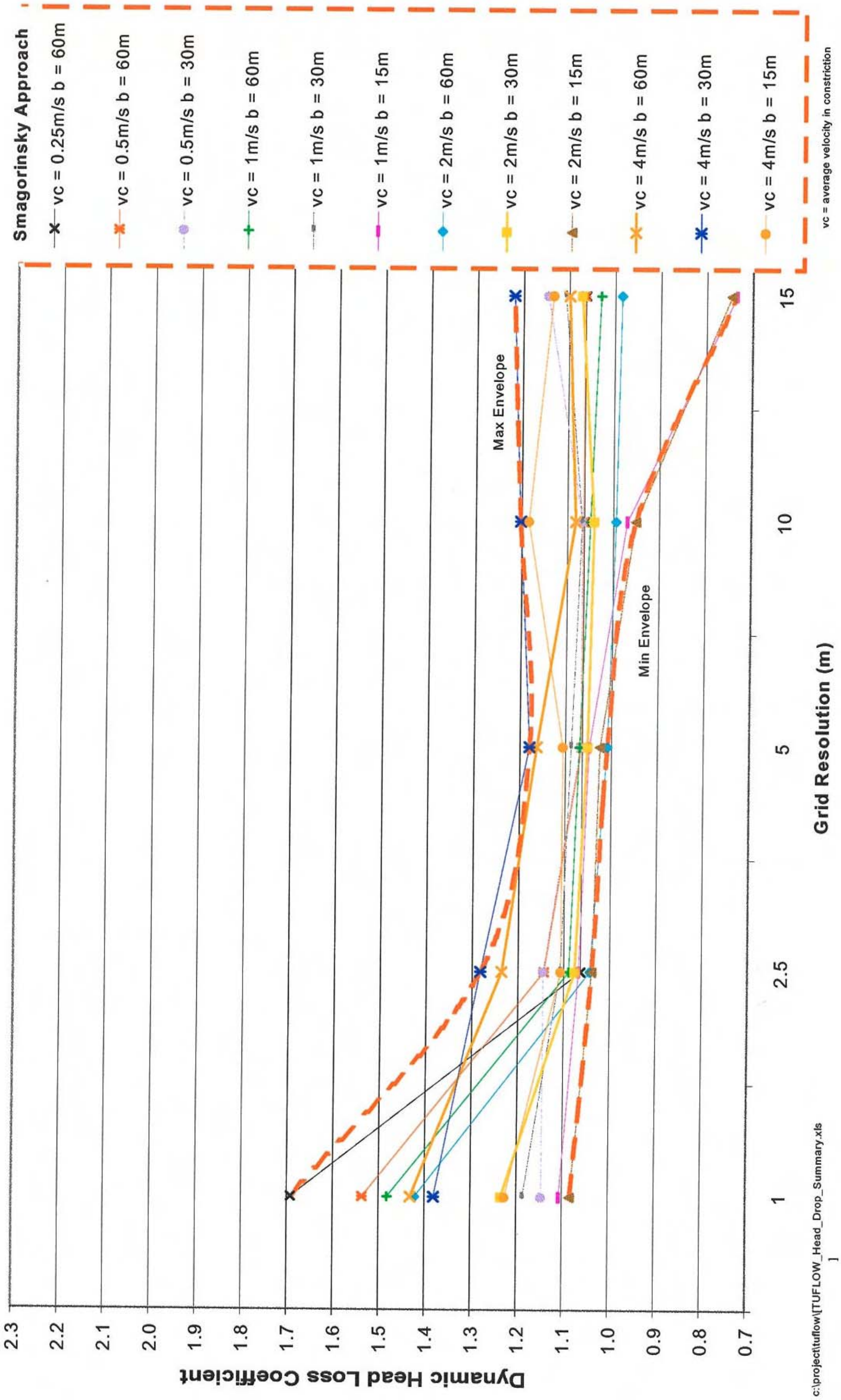


**Figure 3-7 TUFLOW – Dynamic Head Loss Coefficients**

### 3.3.2 Losses

The total head loss across the test channel is shown in Table 3–2 for each scenario. Water levels predicted across the model domain are shown graphically in Figure 3-8 through Figure 3-19. These figures are grouped according to average velocity through the constriction, $v_c$.

**Table 3–2 TUFLOW – Total Head Loss (mm)**

| Width of Constriction (m) | Grid Dimension (m) | Flow | | | | |
|---|---|---|---|---|---|---|
| | | 30m$^3$/s | 60m$^3$/s | 120m$^3$/s | 240m$^3$/s | 480m$^3$/s |
| 15 | 1 | 72 | 283 | 1247 | - | - |
| | 2.5 | 70 | 274 | 1150 | - | - |
| | 5 | 69 | 271 | 1149 | - | - |
| | 10 | 65 | 256 | 1213 | - | - |
| | 15 | 53 | 214 | 1172 | - | - |
| 30 | 1 | 19 | 78 | 321 | 1399 | - |
| | 2.5 | 19 | 74 | 289 | 1319 | - |
| | 5 | 18 | 73 | 284 | 1235 | - |
| | 10 | 18 | 72 | 282 | 1254 | - |
| | 15 | 19 | 74 | 288 | 1268 | - |
| 60 | 1 | 7 | 26 | 101 | 389 | 1546 |
| | 2.5 | 5 | 21 | 81 | 312 | 1387 |
| | 5 | 5 | 20 | 80 | 305 | 1328 |
| | 10 | 5 | 20 | 79 | 302 | 1262 |
| | 15 | 5 | 20 | 78 | 300 | 1276 |

- no result due to model instability

The total head loss results presented in Table 3–2 are used to calculate the dynamic head loss coefficient. The dynamic head loss coefficient is due solely to expansion and contraction losses, that is, frictional losses have been removed (refer to Appendix A). The dynamic head loss coefficient is a factor of the dynamic head, $v_c^2/2g$ (refer to terminology definitions at the beginning of this study report). Dynamic head loss coefficients are presented in Table 3–3 and shown graphically in Figure 3-7.

Dynamic head loss coefficients predicted in TUFLOW are compared to dynamic head loss coefficients predicted by other models and methods in Section 9.

**Table 3–3 TUFLOW – Dynamic Head Loss Coefficient Results ($v_c^2/2g$)**

| Width of Constriction (m) | Grid Dimension (m) | Flow | | | | |
|---|---|---|---|---|---|---|
| | | 30m³/s | 60m³/s | 120m³/s | 240m³/s | 480m³/s |
| 15 | 1 | 1.11 | 1.08 | 1.23 | - | - |
| | 2.5 | 1.07 | 1.04 | 1.11 | - | - |
| | 5 | 1.05 | 1.03 | 1.11 | - | - |
| | 10 | 0.97 | 0.95 | 1.18 | - | - |
| | 15 | 0.73 | 0.75 | 1.13 | - | - |
| 30 | 1 | 1.15 | 1.19 | 1.23 | 1.38 | - |
| | 2.5 | 1.15 | 1.11 | 1.08 | 1.28 | - |
| | 5 | 1.07 | 1.09 | 1.05 | 1.18 | - |
| | 10 | 1.07 | 1.07 | 1.04 | 1.20 | - |
| | 15 | 1.15 | 1.11 | 1.07 | 1.22 | - |
| 60 | 1 | 1.69 | 1.54 | 1.48 | 1.42 | 1.43 |
| | 2.5 | 1.06 | 1.14 | 1.09 | 1.04 | 1.24 |
| | 5 | 1.06 | 1.07 | 1.07 | 1.01 | 1.16 |
| | 10 | 1.06 | 1.07 | 1.05 | 0.99 | 1.08 |
| | 15 | 1.06 | 1.07 | 1.03 | 0.98 | 1.10 |

- no result due to model instability

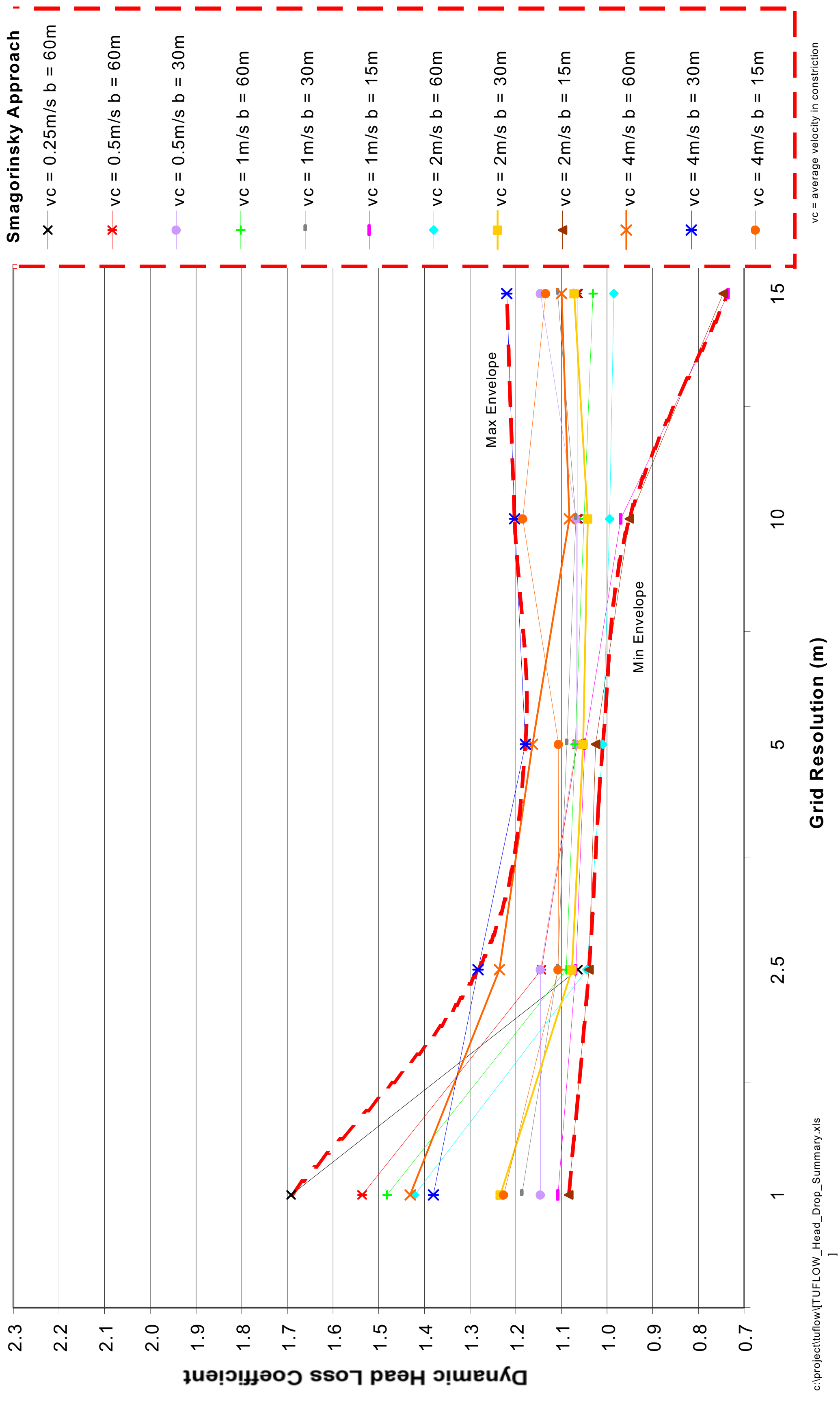


**Figure 3-7 TUFLOW – Dynamic Head Loss Coefficients**

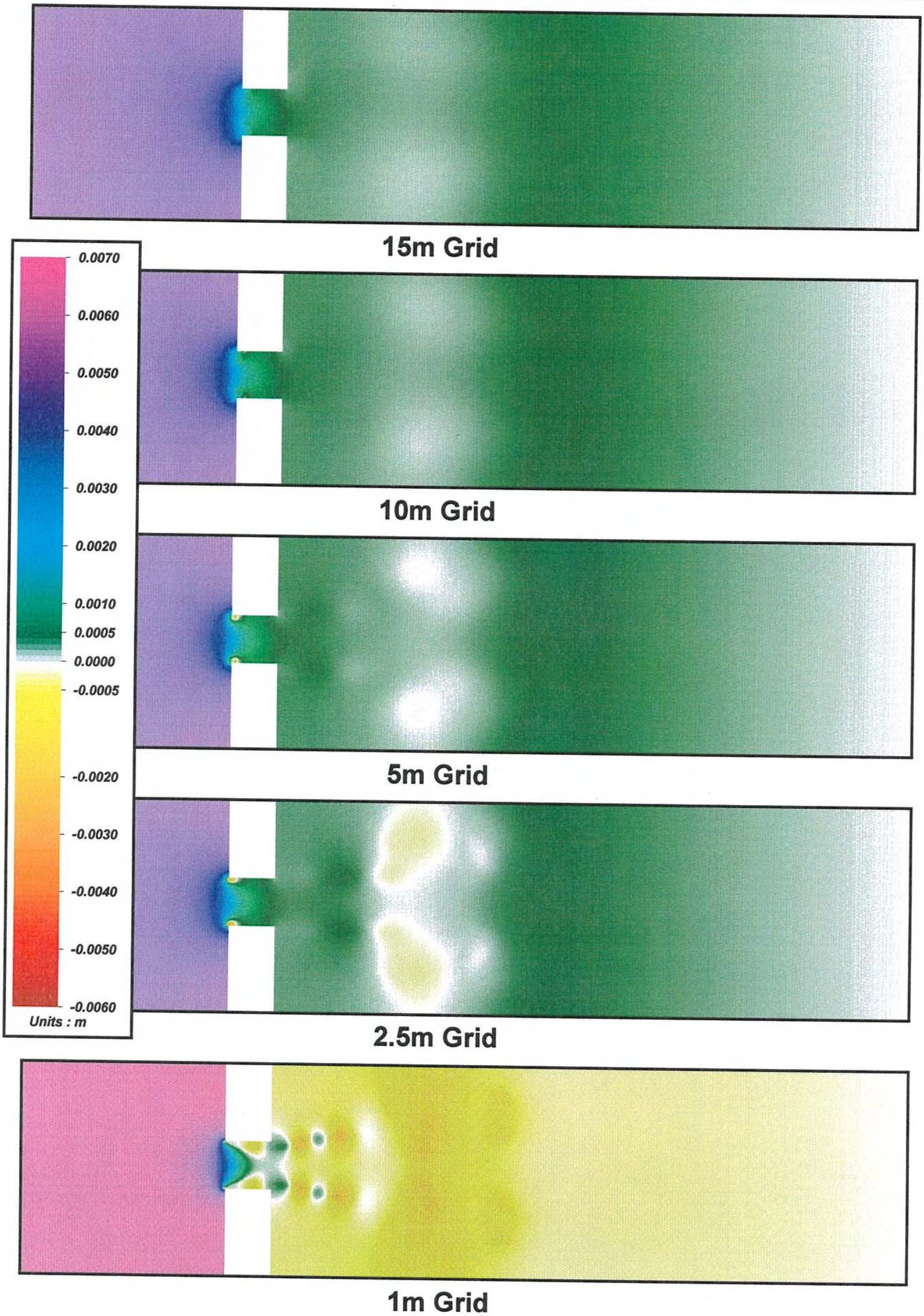


TUFLOW - Water Levels :
Vc = 0.25m/s (Q=30m$^3$/s & b=60m)

Figure 3-8

WATERLEVELS 025_b60.wor

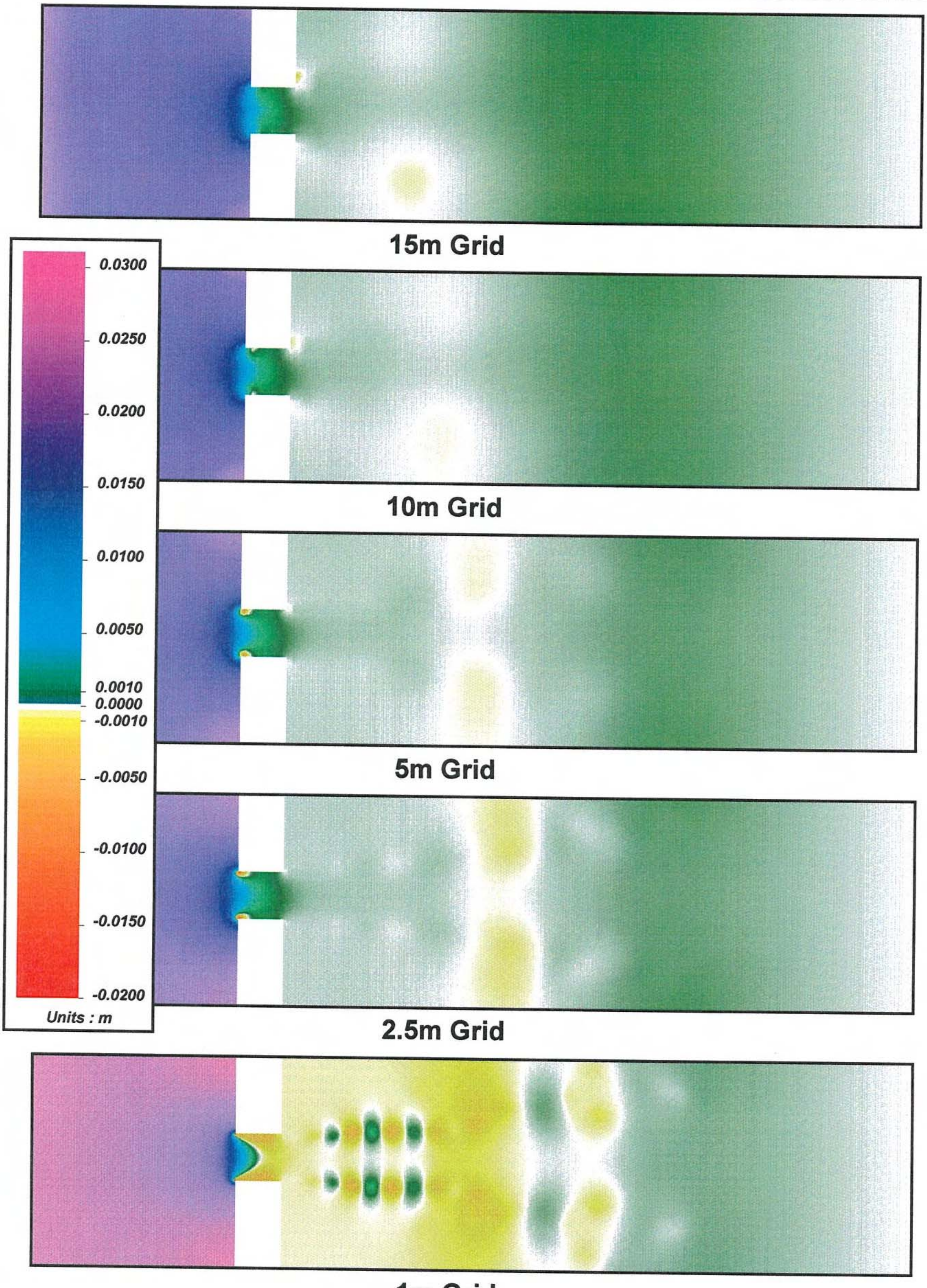


**TUFLOW - Water Levels :**
**Vc = 0.5m/s (Q=60m$^3$/s & b=60m)**

**Figure 3-9**

WATERLEVELS 05_b60.wor

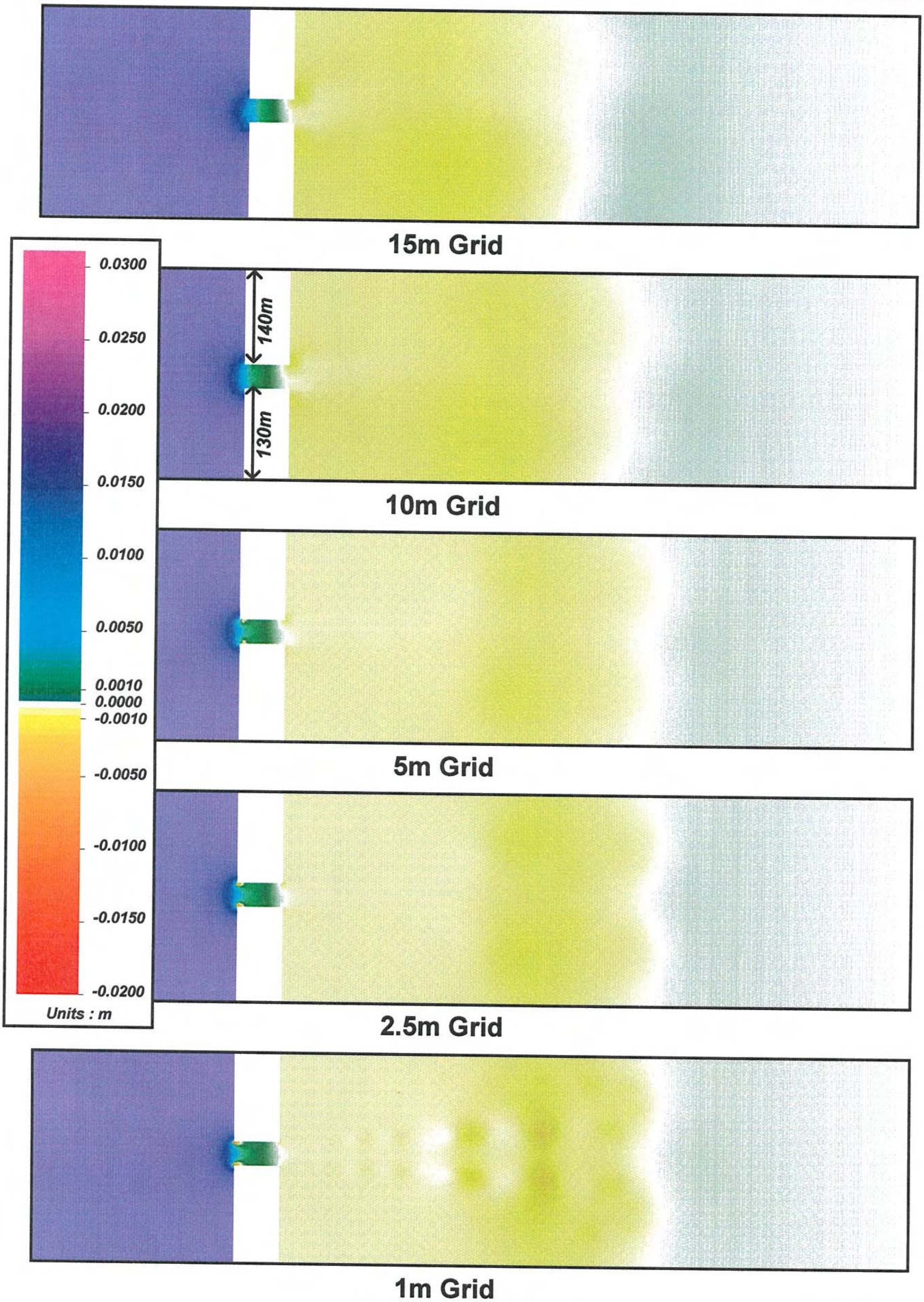


**TUFLOW - Water Levels :**
**Vc = 0.5m/s (Q=30m$^3$/s & b=30m)**

**Figure 3-10**

WATERLEVELS 05_b30.wor

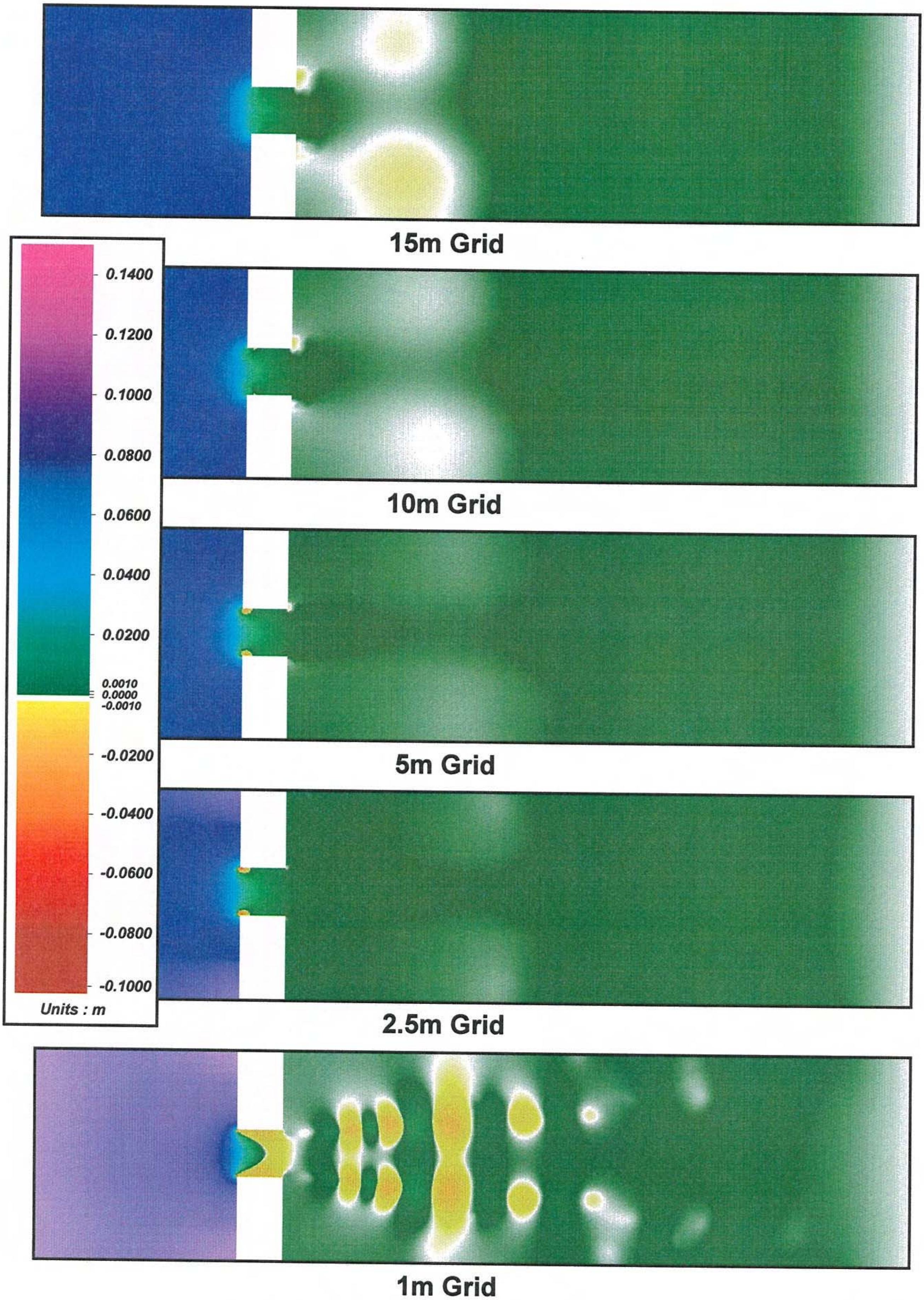


TUFLOW - Water Levels :
Vc = 1m/s (Q=120m³/s & b=60m)

Figure 3-11

WATERLEVELS 1_b60.wor

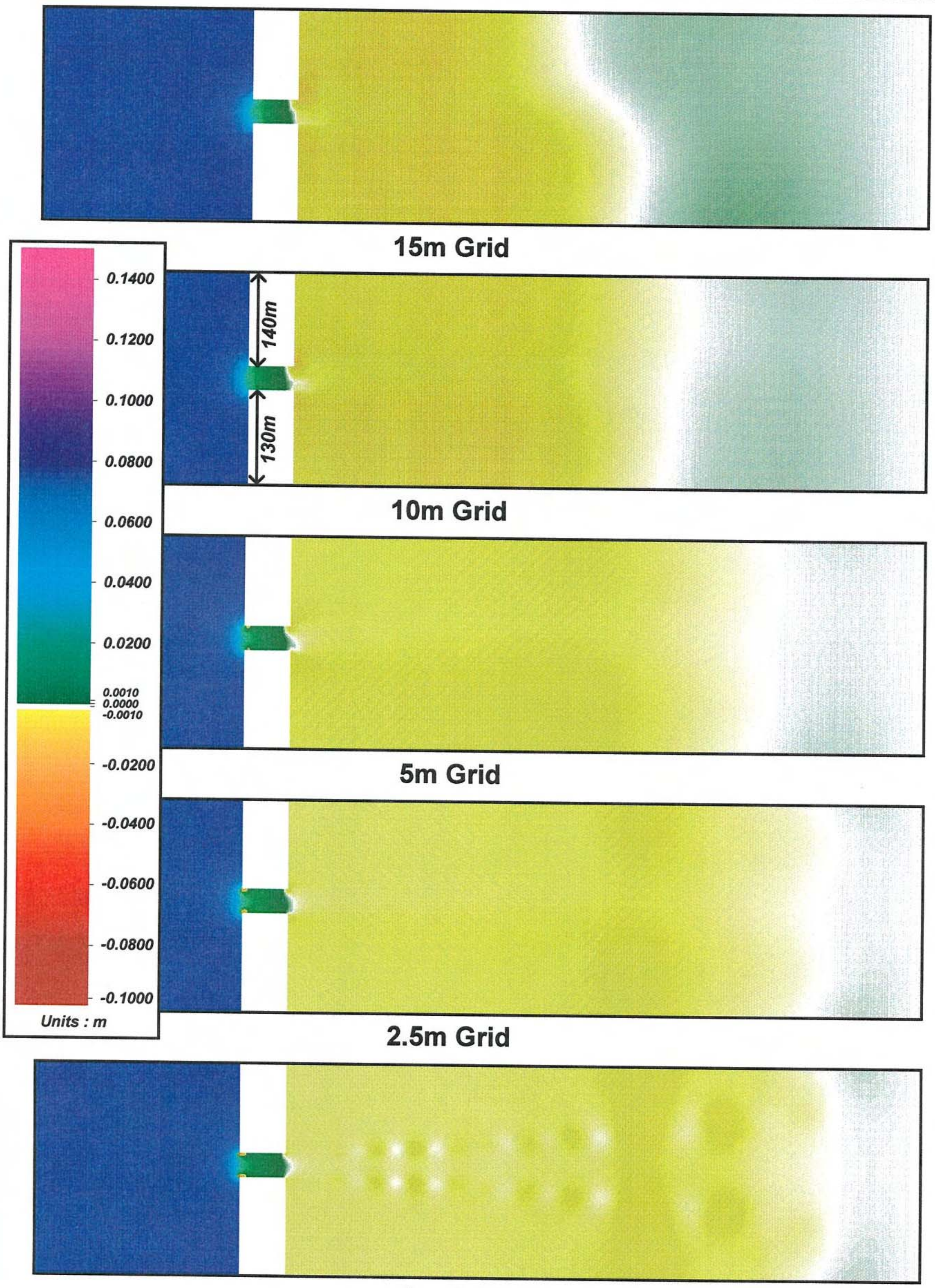


**TUFLOW - Water Levels :**
**Vc = 1m/s (Q=60m$^3$/s & b=30m)**

**Figure 3-12**

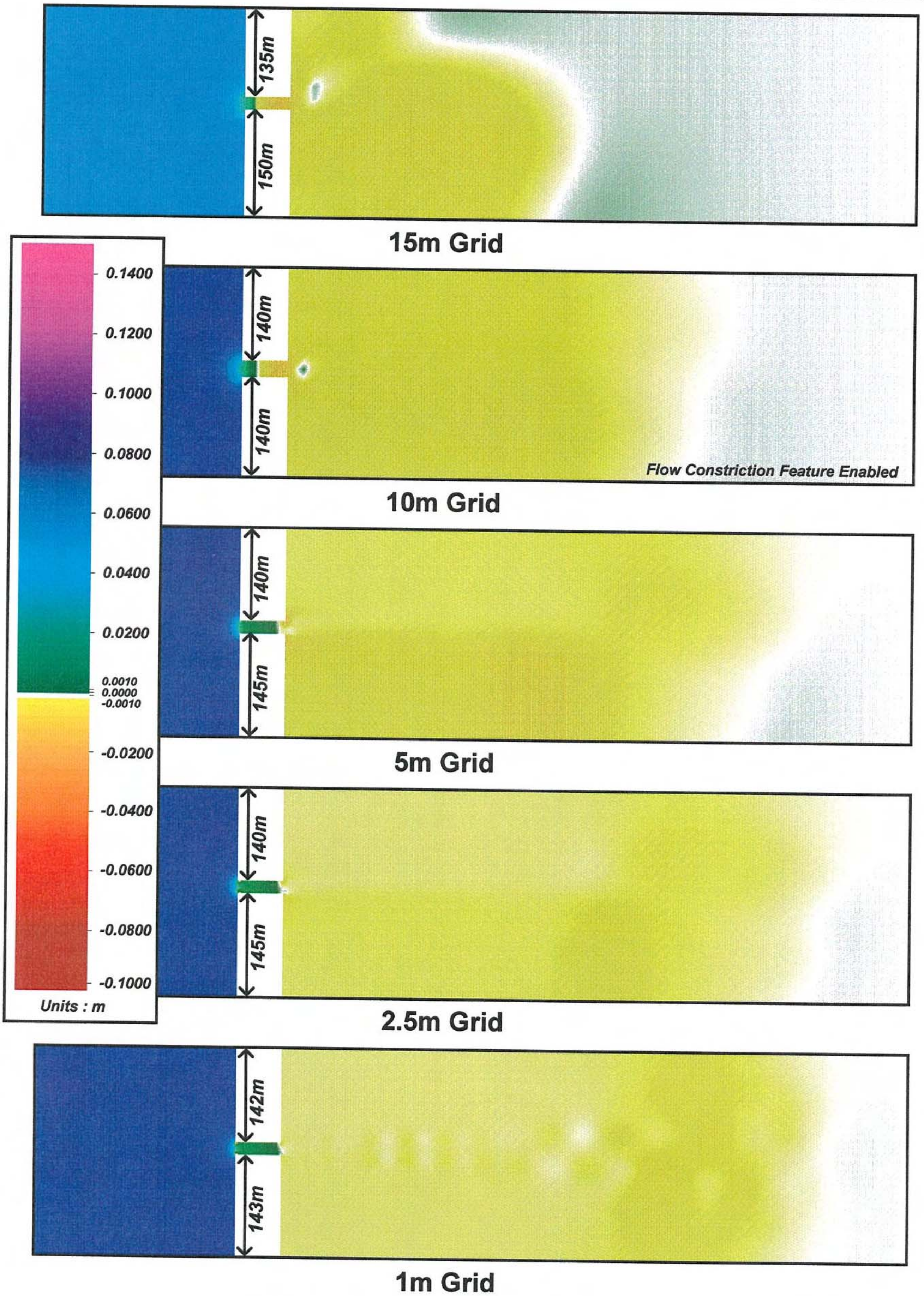


**TUFLOW - Water Levels :**
**Vc = 1m/s (Q=30m$^3$/s & b=15m)**

**Figure 3-13**

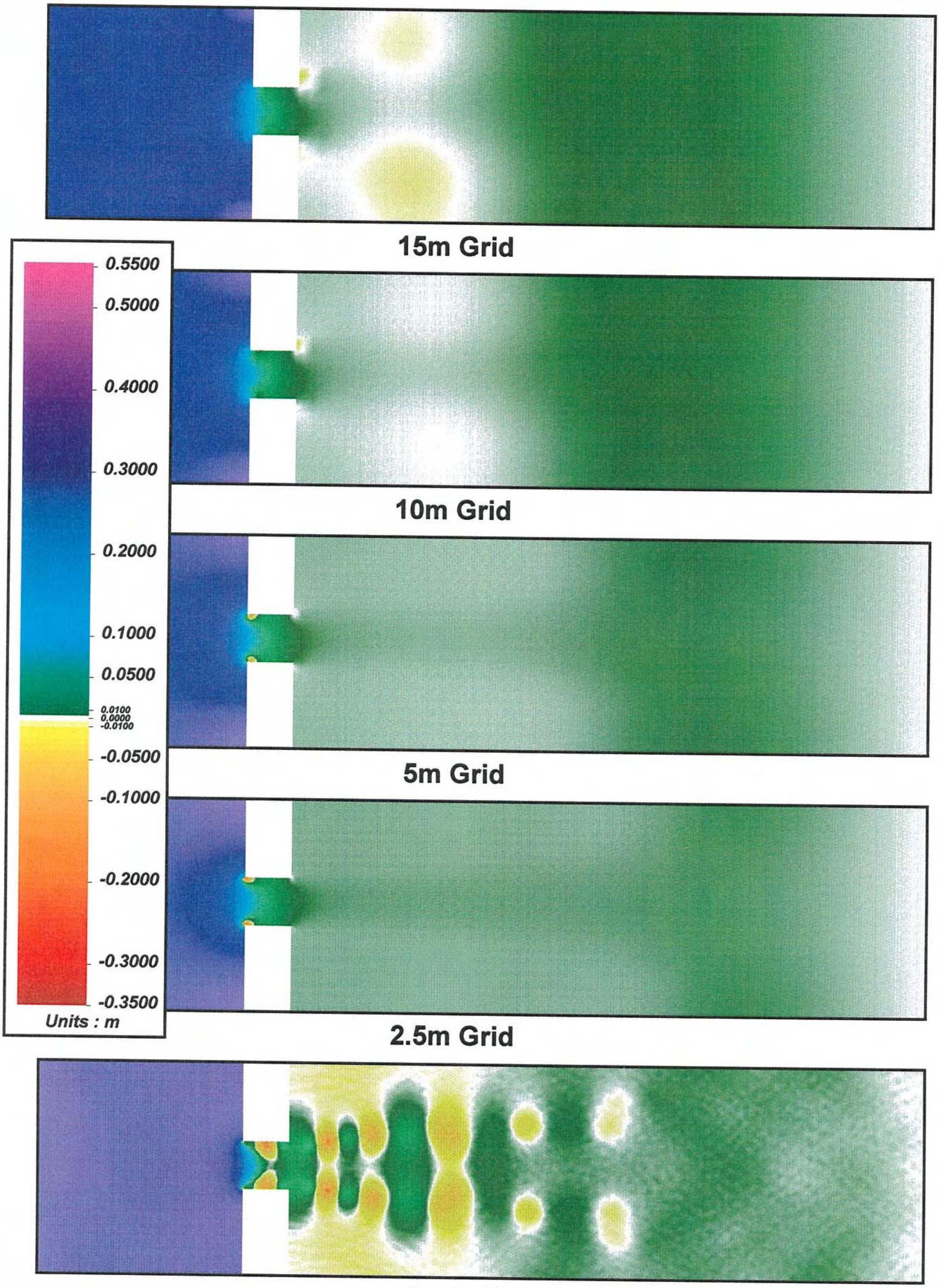


**TUFLOW - Water Levels :**
**Vc = 2m/s (Q=240m³/s & b=60m)**

**Figure 3-14**

WATERLEVELS 2_b60.wor

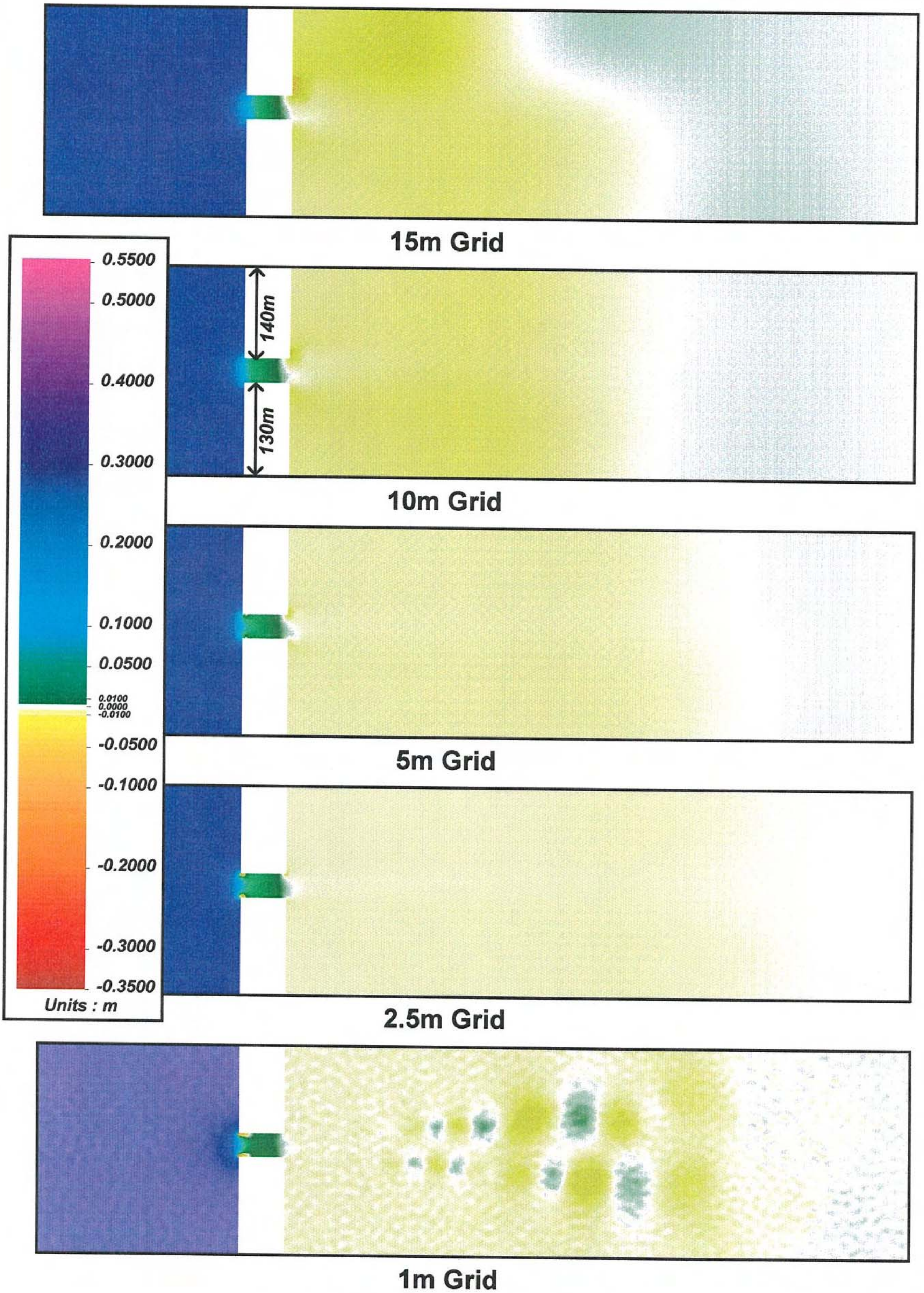


**TUFLOW - Water Levels :**
**Vc = 2m/s (Q=120m$^3$/s & b=30m)**

**Figure 3-15**

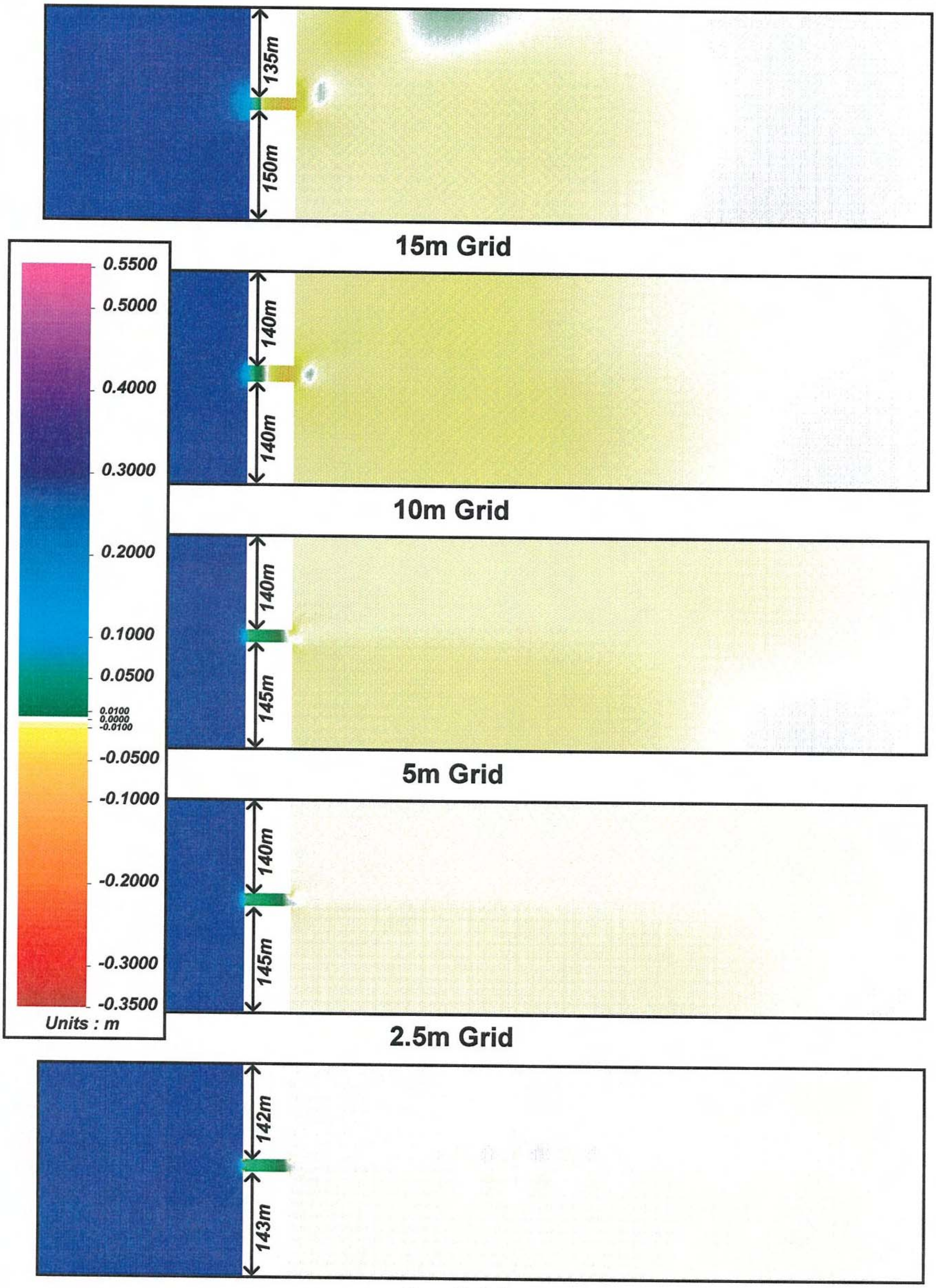


**TUFLOW - Water Levels :**
**Vc = 2m/s (Q=60m$^3$/s & b=15m)**

**Figure 3-16**

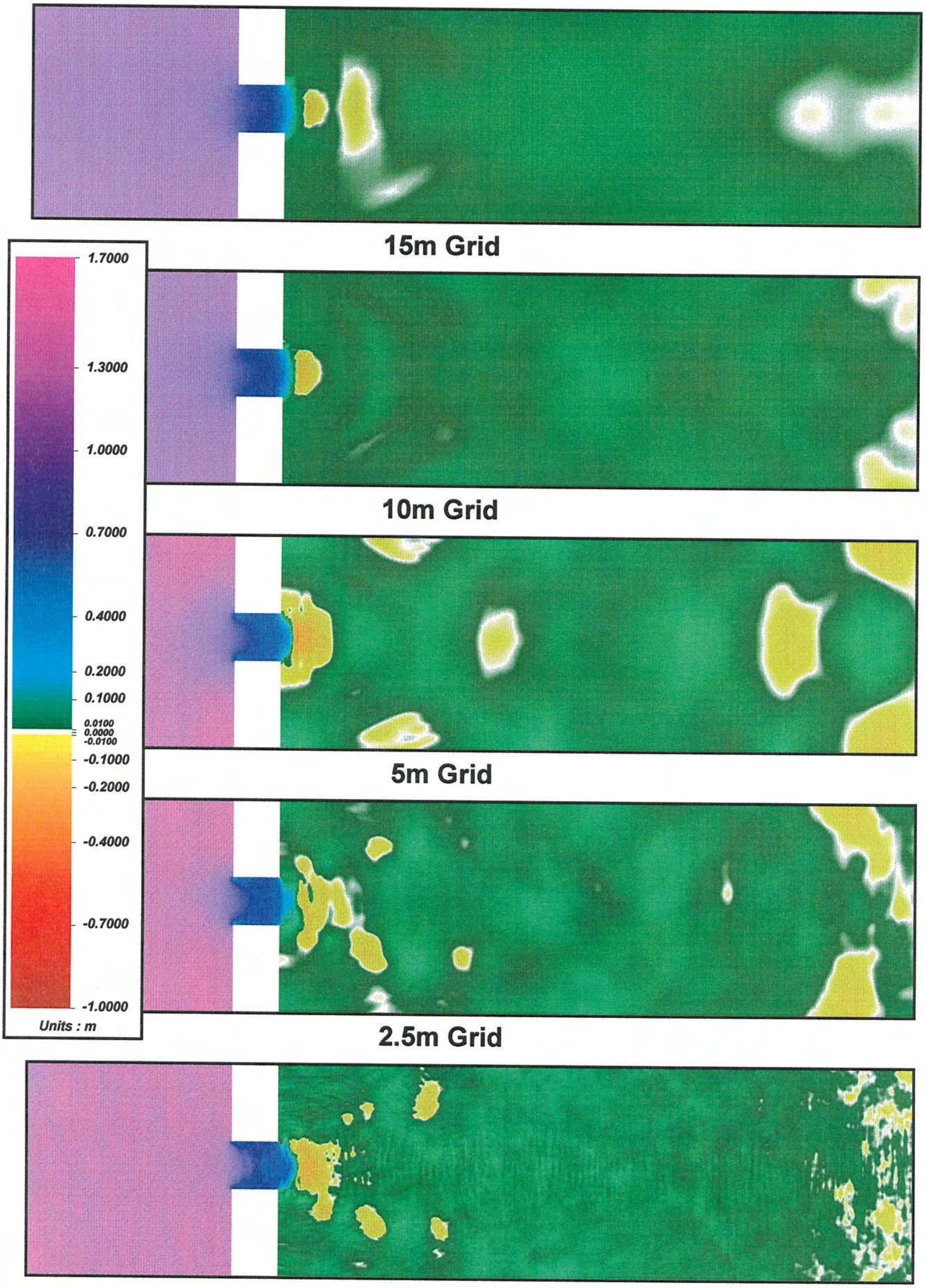


**TUFLOW - Water Levels :**
**Vc = 4m/s (Q=480m$^3$/s & b=60m)**

**Figure 3-17**

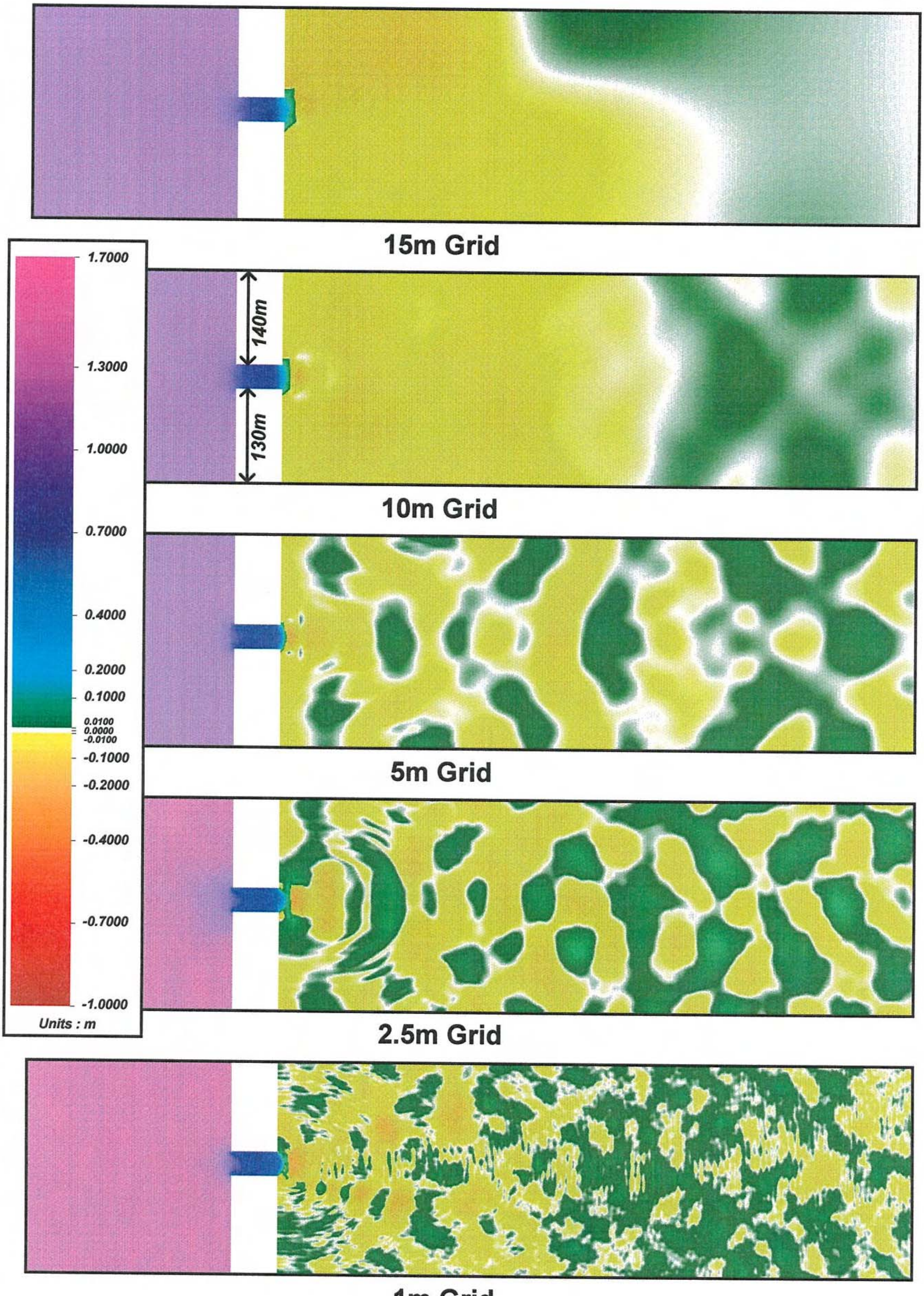


**TUFLOW - Water Levels :**
**Vc = 4m/s (Q=240m³/s & b=30m)**

**Figure 3-18**

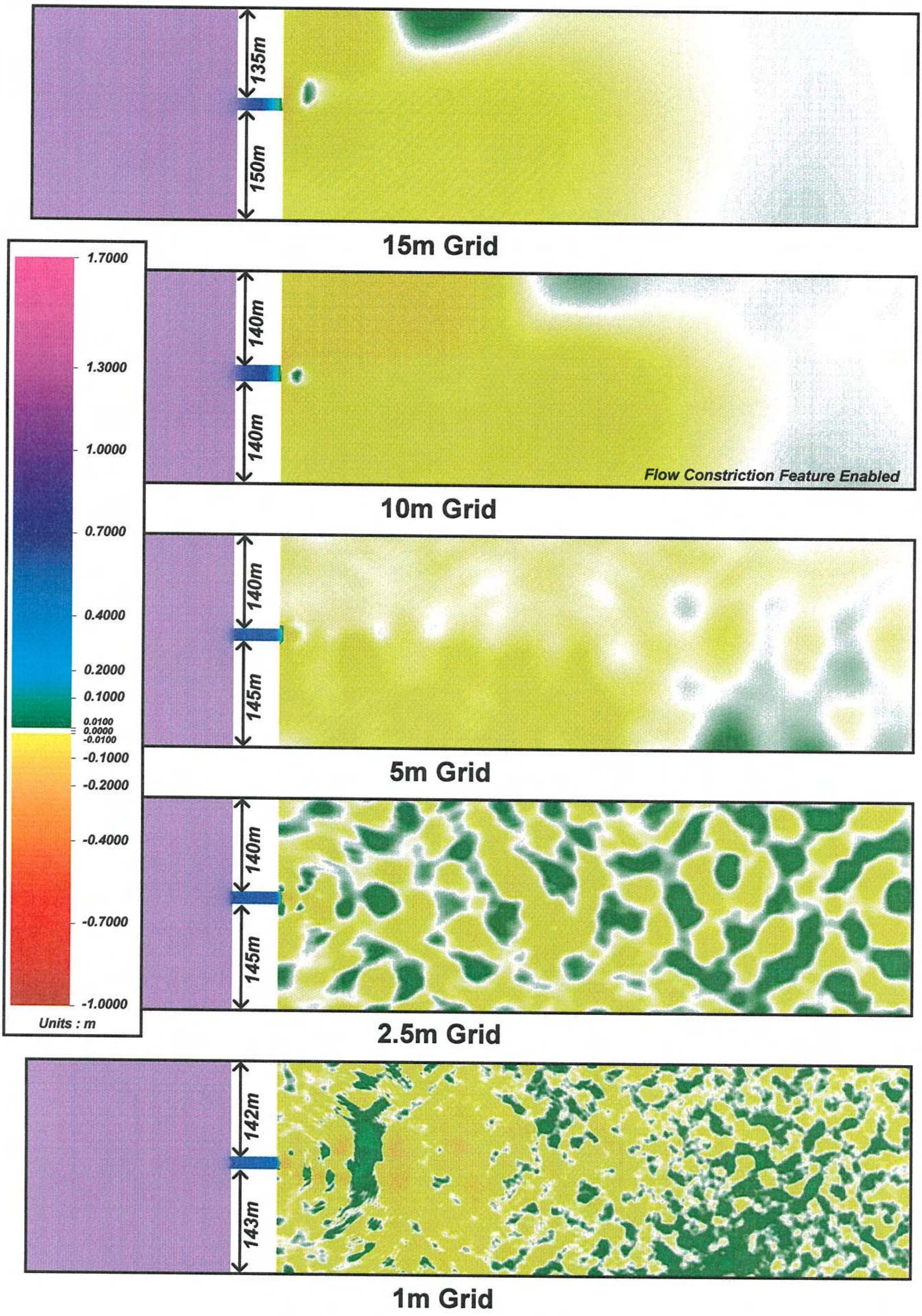


**TUFLOW - Water Levels :**
**Vc = 4m/s (Q=120m$^3$/s & b=15m)**

**Figure 3-19**

## 3.4 Discussion

### 3.4.1 Effects of Spatial Resolution

#### 3.4.1.1 Flow Characteristics

The presence of the vena contracta within the constriction becomes evident as the spatial resolution increases. As the vena contracta is more accurately modelled with increasing spatial resolutions, velocities within the vena contracta increase with increasing model resolution. This trend is evident in Figure 3-1. In addition, the vena contracta is evident in Figure 3-2 through Figure 3-6 as the lower velocity (blue) region within the constriction. This is only apparent for the 1m grid resolution.

Increasing spatial resolution increases the definition of the velocity distribution across the model domain as expected. Differences in flow patterns are particularly evident downstream of the constriction where the eddy patterns are more pronounced with each increase in the spatial resolution. Shedding of eddy vortices from the central flow path were seen when viewing the TUFLOW results as an animation.

Instabilities in the flow patterns at the higher spatial resolutions become evident when the average velocity through the constriction, $v_c$, is 4m/s (Figure 3-6). This may be caused by a supercritical regime developing at this velocity. As discussed in Section 1.4.3, hydrodynamic models are not able to replicate supercritical flow conditions reliably and instabilities typically occur. These instabilities are also believed to be the cause of the water level “ripples” apparent in Figure 3-17 to Figure 3-19.

#### 3.4.1.2 Losses

Figure 3-7 shows that increases in the model resolution result in increases in the predicted dynamic head loss coefficients. As the model resolution increases, it may be argued that the ability of the model to simulate turbulent losses increases. Thus, at higher spatial resolutions a greater loss will be predicted. Use of the Smagorinsky formulation may overcome this to some extent as this method attempts to account for turbulent losses at sub-grid scale. This is discussed further in Appendix B.

As the model resolution increases, the range of the dynamic head loss coefficient envelope contracts around the grid size of 5m before expanding again for the finer grid sizes. At the 1m grid size, the maximum envelope is pushed outward by results for low average constriction velocities. At these very low velocities, the constriction losses are relatively small and the dynamic head loss coefficient becomes sensitive to the dynamic head ($v_c^2/2g$). This is one of the disadvantages of using the average constriction velocity in the dynamic head calculation as discussed in Section 2.6. If the point representing $v_c$=0.25m/s at the 1m grid size was removed from Figure 3-7, the range of the dynamic head loss coefficient at this grid size is substantially reduced.

# 4 RMA2 COMPUTATIONS

## 4.1 Introduction

RMA2 is a two-dimensional finite element hydrodynamic model (King, 1998) and is used for the solution of the two-dimensional depth averaged shallow water flow equations. RMA2 uses a non-uniform mesh of quadrilateral and triangular elements to represent the area being modelled. Variation of the mesh density throughout the model area is possible such that areas of particular interest or complexity can be better represented.

## 4.2 Computational Procedure

RMA2 solves the depth averaged Navier-Stokes equations. Turbulent energy losses are accounted for with allowance for an eddy viscosity effect. Differences in pressure gradient due to pre-determined density gradients are added. Friction losses, Coriolis effects and surface wind stresses are also built into the governing equations. Coefficients associated with these terms may vary from element to element.

**Continuity Equation**

$$D\left(\frac{\partial_u}{\partial_x}+\frac{\partial_v}{\partial_y}\right)+u\frac{\partial_D}{\partial_x}+v\frac{\partial_D}{\partial_y}+\frac{\partial_D}{\partial_t}=0$$

**Momentum Equation X-Direction**

$$\rho\left(D\frac{\partial_u}{\partial_t}+Du\frac{\partial_v}{\partial_x}+Dv\frac{\partial_u}{\partial_y}+gD\frac{\partial_h}{\partial_x}+gn^2u\left|V\right|+uq_s-\Omega_{vh}\right)-D\frac{\partial}{\partial_x}\left(\varepsilon_{xx}\frac{\partial_u}{\partial_x}\right)-D\frac{\partial}{\partial_y}\left(\varepsilon_{xy}\frac{\partial_u}{\partial_y}\right)=F_x$$

**Momentum Equation Y-Direction**

$$\rho\left(D\frac{\partial_v}{\partial_t}+Du\frac{\partial_v}{\partial_x}+Dv\frac{\partial_u}{\partial_y}+gD\frac{\partial_h}{\partial_x}+gn^2v\left|V\right|+vq_s-\Omega_{uh}\right)-D\frac{\partial}{\partial_x}\left(\varepsilon_{yx}\frac{\partial_u}{\partial_x}\right)-D\frac{\partial}{\partial_y}\left(\varepsilon_{yy}\frac{\partial_v}{\partial_y}\right)=F_y$$

| | | |
|---|---|---|
| Where: | x,y | = horizontal cartesian coordinates |
| | t | = time |
| | u,v | = horizontal velocity components in the x and y directions |
| | D | = depth |
| | a | = bottom elevation |
| | $\varepsilon_{yy}, \varepsilon_{xy}, \varepsilon_{yx}, \varepsilon_{xx}$ | = turbulent eddy coefficents |
| | V | = total water velocity |
| | g | = gravitational acceleration |
| | $q_s$ | = tributary inflow into system |

| | |
|---|---|
| $n$ | = Mannings 'n' |
| $\Omega_{vh}, \Omega_{uh}$ | = coriolis forcing in the x and y directions |
| $F_x, F_y$ | = sum of components of external forces in the x and y directions (including wave and wind forces) |

## 4.3 Results

A summary of the simulations undertaken is provided in Table 4–1 with an indication of success of the simulation. For the purposes of this project, comparisons are only undertaken when the average velocity in the constriction is 4m/s or less due to stability problems associated with supercritical flow regimes (refer to Section 2.1).

**Table 4–1 Summary of RMA2 Simulations Undertaken**

| Width of Constriction (m) | Mesh Density | Flow | | | | |
|---|---|---|---|---|---|---|
| | | $30m^3/s$ | $60m^3/s$ | $120m^3/s$ | $240m^3/s$ | $480m^3/s$ |
| 15 | Mesh 5 (Finest) | ✓ | ✓ | ✓ | × | × |
| | Mesh 4 (Fine) | ✓ | ✓ | ✓ | ✓ | × |
| | Mesh 3 (Medium) | ✓ | ✓ | ✓ | ✓ | ✓ |
| | Mesh 2 (Coarse) | ✓ | ✓ | ✓ | ✓ | ✓ |
| | Mesh 1 (Coarsest) | ✓ | ✓ | ✓ | ✓ | ✓ |
| 30 | Mesh 5 (Finest) | ✓ | ✓ | ✓ | ✓ | × |
| | Mesh 4 (Fine) | ✓ | ✓ | ✓ | ✓ | ✓ |
| | Mesh 3 (Medium) | ✓ | ✓ | ✓ | ✓ | ✓ |
| | Mesh 2 (Coarse) | ✓ | ✓ | ✓ | ✓ | ✓ |
| | Mesh 1 (Coarsest) | ✓ | ✓ | ✓ | ✓ | ✓ |
| 60 | Mesh 5 (Finest) | ✓ | ✓ | ✓ | ✓ | × |
| | Mesh 4 (Fine) | ✓ | ✓ | ✓ | ✓ | ✓ |
| | Mesh 3 (Medium) | ✓ | ✓ | ✓ | ✓ | ✓ |
| | Mesh 2 (Coarse) | ✓ | ✓ | ✓ | ✓ | ✓ |
| | Mesh 1 (Coarsest) | ✓ | ✓ | ✓ | ✓ | ✓ |

× Simulation did not run to completion due to instabilities

✓ Simulation ran to completion

Average Velocity in Constriction

| 0.25m/s | 0.5m/s | 1m/s | 2m/s | 4m/s | 8m/s | 16m/s |
|---|---|---|---|---|---|---|

### 4.3.1 Flow Characteristics

Velocities within the vena contracta for the 60m width of constriction subset are shown in Figure 4-1 and are grouped according to $_{average}$ velocity through the constriction, $v_c$. The velocity within the vena contracta has been extracted from the same location for all simulations. This location is within the full contraction region of the vena contracta at the centre of the constriction.

Flow patterns for the all mesh densities are shown for the 60m width of constriction subset of the RMA2 simulations in Figure 4-2 through Figure 4-6. These are grouped according to average velocity through the constriction, $v_c$. The figures show the relative size and direction of the velocity vectors overlain on the colours representing the velocity magnitude as indicated in the legend.

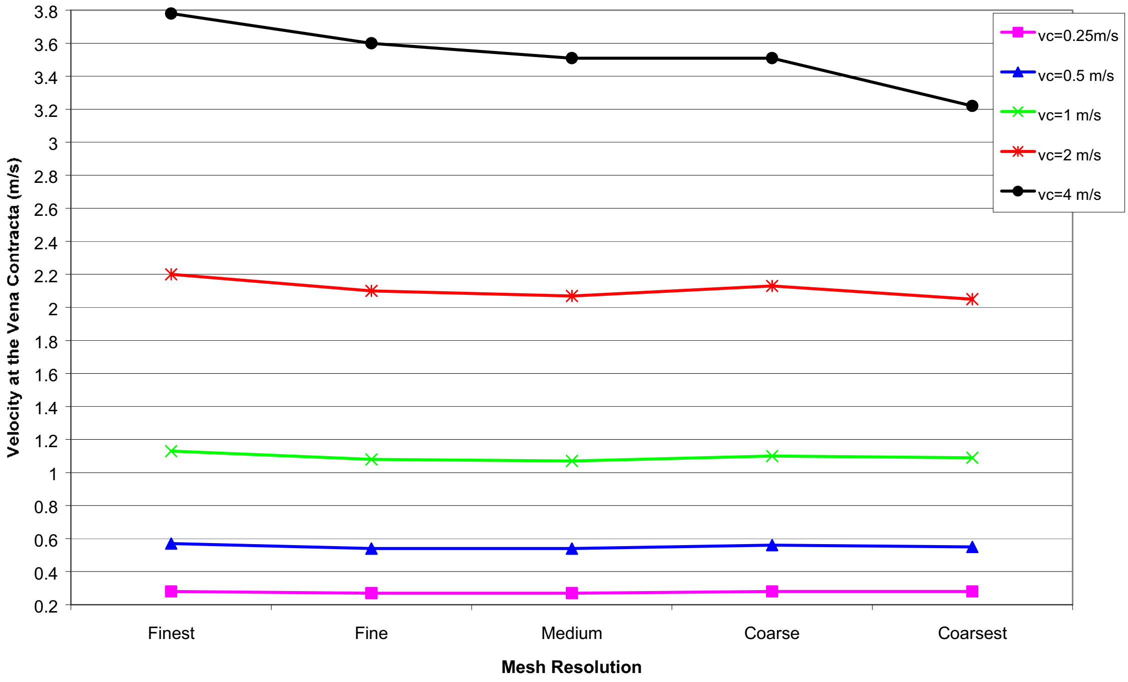


**Figure 4-1 RMA2 – Velocities Within the Vena Contracta: b=60m**

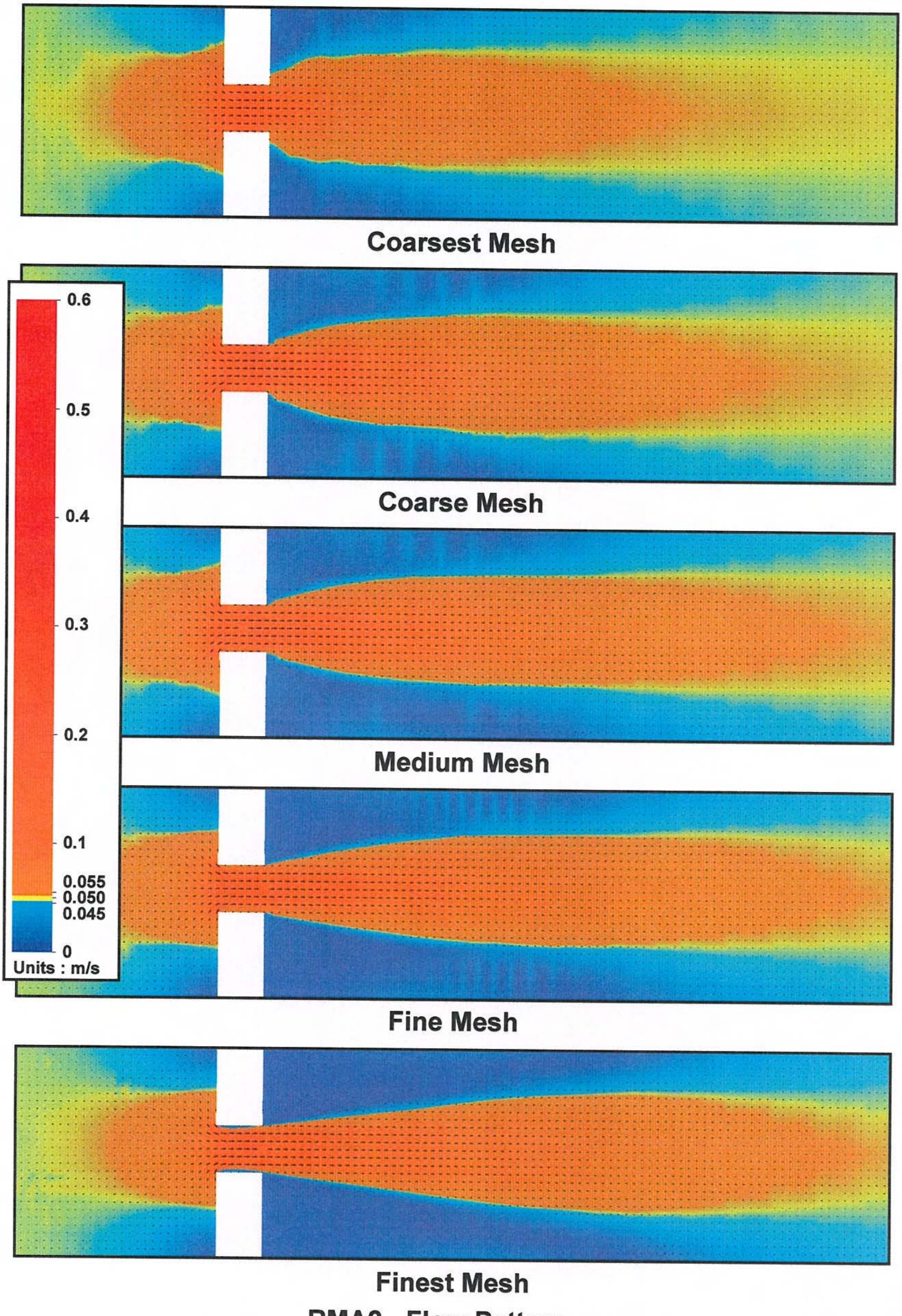


RMA2 - Flow Pattern
Vc = 0.25m/s (Q=30m³/s & b=60m)

Figure 4-2

RMA2-Flow V025_b60.wor

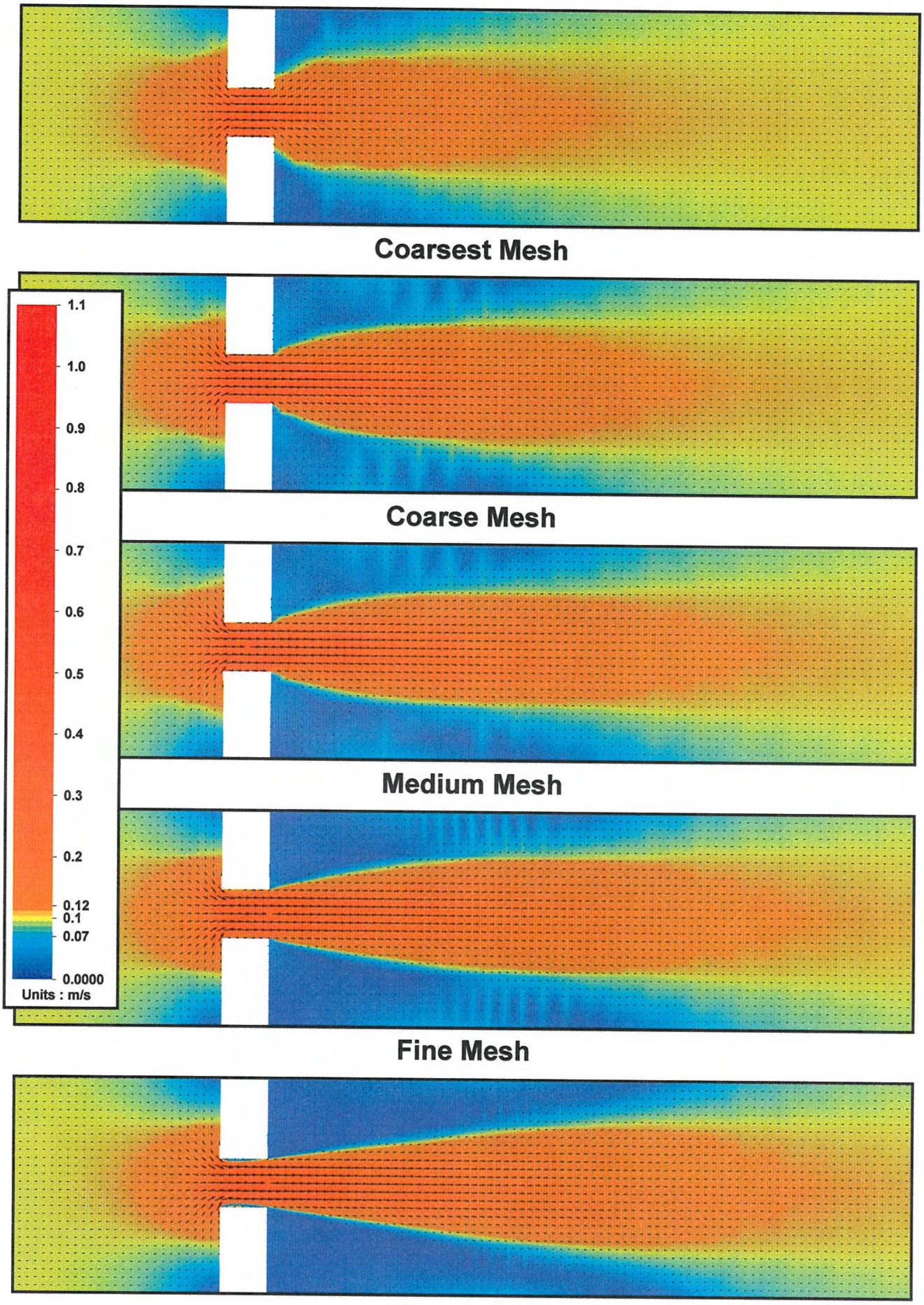


RMA2 - Flow Pattern
Vc = 0.5m/s (Q=60m³/s & b=60m)

Figure 4-3

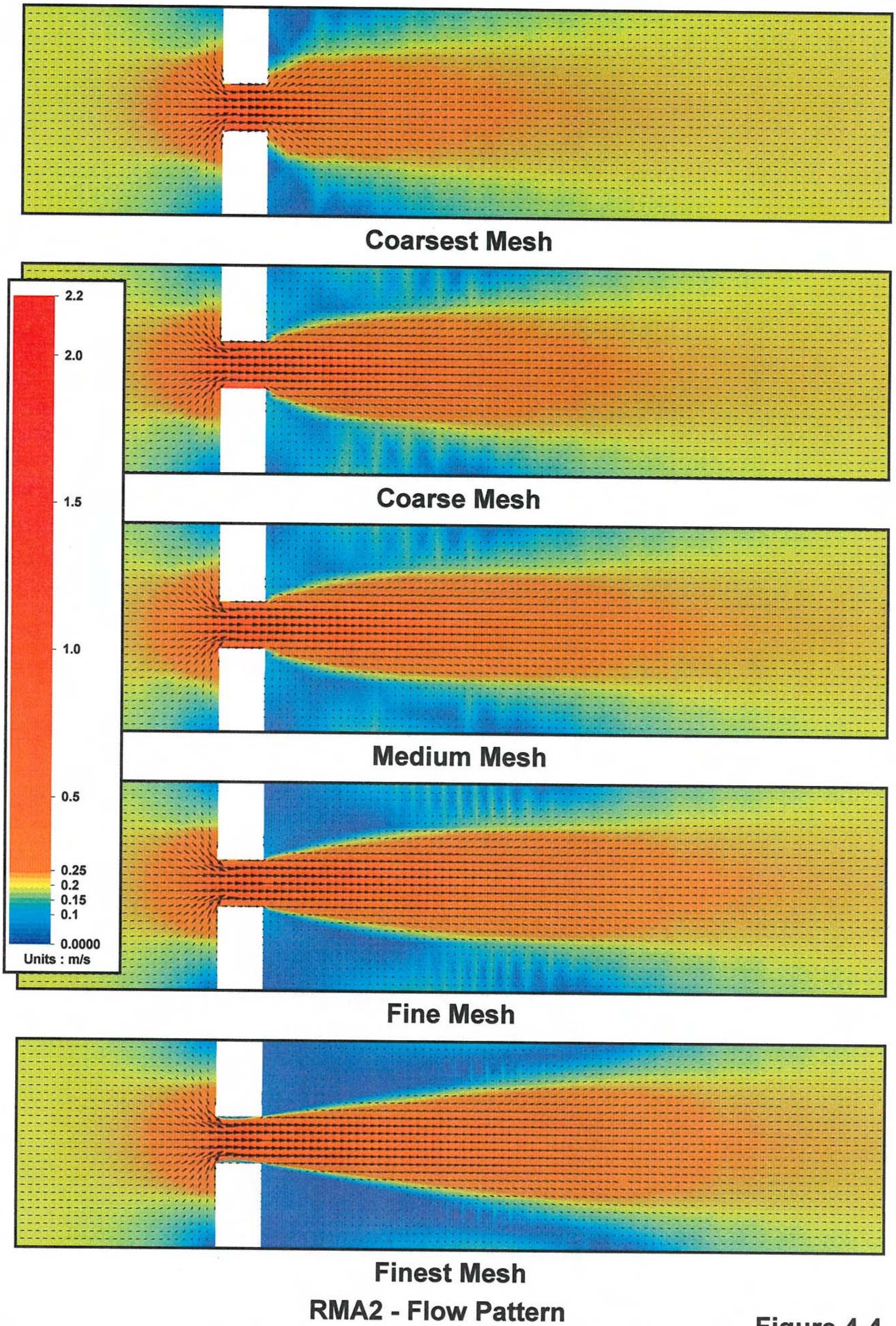


RMA2 - Flow Pattern
Vc = 1m/s (Q=120m$^3$/s & b=60m)

Figure 4-4

RMA2-Flow V1_b60.wor

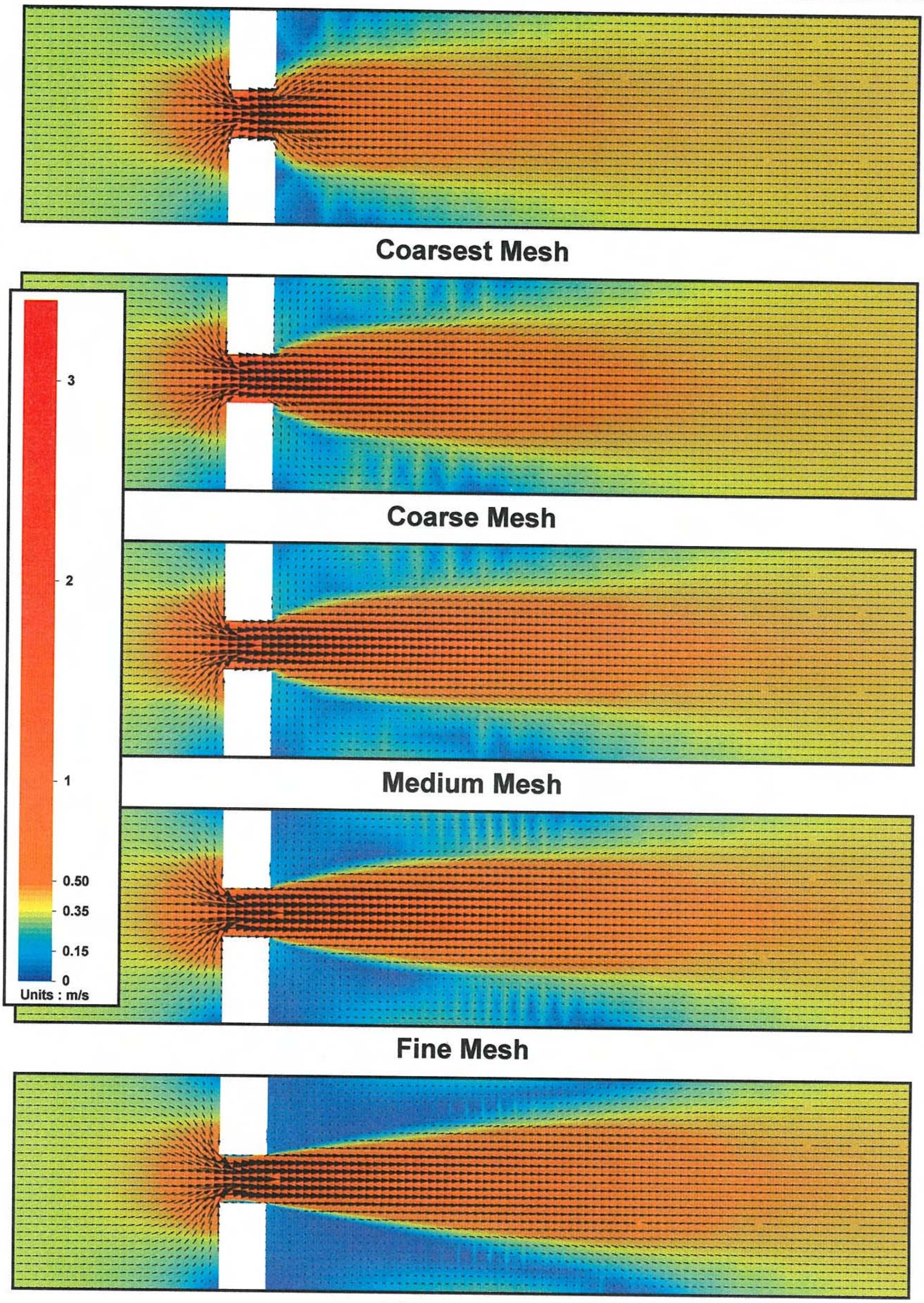


RMA2 - Flow Pattern
Vc = 2m/s (Q=240m³/s & b=60m)

Figure 4-5

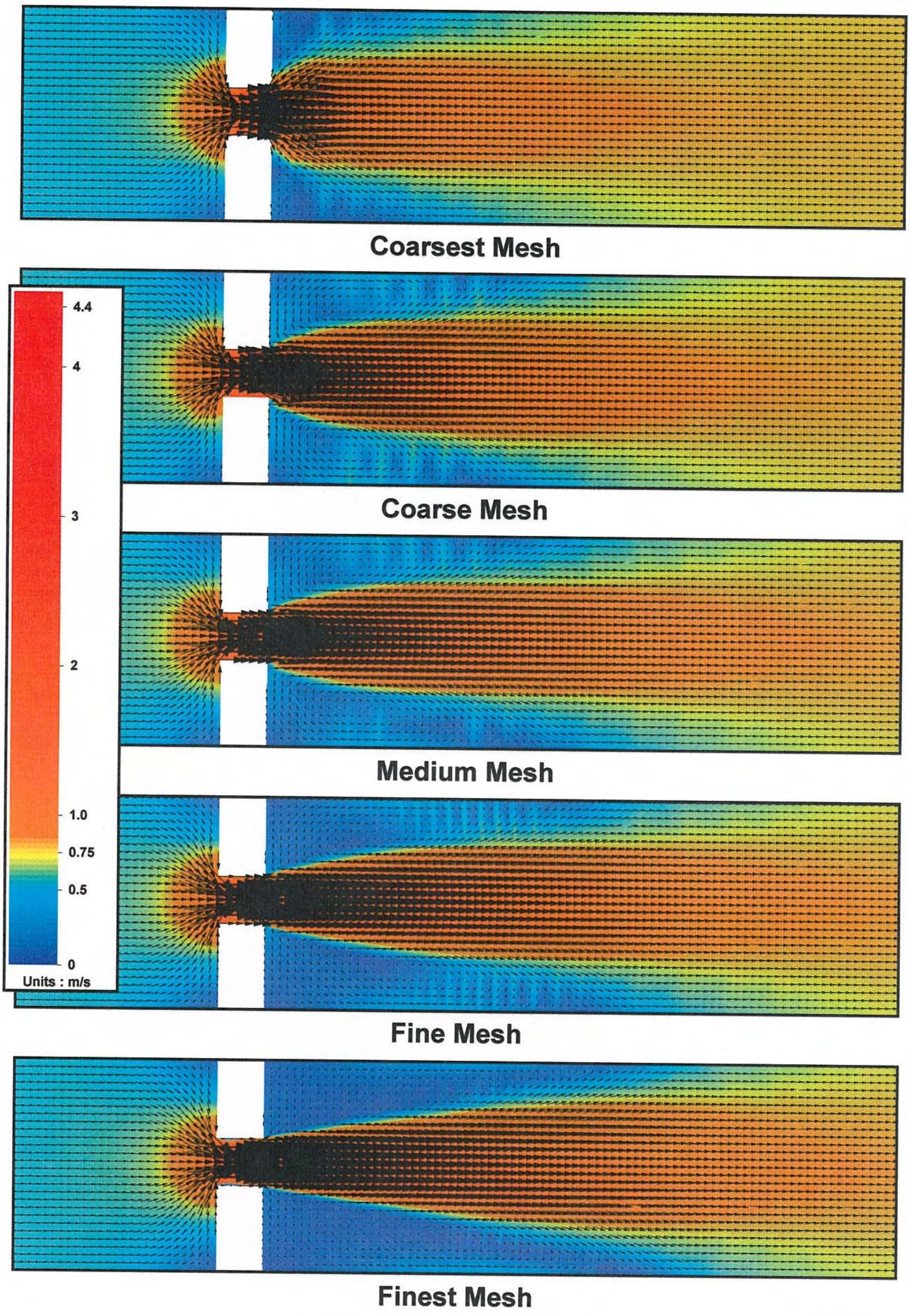


RMA2 - Flow Pattern
$V_c$ = 4m/s (Q=480m$^3$/s & b=60m)

Figure 4-6

### 4.3.2 Losses

The total head loss across the test channel is shown in Table 4–2 for each scenario. Water levels predicted across the model domain are shown graphically in Figure 4-8 through Figure 4-19. These figures have been divided into groups representing average velocity through the constriction.

**Table 4–2 RMA2 - Total Head Loss (mm)**

| Width of Constriction (m) | Mesh Density | Flow | | | | |
|---|---|---|---|---|---|---|
| | | $30m^3/s$ | $60m^3/s$ | $120m^3/s$ | $240m^3/s$ | $480m^3/s$ |
| 15 | Mesh 5 (Finest) | 83 | 326 | 1175 | - | - |
| | Mesh 4 (Fine) | 77 | 307 | 1141 | 2918 | - |
| | Mesh 3 (Medium) | 87 | 352 | 1273 | 3146 | 6116 |
| | Mesh 2 (Coarse) | 65 | 297 | 1286 | 3235 | 6283 |
| | Mesh 1 (Coarsest) | 127 | 519 | 1672 | 3767 | 7122 |
| 30 | Mesh 5 (Finest) | 23 | 92 | 349 | 1195 | - |
| | Mesh 4 (Fine) | 23 | 91 | 350 | 1206 | 2986 |
| | Mesh 3 (Medium) | 24 | 95 | 367 | 1257 | 3066 |
| | Mesh 2 (Coarse) | 23 | 93 | 370 | 1312 | 3172 |
| | Mesh 1 (Coarsest) | 32 | 126 | 486 | 1532 | 3488 |
| 60 | Mesh 5 (Finest) | 6 | 24 | 95 | 360 | - |
| | Mesh 4 (Fine) | 6 | 23 | 93 | 352 | 1189 |
| | Mesh 3 (Medium) | 6 | 24 | 94 | 359 | 1206 |
| | Mesh 2 (Coarse) | 6 | 24 | 93 | 358 | 1216 |
| | Mesh 1 (Coarsest) | 7 | 27 | 108 | 413 | 1347 |

- no result due to model instability

The total head loss results presented in Table 4–2 are used to calculate the dynamic head loss coefficient. The dynamic head loss coefficient is due solely to expansion and contraction losses, that is, frictional losses have been removed (refer to Appendix A). The dynamic head loss coefficient is a factor of the dynamic head, $v_c^2/2g$ (refer to terminology definitions at the beginning of this study report). Dynamic head loss coefficients are presented in Table 4–3 and shown graphically in Figure 4-7.

Results representing average constriction velocities of greater than 4m/s are not presented as a supercritical flow regime is expected at these velocities (refer to 1.4.3).

Dynamic head loss coefficients predicted in RMA2 are compared to dynamic head loss coefficients predicted by other models and methods in Section 9.

**Table 4–3 RMA2 - Dynamic head loss coefficient Results ($v_c^2/2g$)**

| Width of Constriction (m) | Mesh Density | Flow | | | | |
|---|---|---|---|---|---|---|
| | | 30m³/s | 60m³/s | 120m³/s | 240m³/s | 480m³/s |
| 15 | Mesh 5 (Finest) | 1.33 | 1.29 | 1.14 | - | - |
| | Mesh 4 (Fine) | 1.21 | 1.20 | 1.10 | - | - |
| | Mesh 3 (Medium) | 1.41 | 1.42 | 1.26 | - | - |
| | Mesh 2 (Coarse) | 0.98 | 1.15 | 1.27 | - | - |
| | Mesh 1 (Coarsest) | 2.19 | 2.24 | 1.75 | - | - |
| 30 | Mesh 5 (Finest) | 1.45 | 1.45 | 1.37 | 1.13 | - |
| | Mesh 4 (Fine) | 1.44 | 1.44 | 1.38 | 1.14 | - |
| | Mesh 3 (Medium) | 1.53 | 1.52 | 1.46 | 1.21 | - |
| | Mesh 2 (Coarse) | 1.47 | 1.47 | 1.47 | 1.27 | - |
| | Mesh 1 (Coarsest) | 2.14 | 2.13 | 2.04 | 1.54 | - |
| 60 | Mesh 5 (Finest) | 1.31 | 1.39 | 1.37 | 1.28 | - |
| | Mesh 4 (Fine) | 1.30 | 1.34 | 1.32 | 1.24 | 0.99 |
| | Mesh 3 (Medium) | 1.37 | 1.37 | 1.35 | 1.27 | 1.01 |
| | Mesh 2 (Coarse) | 1.34 | 1.35 | 1.33 | 1.27 | 1.03 |
| | Mesh 1 (Coarsest) | 1.64 | 1.64 | 1.62 | 1.54 | 1.19 |

- no result due to model instability or velocity exceeds maximum range for comparison

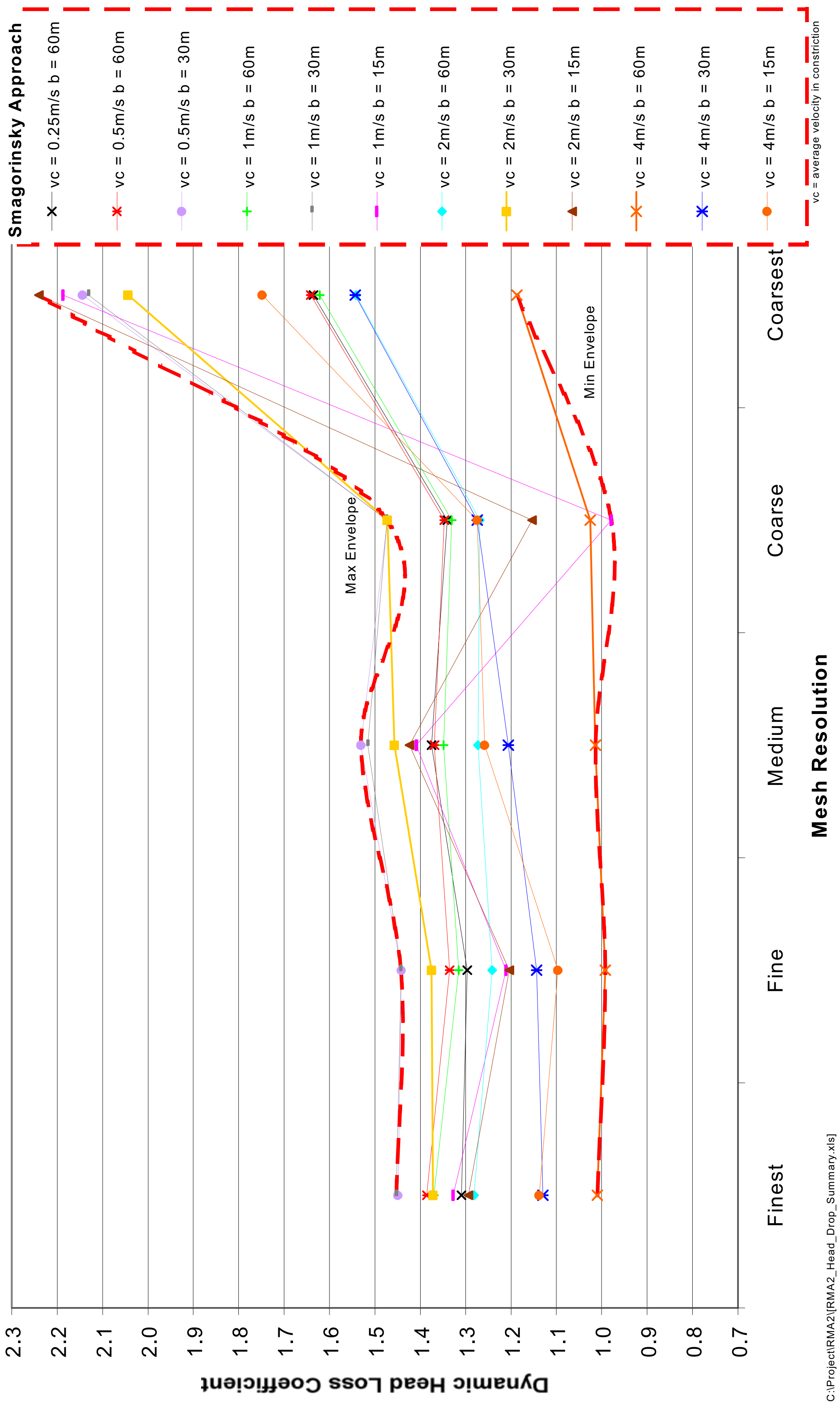


**Figure 4-7 RMA2 - Dynamic Head Loss Coefficients**

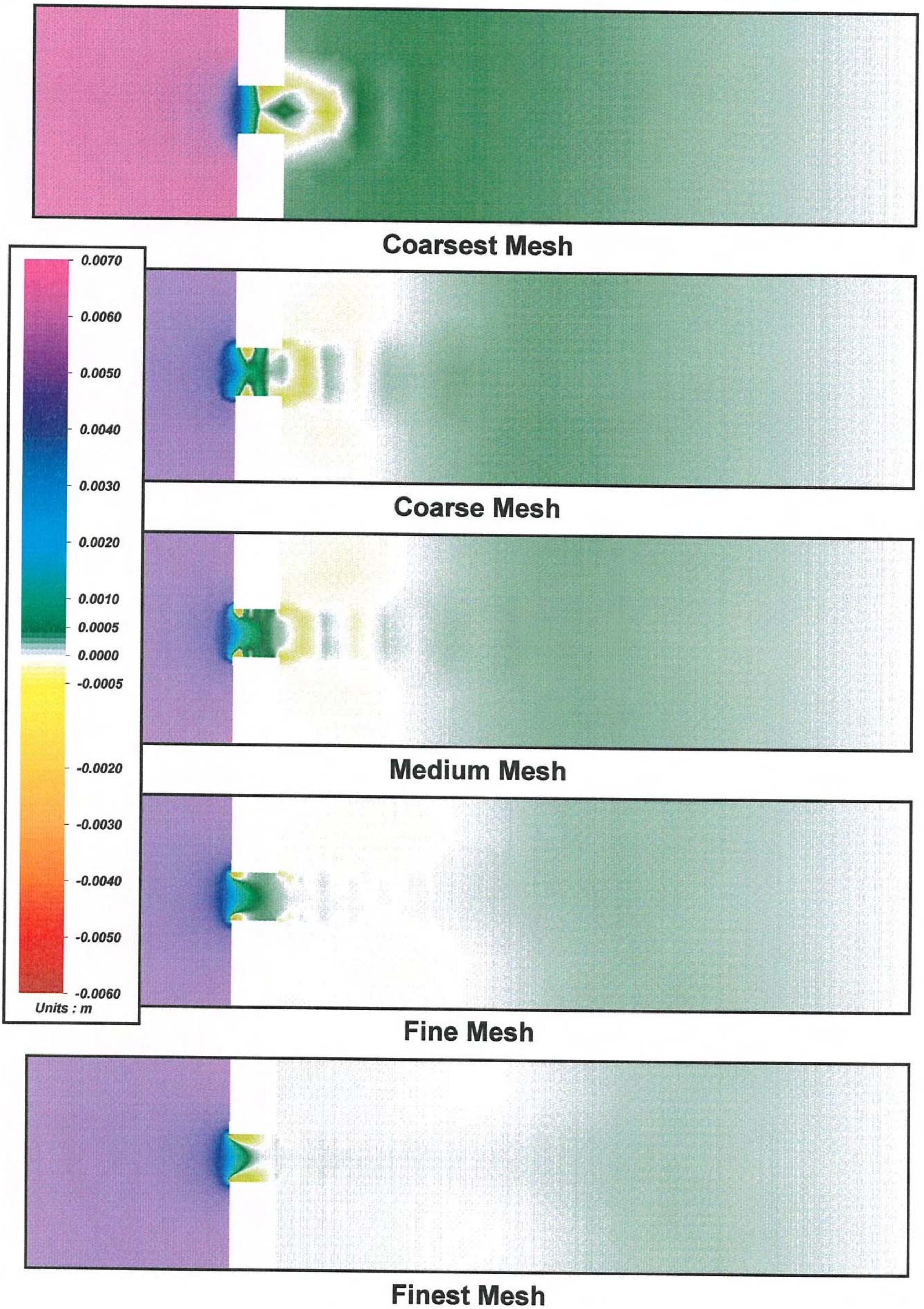


**RMA2 - Water Level**
**Vc = 0.25m/s (Q=30m$^3$/s & b = 60m)**

**Figure 4-8**

RMA2_V0.25_60.wor

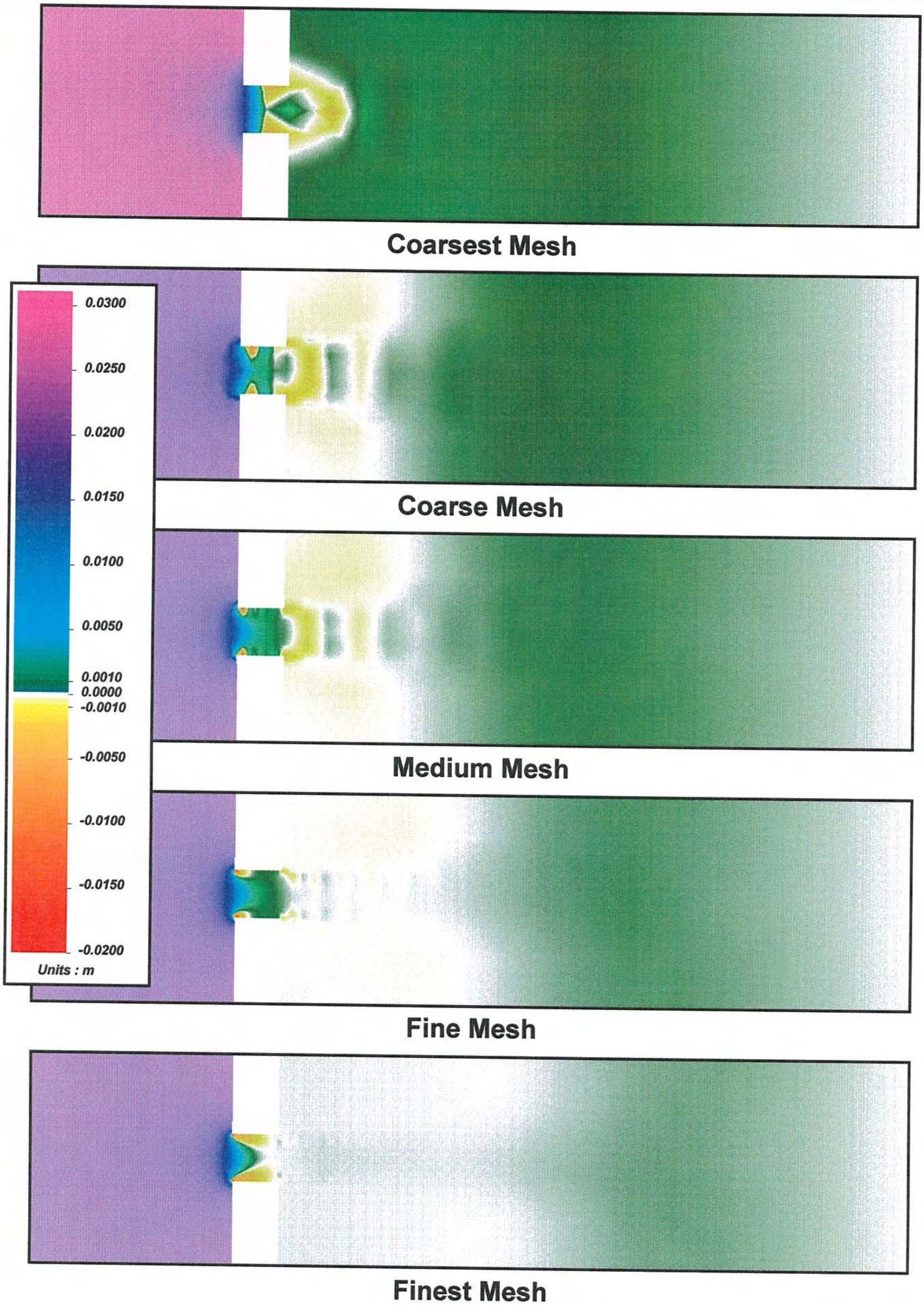


**RMA2 - Water Level**
**Vc = 0.5 m/s (Q=60m³/s b = 60m)**

**Figure 4-9**

RMA2_V0.5_60.wor

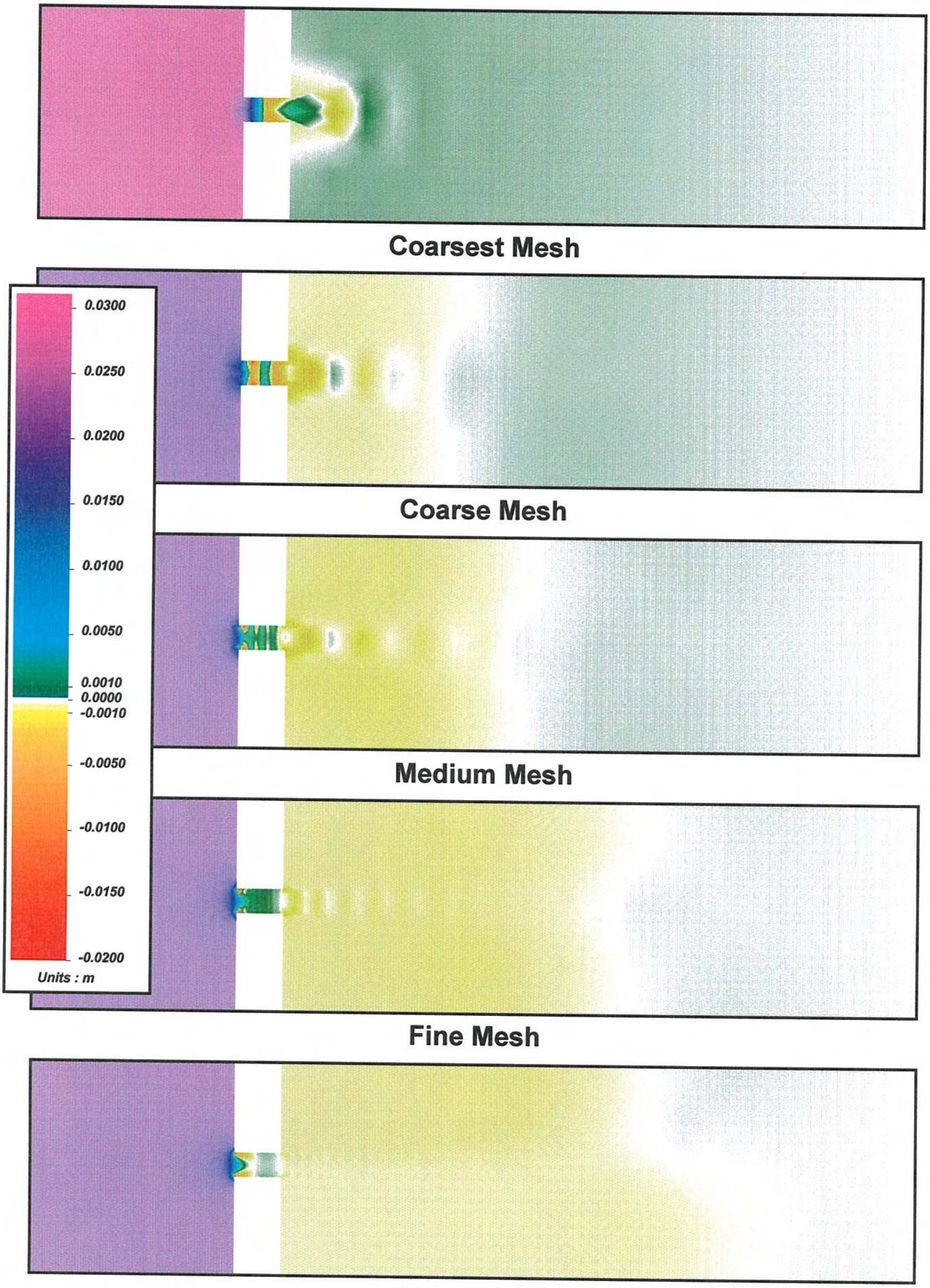


**RMA2 - Water Level**
**Vc = 0.5m/s (Q=30m³/s & b = 30m)**

**Figure 4-10**

RMA2V0.5_30.wor

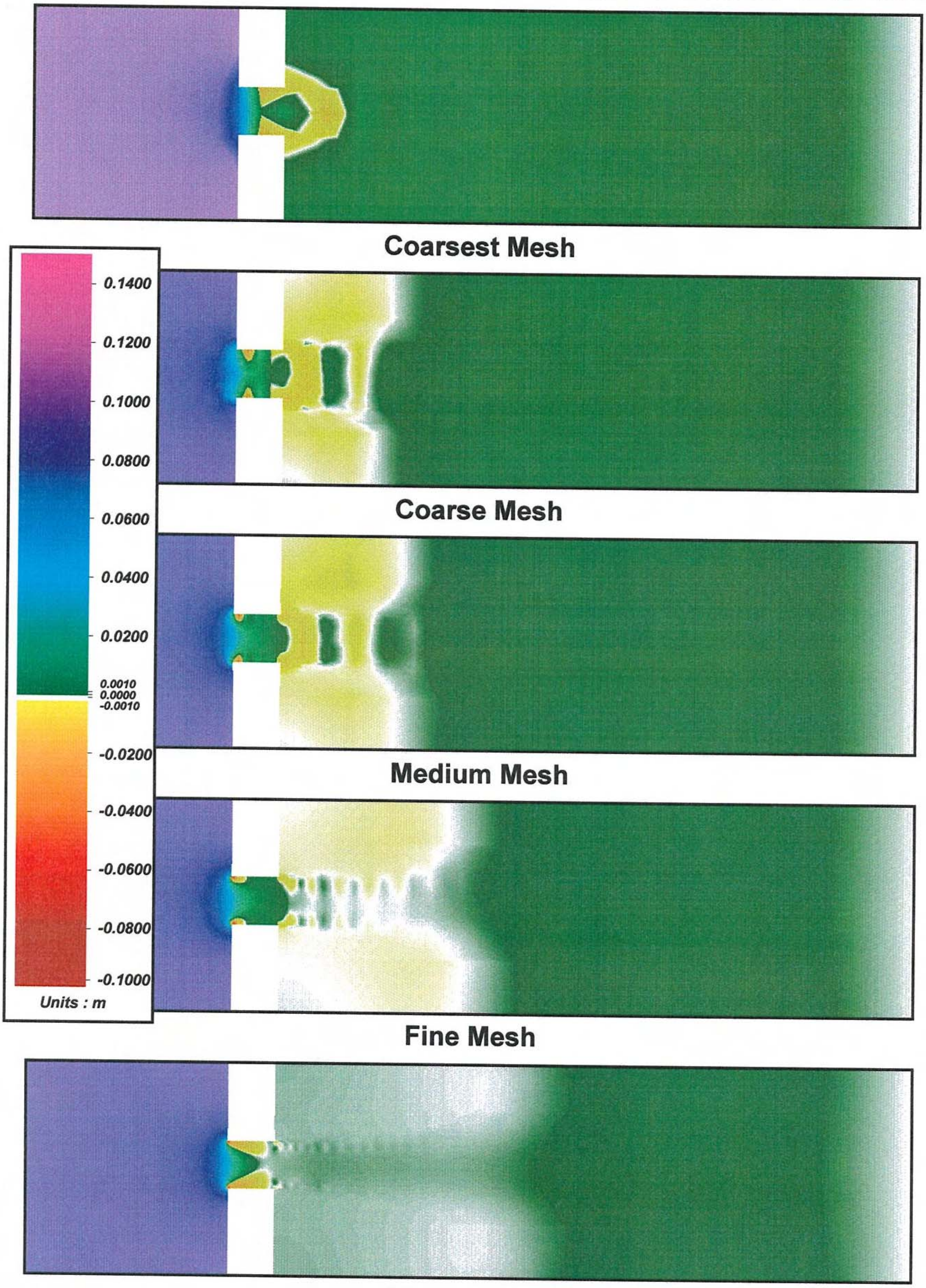


**RMA2 - Water Level**

**Vc = 1m/s ($Q=120m^3/s$ & b = 60m)**

**Figure 4-11**

RMA2V1_60.wor

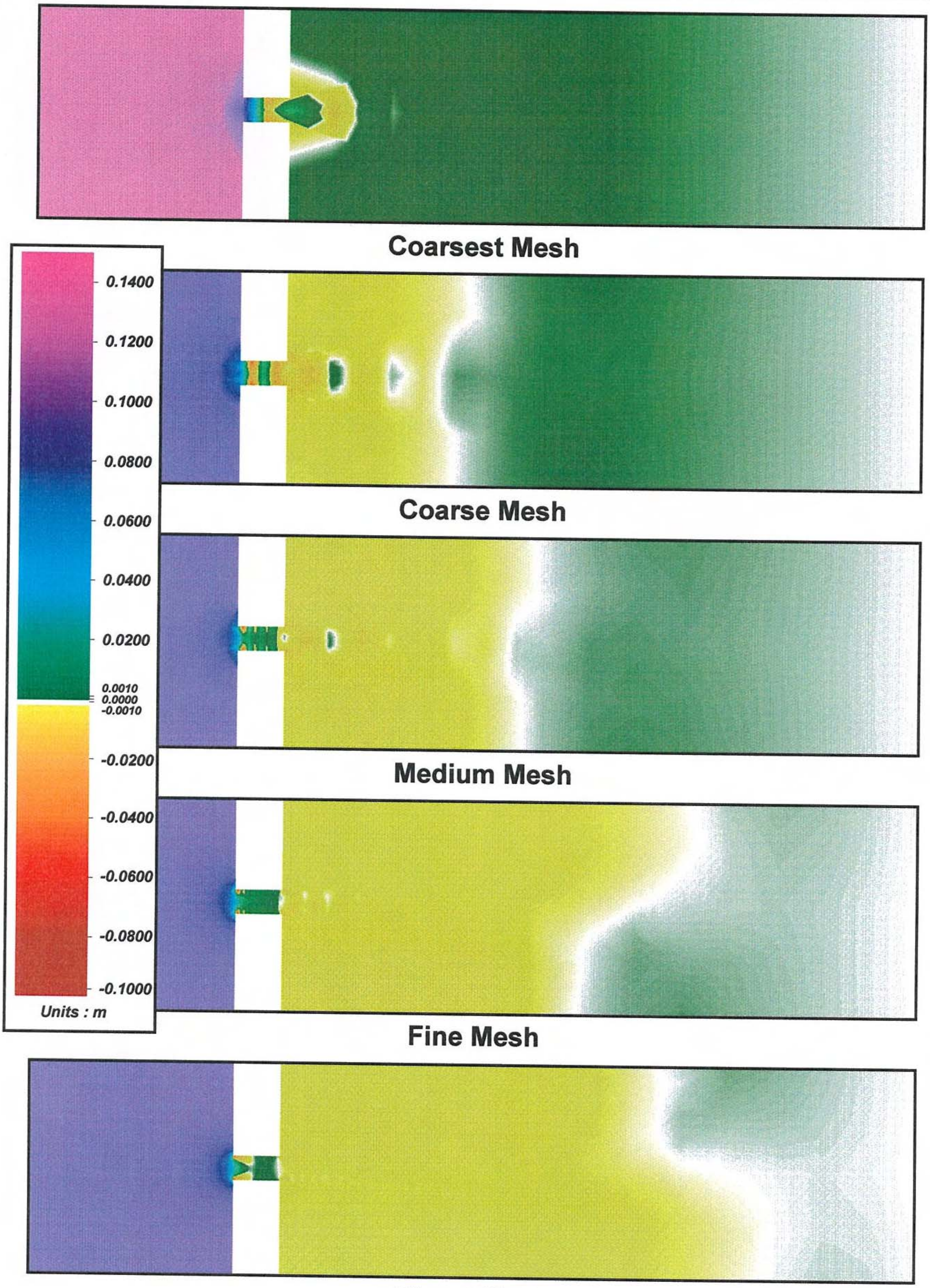


RMA2 - Water Level
Vc = 1m/s (Q=60m$^3$/s & b = 30m)

Figure 4-12

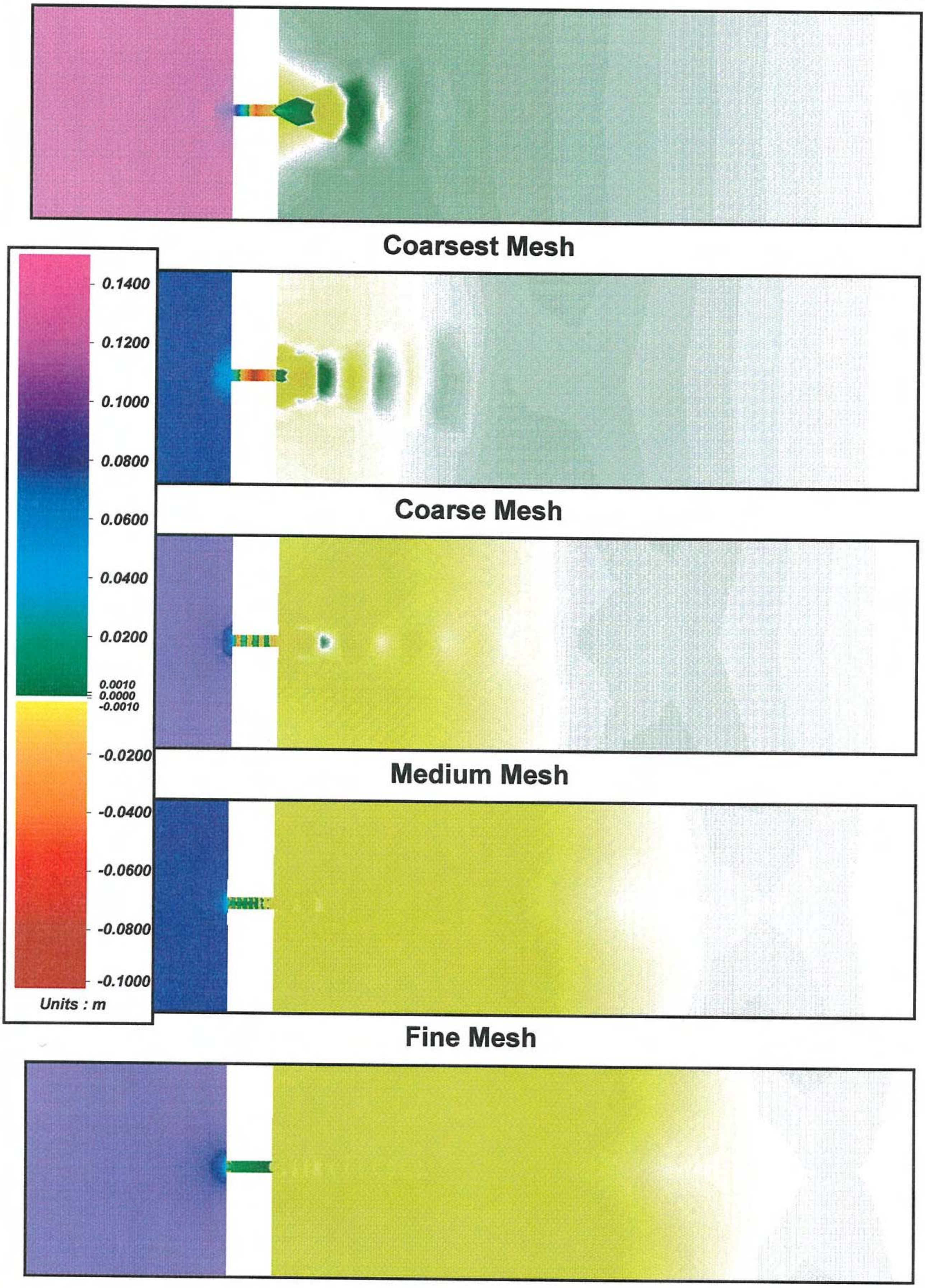


**RMA2 - Water Level**
**Vc = 1m/s (Q=30m³/s & b = 15m)**

**Figure 4-13**

RMA2V1_15.wor

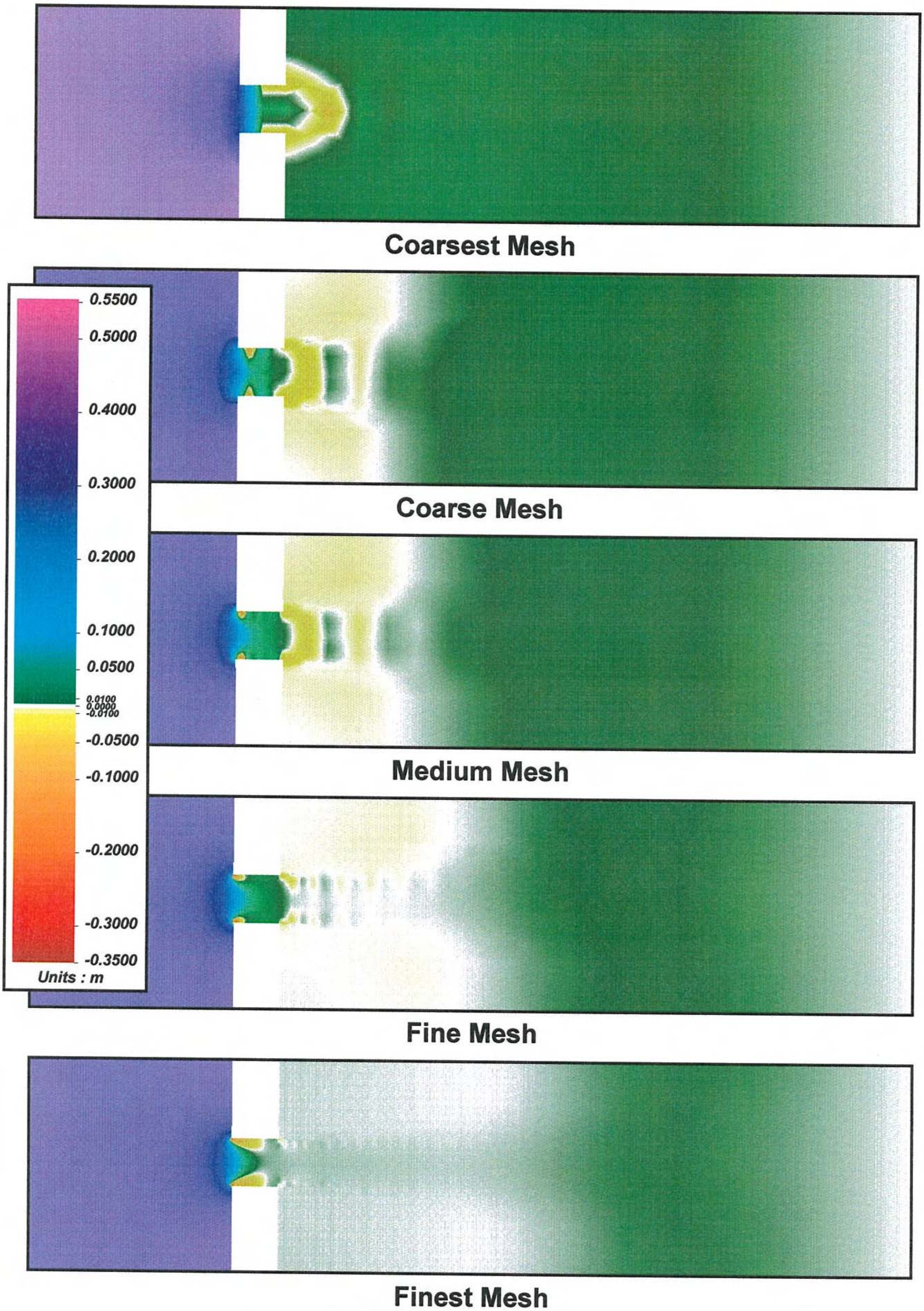


RMA2 - Water Level
Vc = 2m/s (Q=240m$^3$/s & b = 60m)

Figure 4-14

RMA2V2_60.wor

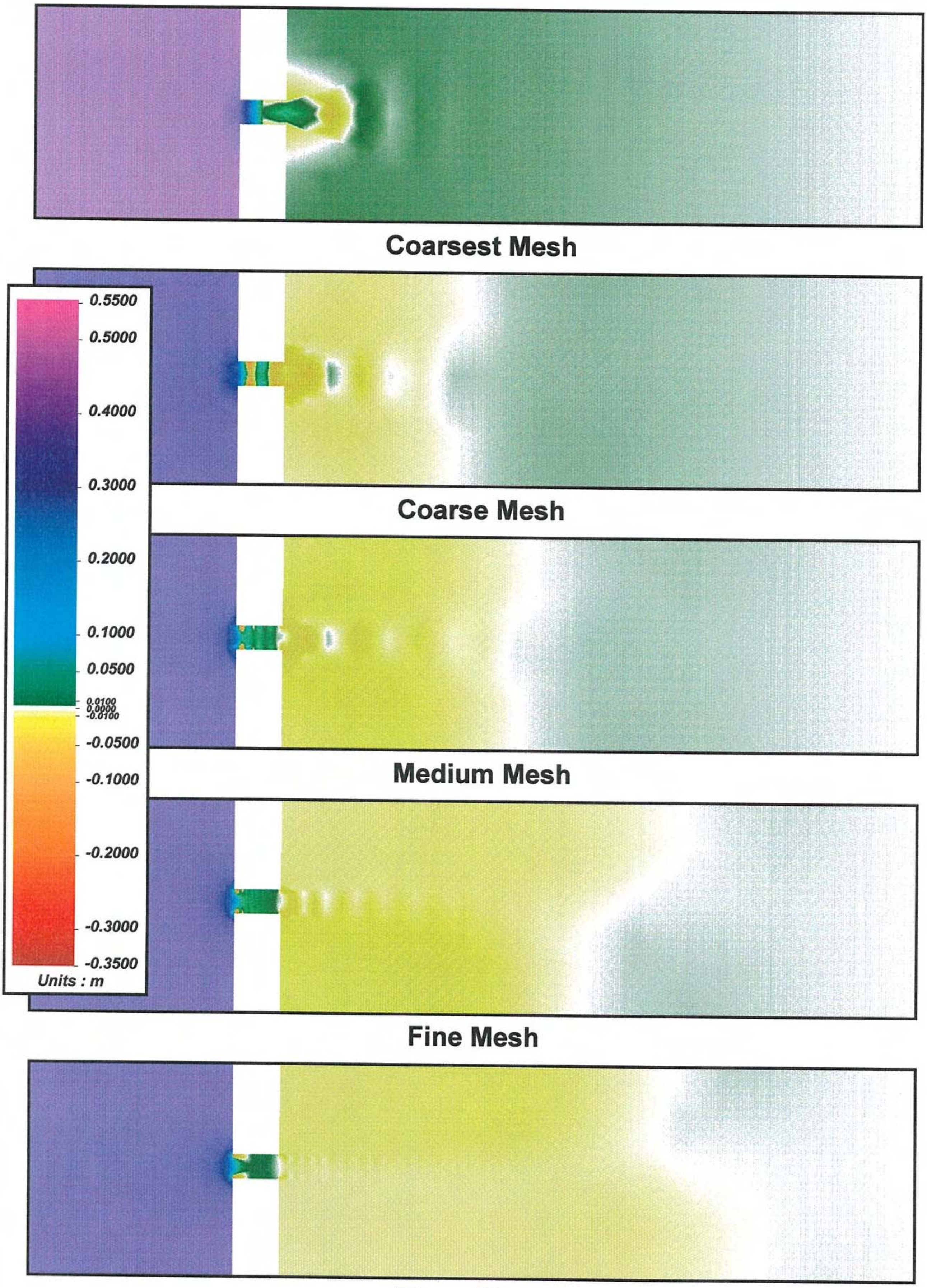


**RMA2 - Water Level**
**Vc = 2m/s (Q=120m³/s & b = 30m)**

**Figure 4-15**

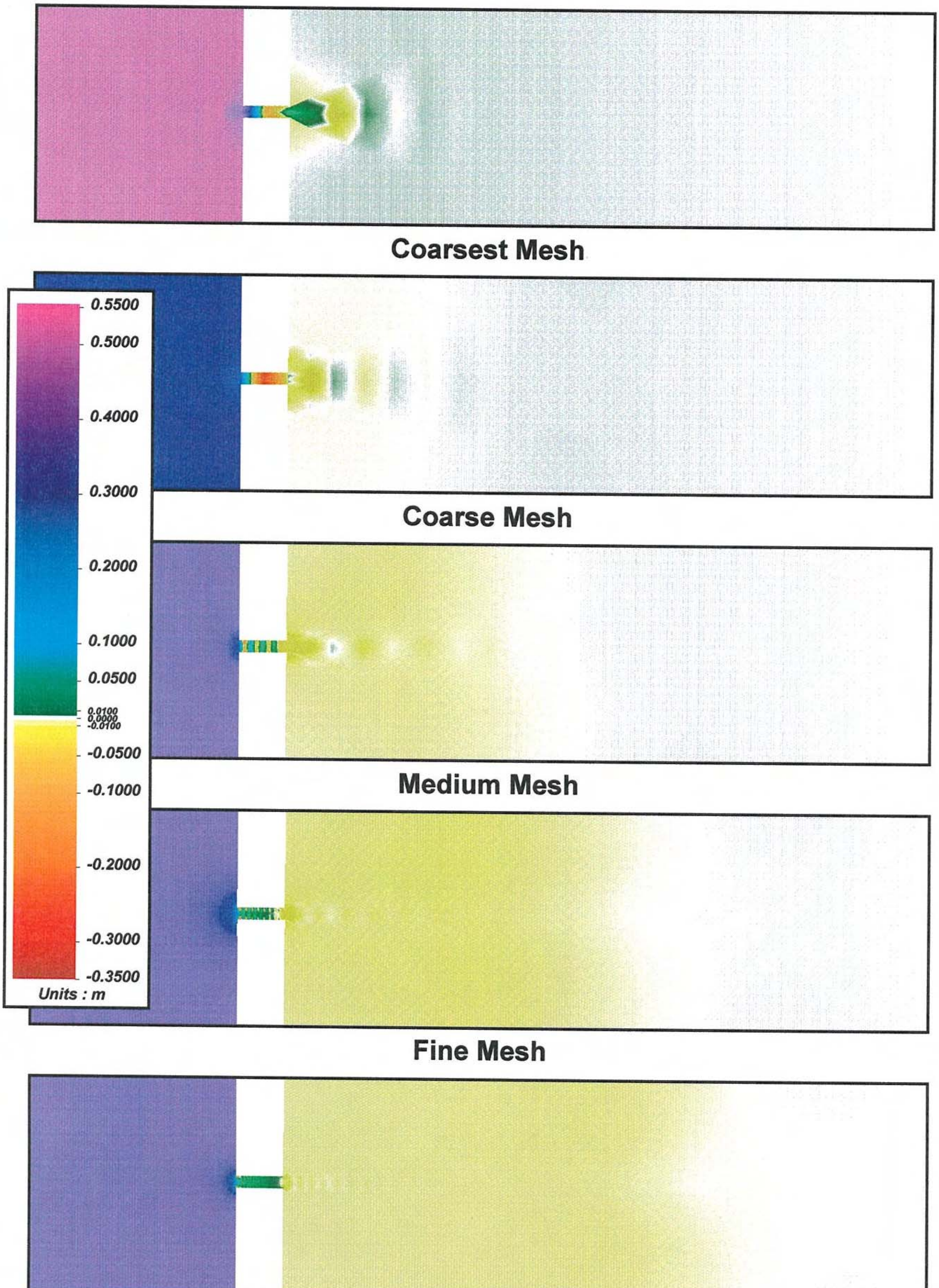


**RMA2 - Water Level**
**Vc = 2m/s (Q=60m$^3$/s & b = 15m)**

**Figure 4-16**

RMA2V2_15.wor

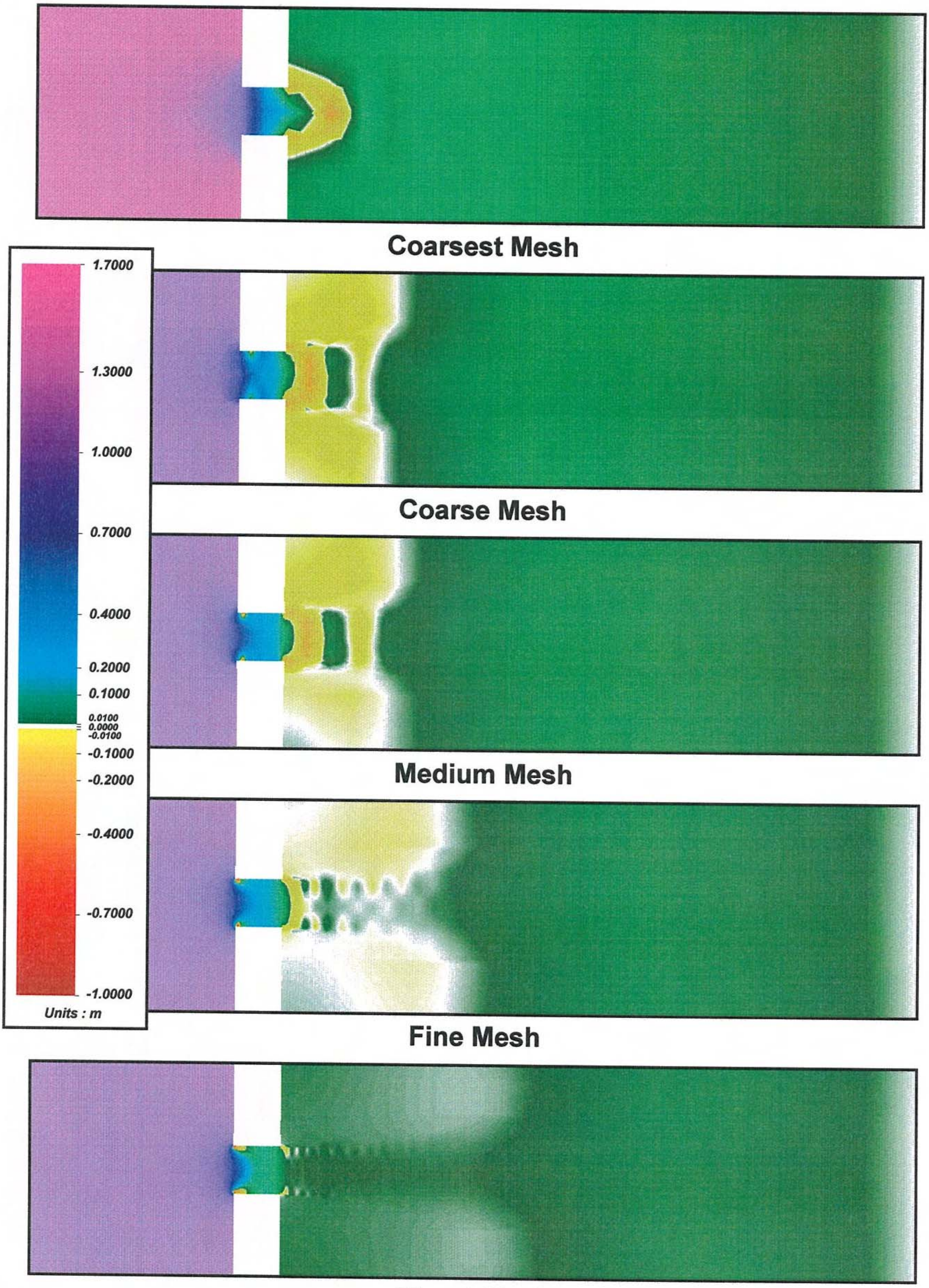


RMA2 - Water Level
Vc = 4m/s (Q=480m³/s & b = 60m)

Figure 4-17

RMA2V4_60.wor

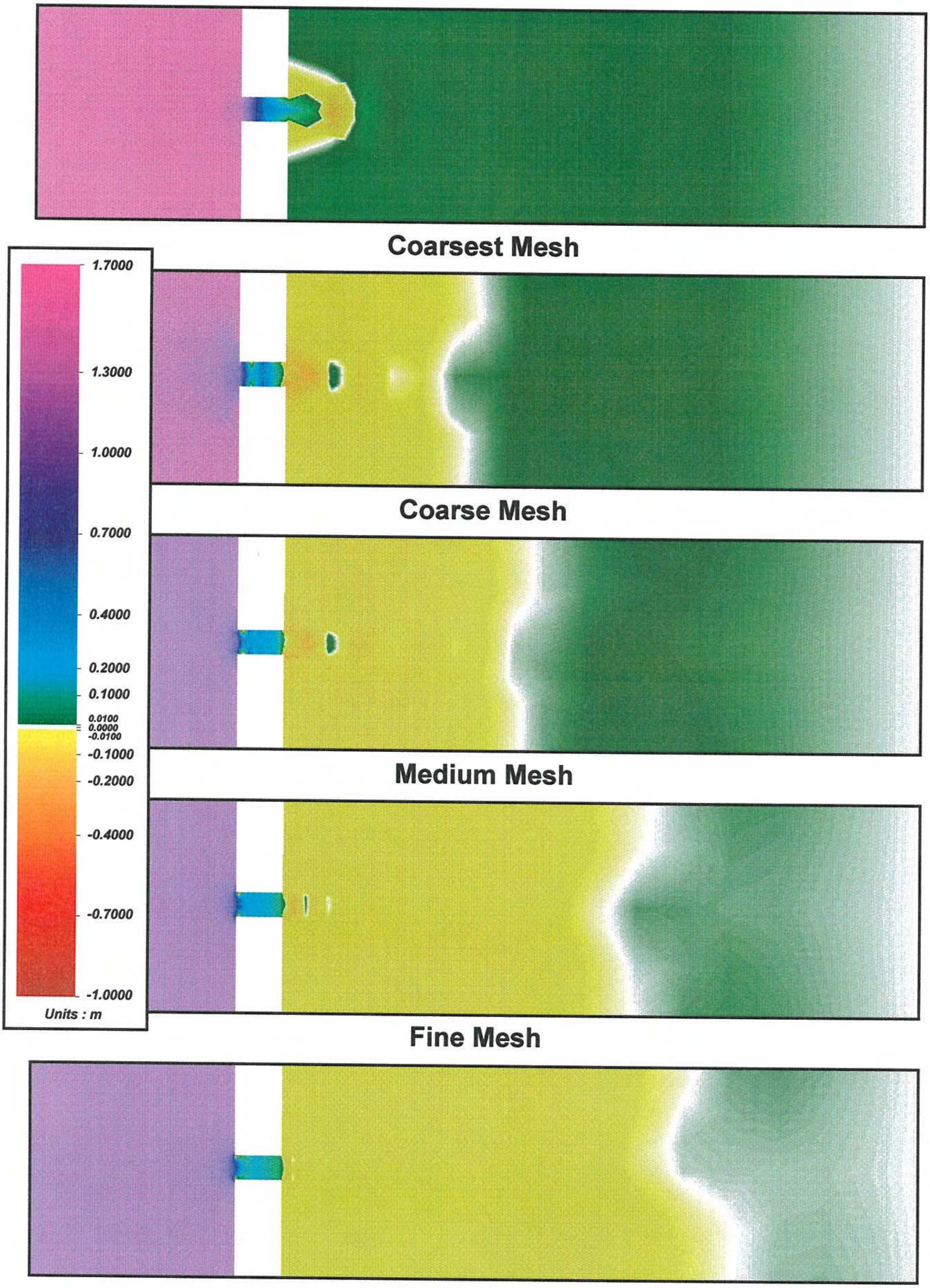


**RMA2 - Water Level**
**Vc = 4m/s (Q=240m$^3$/s & b = 30m)**

**Figure 4-18**

RMA2V4_30.wor

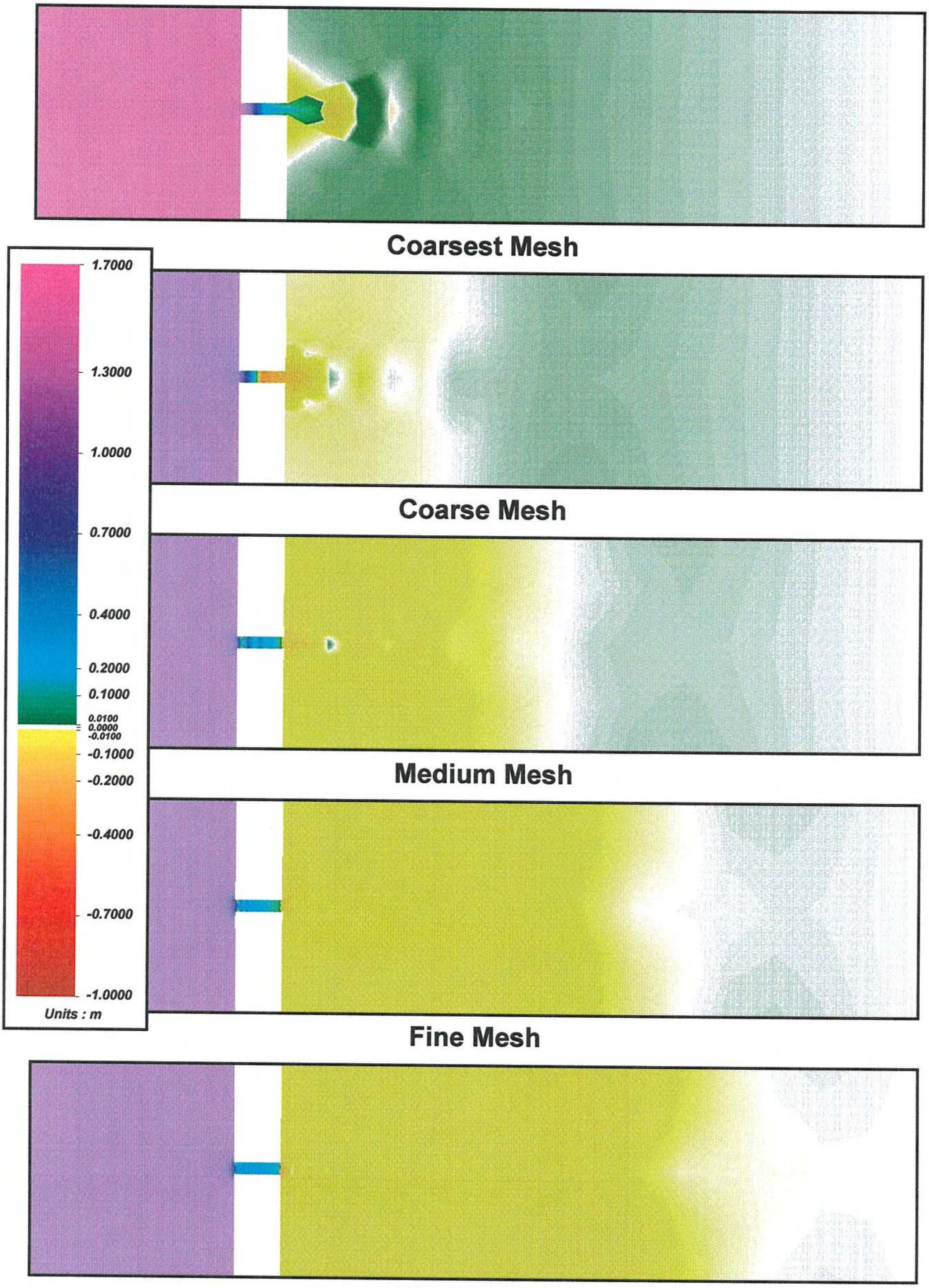


RMA2 - Water Level
Vc = 4m/s (Q=120m³/s & b = 15m)

Figure 4-19

RMA2V4_15.wor

# 4.4 Discussion

## 4.4.1 Flow Characteristics

The presence of the vena contracta within the constriction becomes evident in the finest mesh resolution only. As the vena contracta is more accurately modelled with increasing spatial resolutions, velocities at the location of the vena contracta in the constriction increase with increasing model resolution. This trend is evident in Figure 3-1. In addition, the vena contracta is evident for the finest mesh in Figure 4-2 through Figure 4-6 as the lower velocity (blue) region within the constriction.

Increasing spatial resolution increases the definition of the velocity distribution across the model domain as expected. Differences in flow patterns are particularly evident downstream of the constriction where the eddy patterns are more pronounced with each increase in the spatial resolution.

Instabilities in the flow patterns are evident downstream of the constriction in the lower velocity areas for all average constriction velocities. These may be seen in Figure 4-2 to Figure 4-6 as higher velocity (lighter blue) striations. The location of the striations corresponds to the element boundaries in these regions.

## 4.4.2 Losses

As shown in Figure 4-7, it may be argued that the general trend displayed by RMA2 is a decrease in dynamic head loss coefficients with increasing mesh resolution. However, there are exceptions to this trend, notably those results produced for Mesh 2 (Coarse). Results obtained using this mesh show a decrease in head loss despite a decrease in mesh density. It is unknown why Mesh 2 (Coarse) does not conform to the general trend. However, it is important to note that the range of resolutions covered by the RMA2 meshes is considerably less than that range used for TUFLOW (refer to Section 5.1). As the model resolution increases, the range of the dynamic head loss coefficient envelope contracts and appears to be relatively constant for the finer mesh resolutions. This trend may continue if the mesh resolution was able to be further refined.

# 5 COMPARISON OF TUFLOW AND RMA2

## 5.1 Spatial Resolution

As discussed in Section 1.5, a number of factors must be considered in selecting a suitable spatial resolution for a 2D model. The nature of the RMA2 mesh in comparison with the TUFLOW grid, means that the priority of the selection factors is different for both models. Typically, selection of a grid resolution for TUFLOW involves achieving a balance between practical simulation times and a sufficiently fine resolution to meet the objectives of the modelling. However, an RMA2 mesh resolution is flexible in that that it may be altered on a local scale to smooth any local instabilities or reflect the importance of a particular hydraulic control. An RMA2 mesh is selected in a more intuitive sense and relies far more on the experience of the modeller. It is rare that an RMA2 model would be developed using a coarse mesh, particularly in areas of rapidly varying flow. If a coarse mesh was used in this circumstance any potential inaccuracies may be more accurately attributable to the experience of the modeller rather than the "coarseness" of the mesh as, in theory, there is no need, and in fact, it is bad modelling practice, to assign a coarse mesh to such an area.

However, in developing a TUFLOW grid, it may be a necessity to assign a relatively coarse grid to an area of rapidly varying flow as this area may be small in relation to the remainder of the model. To assign a grid resolution suitable for this small area to the entire model would result in an impractical grid resolution in terms of time and space. In this circumstance it is thus necessary to compensate for the model's inability to provide sufficient representation of the area of rapidly varied flow. This may be achieved using energy loss factors which are available as a TUFLOW input variable. The value of these energy loss factors for a constriction in flow may be determined at a later stage from results presented in this study.

Table 5–1 provides a comparison between the number of computation points in both of the 2D models used in this study. There are major differences between TUFLOW and RMA2 in the number of computation points for all mesh resolutions. There are a number of reasons for this:

- As TUFLOW operates on a regular grid, representation of a constriction width of 15m implies a maximum grid size of 15m. However, TUFLOW does have the capacity to incorporate a width contraction factor over a number of grid cells (termed the "Flow Constriction" feature in WBM, 2000). While this was needed for the 10m grid size to represent the 15m width of constriction (refer to Section 2.4.1.1), this feature was not utilised to investigate larger grid sizes.
- Again, as TUFLOW operates on a regular grid size, it is not possible to increase the grid resolution within the more critical expansion and contraction zone as it is with RMA2. Instead, the grid resolution must be increased over the entire model domain. This expands the number of computation points.
- RMA2 became increasingly unstable as the resolution of the mesh became finer. RMA2 simulations using meshes finer than Mesh 5 were not possible due to instabilities.

**Table 5–1 Comparison of Computation Points in TUFLOW and RMA2**

| Resolution | Name | Approximate Number of Computation Points[a] (Based on 30m Width of Constriction) | | | |
|---|---|---|---|---|---|
| | | Across Model Domain | | Within Expansion and Contraction Zone[1] | |
| | | TUFLOW | RMA2 | TUFLOW | RMA2 |
| Coarsest | 15m Grid / Mesh 1 | 4,400 | 500 | 2,900 | 400 |
| Coarse | 10m Grid / Mesh 2 | 9,800 | 700 | 6,400 | 600 |
| Medium | 5m Grid/ Mesh 3 | 3,900 | 1,000 | 25,500 | 900 |
| Fine | 2.5m Grid / Mesh 4 | 156,000 | 3,400 | 102,000 | 3,300 |
| Finest | 1m Grid / Mesh 5 | 977,000 | 13,200 | 640,000 | 13,000 |

[a] In TUFLOW, there are three computation points per grid element, in RMA2 each element node and mid-side form a computation point.

[1] This zone is arbitrarily defined as 200m upstream from constriction, the constriction itself and 500m downstream of constriction.

### 5.1.1 Simulation Time

Time taken to complete a simulation provides a reflection of the computation intensity and thus the number of computation points. A summary of “time factors” for the two 2D models is provided in Table 5–2. TUFLOW time factors are significantly higher than those of RMA2 due to the relative number of computation points. It is important to be mindful of the differences in computational intensity due to the number of computation points when comparing results from each model.

**Table 5–2 Comparison of Time Factors in TUFLOW and RMA2**

| Resolution | Name | Time Factor $\left(\frac{\text{Actual Run Time}^{a}\ (\text{min})}{\text{Simulation Time}\ (h)}\right)$ | |
|---|---|---|---|
| | | TUFLOW[b] | RMA2[c] |
| Coarsest | 15m Grid / Mesh 1 | 0.38 | < 0.01 |
| Coarse | 10m Grid / Mesh 2 | 1.3 | < 0.1 |
| Medium | 5m Grid/ Mesh 3 | 5.6 | < 0.1 |
| Fine | 2.5m Grid / Mesh 4 | 28 | 0.36 |
| Finest | 1m Grid / Mesh 5 | 730 | 7.3 |

[a] Actual run time on a Pentium 3 933MHz computer with 260Mb of RAM

[b] TUFLOW Simulation Time = 8 hours

[c] RMA2 Simulation Time = 5.5 hours

## 5.2 Results

Figure 3-7 and Figure 4-7 have been combined to create Figure 5-1. This shows a comparison between the dynamic head loss coefficient envelopes for each model across the range of resolutions. It is important to note that this figure compares the envelopes as though the spatial resolutions were similar (that is, finest TUFLOW grid is equivalent to finest RMA2 mesh). As explained in the preceding sections, this is not true due to the differences in the number of computation points. As such, implications of Figure 5-1 should be treated with caution and this figure is not discussed further.

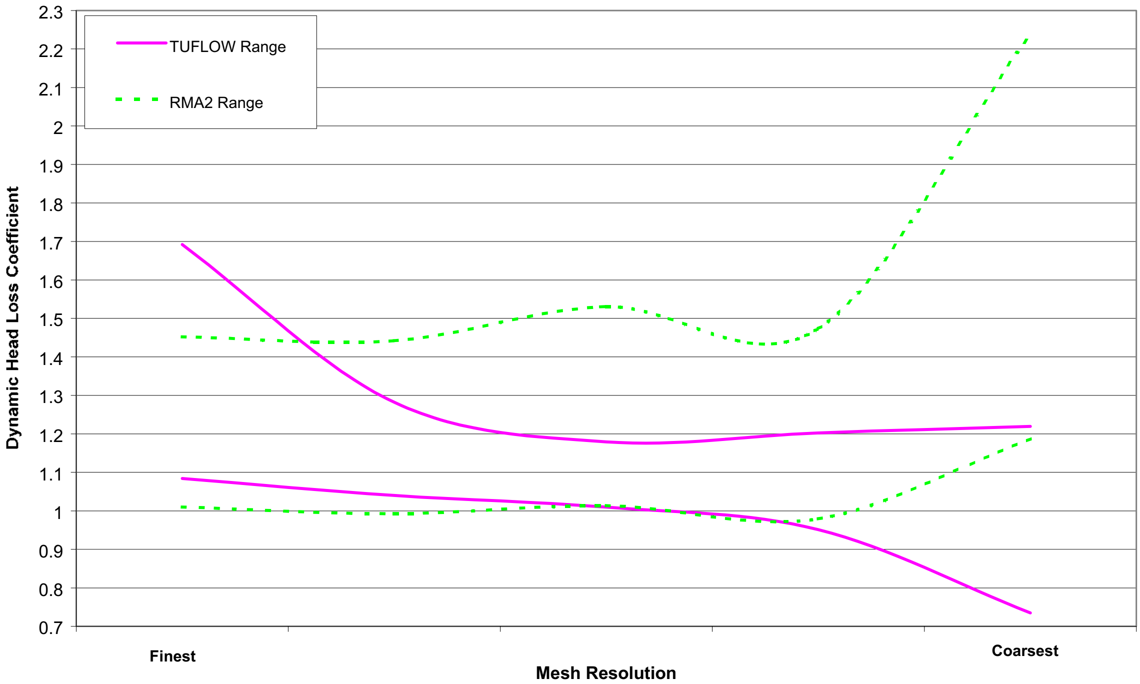


**Figure 5-1 TUFLOW & RMA2 - Dynamic Head Loss Coefficient Envelopes**

As with TUFLOW, increasing the RMA2 spatial resolution increases the definition of the velocity distribution across the model domain. However, the differences are not as extreme as in TUFLOW. Complex eddy patterns in RMA2 results are not obvious downstream of the constriction even for the higher velocities. It is believed that this is a function of the differences in the number of computation points between RMA2 and TUFLOW (refer to Table 5–1). If the RMA2 mesh had been refined further these eddy patterns may have become evident. As discussed, further refinement of the mesh was not possible as the simulation became unstable.

# 6 MIKE 11 COMPUTATIONS

## 6.1 Introduction

The MIKE 11 hydrodynamic (HD) module was developed by DHI Software. It is a one-dimensional, implicit finite difference scheme for the computation of unsteady flows in rivers and estuaries. The module can be used to describe both sub-critical and super-critical flow regimes. Computations at hydraulic structures are possible due to the inclusion of modules developed for this purpose.

## 6.2 Computational Procedure

MIKE 11 solves the vertically integrated equations of conservation of volume and momentum (the "Saint Venant" equations). The equations used by DHI (2000) are as follows:

**Conservation of Volume**

$$\frac{\partial Q}{\partial x} + \frac{\partial A}{\partial t} = q$$

**Conservation of Momentum**

$$\frac{\partial Q}{\partial t} + \frac{\partial \left( \alpha \frac{Q^2}{A} \right)}{\partial x} + gA \frac{\partial h}{\partial x} + \frac{g n^2 Q |Q|}{A R} = 0$$

| | | |
|---|---|---|
| Where: | Q | = discharge |
| | x | = distance |
| | A | = cross-sectional area |
| | t | = time |
| | q | = lateral inflow |
| | $\alpha$ | = vertical velocity distribution coefficient |
| | h | = water elevation |
| | g | = gravitational acceleration |
| | R | = hydraulic radius |
| | n | = Mannings 'n' |

### 6.2.1 Entrance Loss

The contraction loss coefficient, $C_c$ is described as follows:

$$C_c = C_{in}\left(1 - \frac{A_{s1}}{A_1}\right)$$

Where: $C_{in}$ = inflow loss coefficient (typically set to 0.5 as recommended by DHI, 2000)

$A_{s1}$ = constriction inflow cross-sectional area

$A_1$ = inflow channel cross-sectional area

### 6.2.2 Expansion Loss

The expansion loss coefficient, $C_e$, is described as follows:

$$C_e = C_{out}\left(1 - \frac{A_{s2}}{A_2}\right)^2$$

Where: $C_{out}$ = outflow loss coefficient (typically set to 1.0 as recommended by DHI, 2000)

$A_{s2}$ = constriction outflow cross-sectional area

$A_2$ = outflow channel cross-sectional area

### 6.2.3 Friction Loss

The friction loss coefficient, $C_f$, is calculated using the Manning formula:

$$C_f = \frac{2gLn^2}{R^{\frac{4}{3}}}$$

Where: L = length between h-points

n = Manning's 'n'

### 6.2.4 Total Head Loss Through Constriction

The total head loss, $\Delta_h$ , through the constriction is given by:

$$\Delta_h = \frac{Q^2}{2g}\left(\frac{C_c}{A_{s1}^2} + \frac{C_f + C_b}{A_{sa}^2} + \frac{C_e}{A_{s2}^2}\right)$$

Where: $C_b$ = bend loss coefficient which accounts for losses due to damaged culverts, debris etc. For this study it is set to 0.

$A_{sa}$ = mean cross-section area through the constriction

## 6.3 Results

A summary of the MIKE 11 expansion and contraction coefficients is provided in Table 6–1. Total head loss across the full 1140m length of the model is shown in Table 6–2. The total head loss includes the energy loss due to frictional effects. Dynamic head loss coefficients are presented in Table 6–3 and Figure 6-1 and are without frictional losses (as discussed in Section 1.4 and 2.1).

**Table 6–1 MIKE 11 – Contraction and Expansion Coefficients**

| b (m) | Q ($m^3$/s) | $C_c$[1] | $C_e$[1] |
|---|---|---|---|
| 15 | 30 | 0.48 | 0.90 |
| | 60 | 0.48 | 0.90 |
| | 120 | 0.48 | 0.90 |
| 30 | 30 | 0.45 | 0.81 |
| | 60 | 0.45 | 0.81 |
| | 120 | 0.45 | 0.81 |
| | 240 | 0.45 | 0.81 |
| 60 | 30 | 0.40 | 0.64 |
| | 60 | 0.40 | 0.64 |
| | 120 | 0.40 | 0.64 |
| | 240 | 0.40 | 0.64 |
| | 480 | 0.40 | 0.64 |

[1] These coefficients have been calculated manually using equations presented in this Section. MIKE 11 does not output these coefficients.

**Table 6–2 MIKE 11 – Total Head Loss (mm)**

| Width of Constriction (m) | Total Head Loss (mm) Flow ($m^3$/s) | | | | |
|---|---|---|---|---|---|
| | 30 | 60 | 120 | 240 | 480 |
| 15 | 94 | 354 | 1229 | 3096 | 6184 |
| 30 | 23 | 90 | 338 | 1254 | 3139 |
| 60 | 9 | 24 | 80 | 322 | 1216 |

**Table 6–3 MIKE11 – Dynamic Head Loss Coefficients**

| Width of Constriction (m) | Dynamic Head Loss Coefficients ($v^2/2g$) Flow ($m^3$/s) | | | | |
|---|---|---|---|---|---|
| | 30 | 60 | 120 | 240 | 480 |
| 15 | 1.54 | 1.43 | 1.20 | - | - |
| 30 | 1.46 | 1.42 | 1.32 | 1.20 | - |
| 60 | 2.32 | 1.38 | 1.07 | 1.09 | 1.03 |

- not presented to remain consistent with other methods

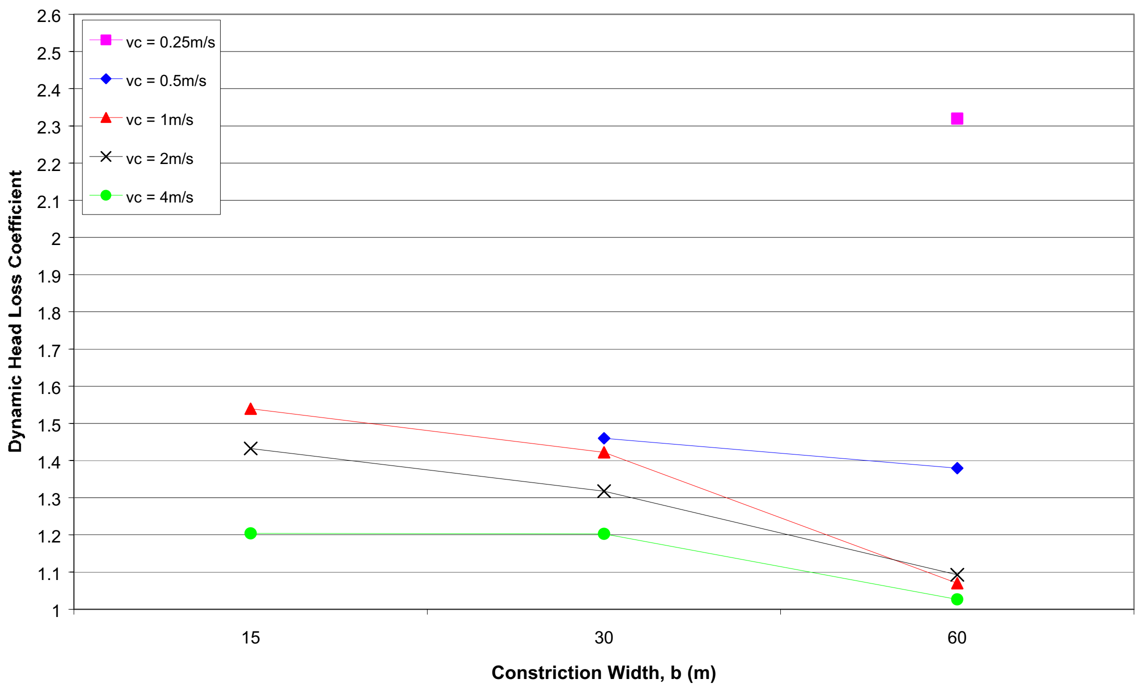


**Figure 6-1 MIKE 11 - Dynamic Head Loss Coefficients**

### 6.3.1 Sensitivity

The sensitivity of the model results to various changes in model set-up is tested. A summary of these tests is provided in Table 6–4.

**Table 6–4 MIKE 11 Sensitivity Tests**

| Description of Sensitivity Test | Change in Total Head Loss Across Model (mm) |
|---|---|
| Move cross-sections adjacent to constriction away from the constriction by 10m | ± 1 |
| Double the expansion reach (from 270m to 540m) | - 1 |
| Double the contraction reach (from 810m to 1620m) | 0 |
| Double the timestep (from 2minutes to 5minutes) | - 5 |
| Halve the timestep (from 2minutes to 1minute) | ± 1 |
| Increase number of cross-sections (add 4 new cross-sections along reach) | ± 1 |

## 6.4 Discussion

Dynamic head loss coefficients predicted by MIKE 11 range from about 1 to 2.3. In general, results from each constriction width in isolation show that dynamic head loss coefficient decreases with increasing average constriction velocity. That is, the higher the average constriction velocity, the lower the dynamic head loss coefficient. As shown in Figure 6-1, the lowest average constriction velocity of 0.25m/s, gives a substantially higher dynamic head loss coefficient. It may be that as the dynamic head at the low velocities is very small, as too is the head loss, the dynamic head loss coefficient becomes very sensitive to accuracy of the values. It is beyond the scope of this study to investigate this phenomenon further. However, it is important to be cognisant of this trend when comparing these results with others. This trend is worthy of further investigation in future work.

The other trend apparent in Figure 6-1 is that for the same average constriction velocities, the dynamic head loss coefficient appears to decrease with increasing constriction width. This is related to the way in which MIKE 11 calculates constriction and expansion losses as described in Sections 6.2.1 and 6.2.2. The equations presented in these sections show that MIKE 11 factors the input expansion and contraction parameters by the constriction area. In general, the larger the constriction width in relation to the channel width, the lower the contraction and expansion coefficients and thus the lower the dynamic head.

Sensitivity tests show that results are relatively insensitive to any of the changes described in Table 6–4. Doubling the expansion and contraction reach lengths provides minimal changes in total head loss which reflects the fact that only a small proportion of total head loss within a 1D model occurs in these reaches (friction losses only). Minimal changes in results produced by changing the timestep reflect that the model is implicit (and therefore unconditionally stable – refer to Section 2.4.3) and that the timestep selected is satisfactory.

# 7 HEC-RAS COMPUTATIONS

## 7.1 Introduction

The HEC-RAS modelling software package was developed by the Hydrologic Engineering Centre within the U.S. Army Corp of Engineers. HEC-RAS (Hyrologic Engineering Centre's River Analysis System) software is used to undertake one-dimensional steady flow hydraulics computations. User documentation for this software system is detailed and well-explained. Version 2.2 of HEC-RAS was used to undertake analyses for this study (HEC, 1998).

HEC-RAS is capable of calculating water surface profiles for one-dimensional, steady, gradually-varied flow in natural or constructed channels. Profiles for sub-critical, supercritical and mixed flow regimes can be calculated. Flow can be rapidly varied at hydraulic structures such as bridges, culverts and weirs. At these locations the momentum equation or other empirical equations are used.

The basic computation procedure employed by HEC-RAS is provided below. HEC (1998) have undertaken substantial research into flow through constrictions and this is detailed in Appendix C.

## 7.2 Computational Procedure

HEC-RAS uses the standard step method (Chow, 1959) from one cross-section to the next to solve both the continuity equation:

$$V_2 A_2 = V_1 A_1$$

Where: $V_1$ and $V_2$ = average velocities ($_1$ signifying downstream, $_2$ signifying upstream)

$A_1$ and $A_2$ = average cross-sectional flow areas

and the energy equation:

$$d_2 + z_2 + \frac{\alpha_2 V_2^2}{2g} = d_1 + z_1 + \frac{\alpha_1 V_1^2}{2g} + \Delta h$$

Where: $d_1$ and $d_2$ = depth of water at cross-sections ($_1$ signifying downstream, $_2$ signifying upstream)

$z_1$ and $z_2$ = elevation of the main channel inverts

$\alpha_1$ and $\alpha_2$ = velocity weighting coefficients

$g$ = gravitational acceleration

$\Delta h$ = energy head loss

The energy head loss between two cross-sections is comprised of friction losses and contraction and expansion losses as represented in the following equation:

$$\Delta_h = L_{1-2}\bar{S}_f + C\left(\frac{\alpha_2 V_2^2}{2_g} - \frac{\alpha_1 V_1^2}{2_g}\right)$$

Where: $L_{1-2}$ = discharge weighted reach length ($_1$ signifying downstream, $_2$ signifying upstream)

$\bar{S}_f$ = representative friction slope between two sections

$C$ = expansion ($C_e$) or contraction ($C_c$) loss coefficient

## 7.3 Results

Total head loss across the full 1140m length of the model is shown in Table 7–1. The total head loss includes the energy loss due to frictional effects. Dynamic head loss coefficients are presented in Table 7–2 and Figure 7-1 are without frictional losses (as discussed in Section 2.1).

**Table 7–1 HEC-RAS – Total Head Loss (mm)**

| Width of Constriction (m) | Total Head Loss (mm) Flow ($m^3/s$) | | | | |
|---|---|---|---|---|---|
| | 30 | 60 | 120 | 240 | 480 |
| 15 | 103 | 372 | 1276 | 3196 | 6243 |
| 30 | 27 | 103 | 368 | 1276 | 3195 |
| 60 | 8 | 30 | 114 | 409 | 1319 |

**Table 7–2 HEC-RAS - Dynamic Head Loss Coefficients**

| Width of Constriction (m) | Dynamic Head Loss Coefficient ($v^2/2g$) Flow ($m^3/s$) | | | | |
|---|---|---|---|---|---|
| | 30 | 60 | 120 | 240 | 480 |
| 15 | 1.72 | 1.52 | 1.26 | - | - |
| 30 | 1.77 | 1.68 | 1.46 | 1.23 | - |
| 60 | 1.89 | 1.85 | 1.74 | 1.52 | 1.15 |

- not presented to remain consistent with other methods

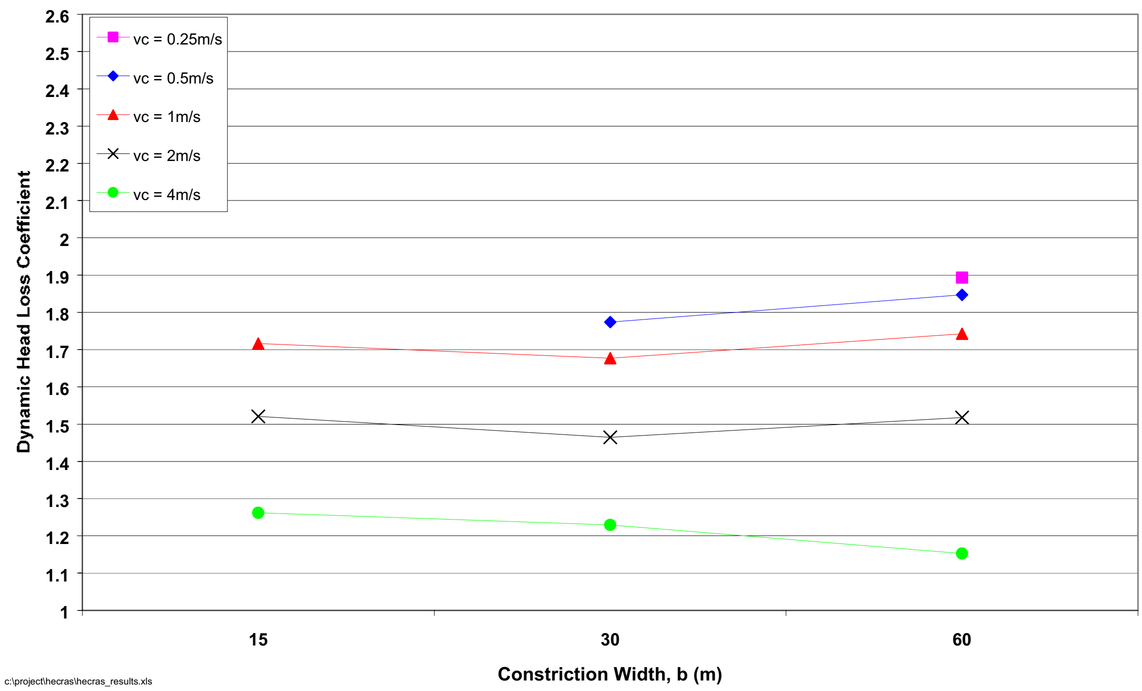


**Figure 7-1 HEC-RAS - Dynamic Head Loss Coefficients**

### 7.3.1 Sensitivity

The sensitivity of the model results to various changes to model set-up has been tested. The sensitivity tests performed relate directly to the research undertaken by HEC (1998) into contraction and expansion losses. As the details of this research are provided in Appendix C, sensitivity results are also contained within that Appendix. Discussion on the sensitivity analysis is provided in Section 7.4 with more detailed discussion is provided in Appendix C.

## 7.4 Discussion

Dynamic head loss coefficients predicted by HEC-RAS range from about 1.1 to 1.9. Results from each constriction width in isolation show that dynamic head loss coefficient decreases with increasing average constriction velocity. That is, the higher the average constriction velocity, the lower the dynamic head loss coefficient. It may be that as the dynamic head at the low velocities is very small, as too is the head loss, the dynamic head loss coefficient becomes very sensitive to accuracy of both of these values. As recommended in Section 6.4, this trend is worthy of further investigation, however it is beyond the scope of the current study.

Results presented for HEC-RAS have been computed following the recommendations contained in HEC (1998). Sensitivity tests have been undertaken in relation to these recommendations and details are provided in Appendix C. In general, these tests show that the results are very sensitive to changes in the ineffective flow areas and positioning of cross-sections adjacent to the constriction for average constriction velocities of 4m/s. For example, widening the ineffective flow area by about 3m (1% of the total channel width), produced a decrease in head loss of up to 25% for average constriction velocities of 4m/s and more. Sensitivity of the results to changes in the position cross-sections adjacent to the constriction were also tested. By moving the cross-sections away from the constriction, differences in head losses of up to 40% were found for average constriction velocities of 4m/s and more. It is not within the scope of this study to determine the reasons for these sensitivities. However, it is important to be cognisant of the sensitivities for the 4m/s average constriction velocity situations when comparing the results with that of other models.

# 8 MANUAL CALCULATIONS

## 8.1 Introduction

A number of hand calculations have been undertaken as part of this project to provide another means of comparison of head loss results. The following sections provide details of these methods.

## 8.2 Henderson (1966)

Henderson (1966) deals with channel transitions from a theoretical and empirical point of view. Of particular interest in this chapter is the section on abrupt expansion and contraction in artificial channels. Henderson (1966) separates the treatment of energy losses into the expansion and contraction components.

### 8.2.1 Expansion Losses

The energy loss across an abrupt channel expansion (between sections 1 and 2 in Figure 8-1) is given by Henderson (1966) as

$$Energy\ Loss = \frac{v_1^2}{2g}\left[\left(1-\frac{b_1}{b_2}\right)^2 + \frac{2 Fr_1^2 b_1^3 (b_2 - b_1)}{b_2^4}\right] \qquad Equation\ 8.1$$

Where: b = width of channel

$_{1,2,3}$ (defined in Figure 8-1)

Fr = Froude number

Thus the bracketed section in the above equation is considered to be the dynamic expansion loss coefficient $\left(v_1^2/2g\right)$ or "expansion coefficient" through the expansion. Expansion coefficients for the varying constriction widths and discharges are provided in Table 8–1. As an aside, as $Fr_1$ tends to zero, the last term in the bracket also tends to zero and the equation reduces to

$$Energy\ Loss = \frac{(v_1 - v_3)^2}{2g} \qquad Equation\ 8.2$$

Equation 8.2 may be used to estimate the energy loss due to the expansion. For this study, both Equation 8.1 and 8.2 give the same set of expansion coefficients since the maximum value of the last term in brackets in Equation 8.1 is 0.006 and thus this term contributes little to the expansion loss value. Henderson (1966) indicates that experiments by Formica (1955) have yielded expansion losses about 10% less than the value given by the second equation and thus the use of this equation is recommended as safe for most normal circumstances.

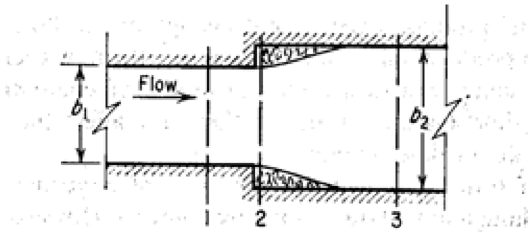


Source: Henderson (1966)

**Figure 8-1 Plan View of Abrupt Channel Expansion (Henderson, 1966)**

**Table 8–1 Expansion Coefficients (Henderson, 1966)**

| Width of Constriction (m) | b1/b2 | Expansion Coefficient (Theoretical) | | | | |
|---|---|---|---|---|---|---|
| | | Flow ($m^3$/s) | | | | |
| | | 30 | 60 | 120 | 240 | 480 |
| 15 | 0.05 | 0.90 | 0.90 | 0.90 | - | - |
| 30 | 0.1 | 0.81 | 0.81 | 0.81 | 0.81 | - |
| 60 | 0.2 | 0.64 | 0.64 | 0.64 | 0.64 | 0.65 |

- not presented to remain consistent with other methods

### 8.2.2 Contraction Losses

Henderson (1966) notes that contraction losses are smaller than expansion losses and that an equation analogous to that above could be derived with section 2 taken at the vena contracta and section 3 where the flow has become uniform again downstream. However, Henderson (1966) indicates that direct experimental measurements provide a better approach as experiments are needed in any case to determine the contraction coefficient. Experiments undertaken by Formica (1955) provide results which indicate head losses of up to 0.23 $v_1^2/2g$ for square-edged contractions in rectangular channels. Formica (1955) found that the coefficients increased with the ratio $y_3/b_2$, reaching the maximum when this ratio was about 1.3. The test channel for this project has a ratio ranging from 0.1 to 0.03. In cases where the ratio is less than 1, Formica (1955) found that the coefficients reduce to about 0.1.

Henderson (1966) also cites the investigation work undertaken by Yarnell (1934b) in connection with bridge piers. This work indicated a larger coefficient of 0.35 for a square-edged contraction and did not report the relationship of this coefficient to the depth : width ratio.

For the purposes of this project a value of between 0.1 and 0.35 is considered to represent the dynamic head loss coefficient due to contraction of the flow based on both Yarnell (1934b) and Formica (1955) as presented in Henderson (1966). Both these values are used to provide a range of contraction coefficients.

### 8.2.3 Dynamic Head Loss Coefficient

Dynamic head loss coefficients due to both contraction and expansion of flow through the constriction are presented in Table 8–2 and Figure 8-2. Two contraction coefficients (0.1 and 0.35) have been used to calculate the head loss coefficients provided in this table. The actual coefficient provided in Table 8–2 is calculated using the average contraction coefficient (0.225) with a range provided. Note that the range is specified as ± 0.13 for all values provided.

**Table 8–2 Dynamic Head Loss Coefficients (Henderson, 1966)**

| Width of Constriction (m) | Dynamic Head Loss Coefficients ($v^2/2g$) ± 0.13 | | | | |
|---|---|---|---|---|---|
| | Flow ($m^3/s$) | | | | |
| | 30 | 60 | 120 | 240 | 480 |
| 15 | 1.13 | 1.13 | 1.13 | - | - |
| 30 | 1.04 | 1.04 | 1.04 | 1.04 | - |
| 60 | 0.87 | 0.87 | 0.87 | 0.87 | 0.87 |

- not presented to remain consistent with other methods

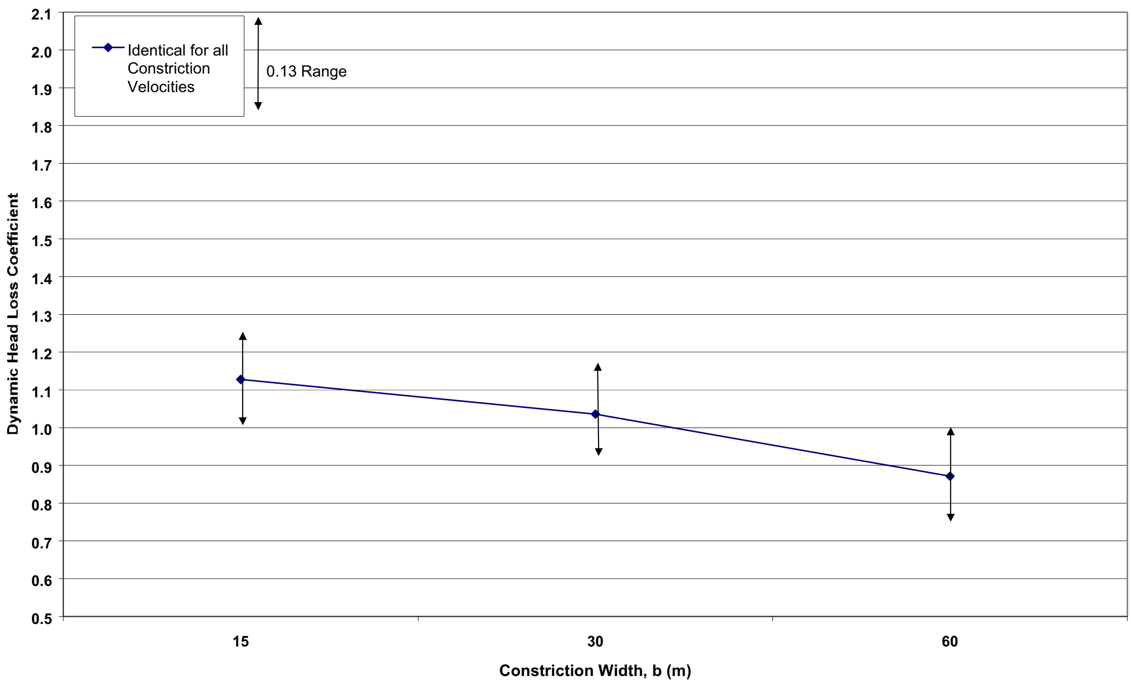


**Figure 8-2 Dynamic Head Loss Coefficients (Henderson, 1966)**

### 8.2.4 Discussion

The dynamic head loss coefficients calculated according to Henderson (1966) are relatively low even accounting for the potential range in values. Henderson (1966) provides a summary of theoretical and empirical techniques developed in other studies. A more detailed assessment of these studies may provide and explanation for these results. However, it is beyond the scope of this study to investigate this further.

## 8.3 Waterway Design

AUSTROADS (1994) has produced the manual entitled *Waterway Design – A Guide to the Hydraulic Design of Bridges, Culverts and Floodways*. AUSTROADS is the national association of road transport and traffic authorities in Australia. The manual is written to provide a guide to good practice for engineers involved in the design of waterway structures. The chapter on bridges contained within the manual is based on *Hydraulics of Bridge Waterways* by Bradley (1978). The empirical methods presented for calculating energy losses through bridge structures are based upon results of model tests verified by measurements made at a number of bridges in the field during floods. For the purposes of this project it is assumed that the empirical relationships provided by AUSTROADS (1994) for bridge constrictions may be applied to the test model under consideration here to determine energy losses through the artificial constriction.

A number of parameters are needed to undertake the empirical methods presented. These are explained and evaluated in the following sections.

### 8.3.1 Parameters

**Bridge Opening Ratio**

The bridge opening ratio, M, defines the degree of flow constriction involved. As the channel cross-section in the test channel is regular in nature, the bridge opening ratio may be evaluated using the following equation. For the test channel the values of M range from 0.05 for the 15m width of constriction to 0.2 for the 60m width of constriction.

$$M = \frac{b}{B}$$

Where: B = total width of channel

b = width of constriction

**Kinetic Energy Coefficients**

The kinetic energy coefficients, $\alpha_1$ and $\alpha_2$ are introduced to account for the non-uniform velocity distribution occurring due to depth changes in a river channel. Due to the regular nature of the test channel considered here, it is sufficient to assume that $\alpha_1 = \alpha_2 = 1$.

**Backwater Coefficient**

The backwater coefficient, $K^*$, is evaluated using the base backwater coefficient, $K_b$, to which are added incremental coefficients to account for the effect of piers, eccentricity and skew. The base backwater coefficient is dependent on M, the bridge opening ratio and the type of abutment. $K_b$ is evaluated using empirical curves supplied by AUSTROADS (1994). As the test channel does not have any piers or exhibit any eccentricity or skewness to the flow, the incremental coefficients used to represent these physical characteristics may all be set to 0. Thus, in this case, $K^* = K_b$.

A set of three empirical curves are provided by AUSTROADS (1994) to evaluate $K_b$ and these are reproduced as Figure 8-3. The three curves relate to the wingwall formation. It is assumed that the lower curve be applied to the test channel to represent a 90° wingwall with a bridge length of 60m. However, this curve does not extend below a bridge opening ratio of 0.15. As the bridge opening ratio considered in the case of the test channel ranges from 0.05 to 0.2, the curve needs to be extrapolated below that presented. Thus, the validity of the value of $K_b$ obtained in this manner is questionable. It is estimated that the values of $K_b$ are within the range 3.5 to 2.5 for the 15m width of constriction to 60m width of constriction respectively.

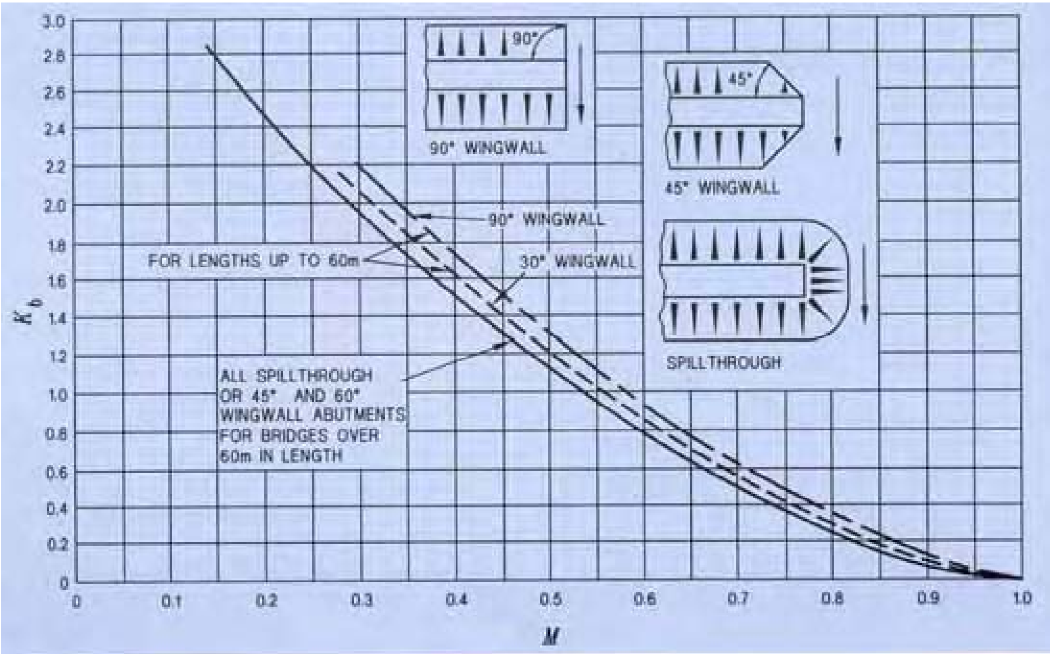


**Figure 8-3 Backwater Coefficient Base Curves from AUSTROADS (1994)**

### 8.3.2 Computation of Backwater

The expression provided by AUSTROADS (1994) for calculation of backwater has been formulated applying the principle of conservation of energy between the point of maximum backwater upstream from a bridge and a point downstream from a bridge at which normal stage has been established.

$$h_1^* = K^* \alpha_2 \frac{v_{cn}^2}{2g} + \alpha_1 \left[ \left( \frac{A_{cn}}{A_{ds}} \right)^2 - \left( \frac{A_{cn}}{A_{us}} \right)^2 \right] \frac{v_{cn}^2}{2g}$$

Where:

| | | |
|---|---|---|
| | $h_1^*$ | = total backwater (m) |
| | $K^*$ | = total backwater coefficient |
| | $\alpha_1$ and $\alpha_2$ | = kinetic energy coefficients = 1 |
| | $A_{cn}$ | = gross water area ($m^2$) in constriction below normal stage |
| | $v_{c2}$ | = average velocity (m/s) in constriction or $Q/A_{cn}$ |
| | $A_{ds}$ | = water area ($m^2$) downstream where normal stage is re-established |
| | $A_{us}$ | = water area ($m^2$) upstream where normal stage is re-established |

To compute backwater it is first necessary to obtain an approximate value of $h_1^*$ as the value of $A_{ds}$ is dependent on $h_1^*$. This approximation is calculated by using the first term of the above equation.

### 8.3.3 Contraction and Expansion Losses

The total backwater evaluated according the above AUSTROADS (1994) procedure will include energy losses due to contraction, expansion and friction. In order to assess the contraction and expansion losses only, the friction losses are removed from the total backwater obtained. Friction losses for the test channel are evaluated by manual methods as described in Appendix A.

The contraction and expansion losses are provided in Table 8–3. Dynamic losses are provided in Table 8–4 and shown in Figure 8-4.

**Table 8–3 Waterway Design - Evaluation of Contraction and Expansion Losses**

| Width of Constriction (m) | Discharge ($m^3/s$) | Bridge Opening Ratio, M | Backwater Coefficient, $K^*$ | Total Backwater, $h_1$* (m) | Contraction & Expansion Loss (mm) |
|---|---|---|---|---|---|
| 15 | 30 | 0.05 | 3.2 [a] | 0.16 [a] | 161 |
| | 60 | 0.05 | 3.2 [a] | 0.65 [a] | 651 |
| | 120 | 0.05 | 3.2 [a] | 2.61 [a] | 2609 |
| 30 | 30 | 0.1 | 3.1 [a] | 0.04 [a] | 38 |
| | 60 | 0.1 | 3.1 [a] | 0.16 [a] | 156 |
| | 120 | 0.1 | 3.1 [a] | 0.63 [a] | 631 |
| | 240 | 0.1 | 3.1 [a] | 2.53 [a] | 2533 |
| 60 | 30 | 0.2 | 2.4 | 0.01 | 6 |
| | 60 | 0.2 | 2.4 | 0.03 | 29 |
| | 120 | 0.2 | 2.4 | 0.12 | 123 |
| | 240 | 0.2 | 2.4 | 0.49 | 492 |
| | 480 | 0.2 | 2.4 | 1.98 | 1981 |

[a] As explained in Section 8.3.1, these values are based on the extrapolation of the $K_b$ curves in AUSTROADS (1994) and are thus questionable.

**Table 8–4 Dynamic Head Loss Coefficients (AUSTROADS, 1994)**

| Width of Constriction (m) | Dynamic Head Loss Coefficients ($v_c^2$ /2g) Flow ($m^3/s$): 30 | 60 | 120 | 240 | 480 |
|---|---|---|---|---|---|
| 15 | 3.16 [a] | 3.19 [a] | 3.20 [a] | - | - |
| 30 | 2.95 [a] | 3.06 [a] | 3.09 [a] | 3.11 [a] | - |
| 60 | 1.78 | 2.25 | 2.40 | 2.41 | 2.43 |

[a] As explained in Section 8.3.1, these values are based on the extrapolation of the $K_b$ curves in AUSTROADS (1994) and are thus questionable.

- not presented to remain consistent with other methods

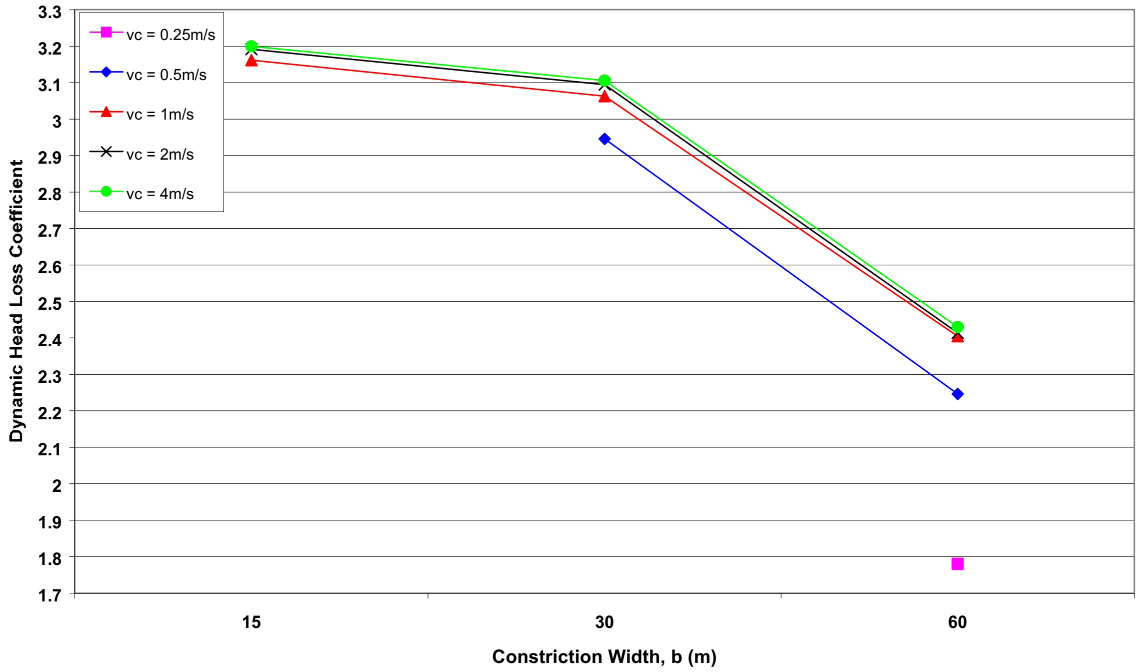


**Figure 8-4 Dynamic Head Loss Coefficients (AUSTROADS, 1994)**

### 8.3.4 Discussion

The dynamic head loss coefficients using AUSTROADS (1994) are extremely high. It is beyond the scope of this study to fully investigate the reasons for this. However, it is believed that the following points may contribute:

- The AUSTROADS (1994) curves have been extrapolated to produce the results for the 15m and 30m width of constriction.
- Original data used to produce these curves (Bradley, 1978) indicates that loss coefficients obtained from model studies are much less than those obtained from field measurements. The reason for this is not discussed within Bradley (1978) but may be worth further investigation.
- Data presented in Mattai (1976) (refer to Section 8.4) indicates that the original loss coefficients are much lower than those presented by Bradley (1978). However, Bradley (1978) does not discuss why the coefficients had been altered in the intervening two years. Again, this may be worth further investigation.

## 8.4 Other Manual Methods

French (1985) cites Yarnell (1934a & b), Henderson (1966) and Mattai (1976) as providing guidance on head losses through bridge contractions. Recommendations by Henderson(1966) have been discussed in Section 8.2.

Recommendations by Yarnell (1934a & b) have been briefly discussed in Section 8.2.2. The majority of investigations undertaken by Yarnell(1934) are in relation to the increase in upstream depth due to the presence of **bridge piers** in a crossing. Thus the majority of results and empirical equations developed by Yarnell (1934a and b) are not applicable to this project except where previously described.

Mattai (1976) undertook detailed investigations on bridge contractions and their effect on upstream water levels. In developing extensive empirical relationships and charts, Mattai's work in 1976 forms the basis for the updated standards developed by Bradley (1978) and incorporated into the Australian guidelines developed by AUSTROADS (1994). Methods recommended by AUSTROADS (1994) have been described and utilised in Section 0.

# 9 COMPARISON OF ALL COMPUTATION METHODS

One of the three primary objectives of this study is to assess the ability of 2D models in predicting energy losses through an abrupt constriction. In order to quantitatively assess this ability, energy losses predicted by 1D models and calculated using manual techniques are compared to those losses predicted by the 2D models. These energy losses are expressed as dynamic head loss coefficients and are presented together in Figure 9-1.

As discussed in Section 1.4.2, the aim was to assess the 2D model predictions against a goal standard for energy losses through a constriction. However, a reliable goal standard was not found. The two manual calculation methods utilised (AUSTROADS, 1994 and Henderson, 1966) produced significantly different results. The 1D models also produced a relatively broad range of dynamic head loss coefficients.

The following points should be remembered when assessing Figure 9-1:

- Values for Waterway Design for constriction widths of 15m and 30m are based on parameters selected by extrapolation of the curves presented by AUSTROADS (1994) The reliability of values produced is questionable (refer to Section 8.3).
- Values for Henderson are based on both theoretical and empirical methods presented by Henderson (1966). It is recommended that the original source of these methods be further investigated as the values appear low. In addition, an "uncertainty" band of ±0.13 should be applied to the values presented here (refer to Section 8.2).
- Values for MIKE 11 are based on predictions from the MIKE 11 1D model. The high value presented may be considered an outlier as it occurs at the lowest value of $v_c$. It is believed that dynamic head loss coefficients are very sensitive at low values of $v_c$ (refer to Section 6).
- Values from HEC-RAS are based on predictions from the HEC-RAS 1D model. HEC(1998) have undertaken substantial research into losses through constrictions and is able to provide significant direction in developing a suitable and reliable model layout. Energy losses for average constriction velocities of 4m/s are very sensitive to changes in model layout and results at these velocities should be treated with caution (refer to Section 7 and Appendix C).
- TUFLOW values are based on predictions from the TUFLOW 2D model. The values exhibit a trend of increasing dynamic head loss coefficients with increasing spatial resolution. The highest value for the 1m grid may be treated as an outlier as it occurs at the lowest value of $v_c$. It is believed that dynamic head loss coefficients are very sensitive at low values of $v_c$ (refer to Section 3).
- RMA2 values are based on predictions from the RMA2 2D model. The values are relatively constant for the finest two mesh resolutions utilised. The trend for the coarser mesh resolutions appears to indicate that the dynamic head losses coefficients decrease with increasing spatial resolution (refer to Section 4).

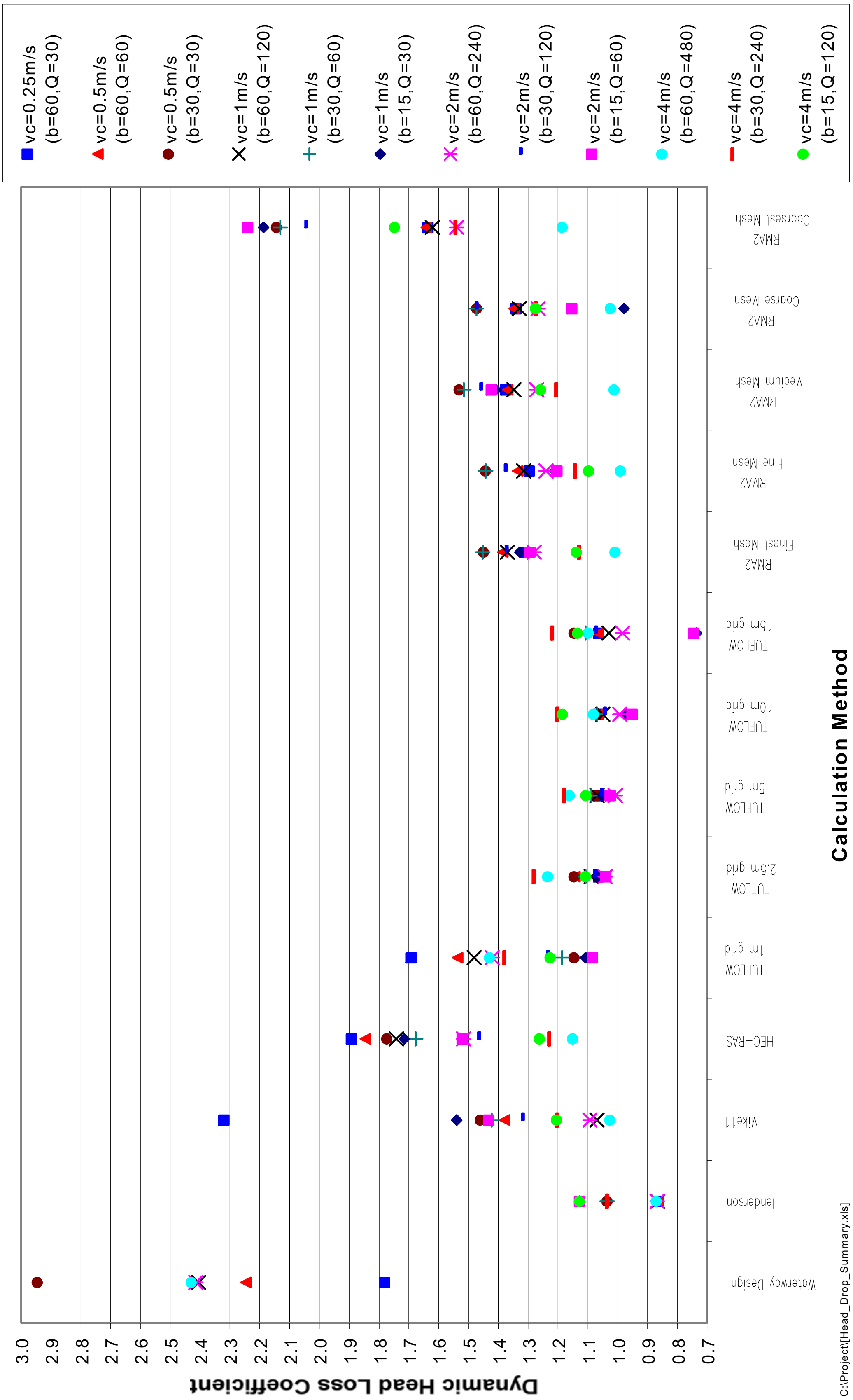


**Figure 9-1 Dynamic Head Loss Coefficients – All Calculation Methods**

# 10 CONCLUSIONS AND RECOMMENDATIONS

A summary of conclusions and recommendations arising from this study are provided below:

- Numerous methods can be used to estimate and predict energy losses through an abrupt constriction. The methods utilised here include manual methods (theoretical and empirical), 1D models and 2D models.
- On the basis of this study, none of the methods tested appear worthy of becoming a "goal standard" against which other methods may be compared. Although it was initially intended that a combination of the manual methods and the 1D models provide such a standard, the range of results for these methods, and remaining uncertainties, meant that this intention was not able to be fulfilled. Further investigation is needed to determine a suitable and reliable "goal standard" such that this type of comparison may be made.
- The spatial resolution of 2D models has an impact on their predictive ability. The nature of the impact is closely related to the technique used to evaluate the eddy viscosity. Further work is needed to investigate this impact to determine the most suitable eddy viscosity formulation technique for use with each model.
- For the 2D model TUFLOW, the higher resolution models produce higher dynamic head loss coefficients. This is a direct result of the ability of the higher resolution models to more accurately portray turbulent losses.
- For the 2D model, RMA2, the higher resolution models produce lower dynamic head loss coefficients. However, further investigation is needed to determine if this trend continues at finer mesh resolutions as the trend is not evident at the two finest mesh resolutions considered in this study.

# 11 REFERENCES

**Abbot, M.B. (1979),** "Computational Hydraulics – Elements of the Theory of Free Surface Flows", Pitman Publishing Limited, London, UK.

**AUSTROADS (1994), "**Waterway Design", *A Guide to the Hydraulic Design of Bridges Culverts and Floodways*, Austroads Publication AP-23/94, 1994.

**Bradley, J.N. (1978),** *Hydraulics of Bridge Waterways*, Hydraulic Design Series No 1, US Federal Highway Administration, Washington DC.

**Chow, V.T. (1959),** *Open Channel Flow*, McGraw Hill Book Company, New York.

**Crowder, D.W., and Diplas, P. (2000), "**Using Two-Dimensional Hydrodynamic Models at Scales of Ecological Importance", *Journal of Hydrology*, No. 230, p172-191.

**Cunge, J.A., Holly, F.M., and Verwey, A. (1980),** *Practical Aspects of Computational River Hydraulics*, Pitman Publishing, 1980.

**DHI (1992)**, "MIKE11 Users and Reference Manual", Version 3.01.

**DHI (1998)**, "MIKE21 Users Manual"

**DHI (2000)**, "MIKE11 Users and Reference Manual", Version 2000.

**El-Sherwey, M.I.A., Joshi, S.G., and Sharma, S.D. (1996),** "A Study of Turbulent Flows Through Sudden Open Channel Transitions Using Laser Doppler Velocimetery", *Proceedings Fluids Engineering Division Conference* Volume 2, FED-Vol. 237, ASME.

**Farajalla, R.A., and Vieux, B.E. (1995),** "Capturing the essential spatial variability in distributed hydrological modelling: Infiltration parameters", *Hydrological Proceedings No 9*, p55-68.

**FHA**, "Finite Element Surface-Water Modelling System Two Dimensional Flow in a Horizontal Plane, Version 2 Users Manual", US Department of Transportation, Federal Highway Administration.

**Formica, G. (1955),** *Preliminary Tests on Head Losses in Channels due to Cross-sectional Changes*, L'Energia Elletrica, Milan, vol. 32, no.7, p554, July 1995.

**French, R.H. (1985),** *Open Channel Hydraulics*, McGraw Hill Book Company.

**Hardy. R.J., Bates, P.D., and Anderson, M.G. (1999), "**The Importance of Spatial Resolution in Hydraulic Models for Floodplain Environments", *Journal of Hydrology*, No. 216, p124-136.

**HEC (1995),** RD-42, "Flow Transitions in Bridge Backwater Analysis, U.S. Army Corp of Engineers, Hydraulic Engineering Centre, Davis CA., September 1995.

**HEC (1998),** *HEC-RAS River Analysis System – Hydraulic Reference Manual Version 2.2*, U.S. Army Corps of Engineers, Hydraulic Engineering Centre, August 1998.

**Henderson, F.M. (1966),** *Open Channel Flow*, MacMillan Publishing Co.,1966.

**Hunt, J., Brunner, G.W., Larock, B.E. (1999),** "Flow Transitions in Bridge Backwater Analysis", *Journal of Hydraulic Engineering*, Vol. 125, No. 9, September 1999.

**King, I.P. (1994),** *RMA-2 Two-dimensional Finite Element Hydrodynamic Model,* Resource Management Associates, Lafayette, Calif. 1994.

**King, I.P. (1998),** "RMA-2 Users Manual"

**Mattai, H.F. (1976), "**Measurement of Peak Discharge at Width Contractions by Indirect Methods", *Techniques of Water-Resources Investigations of the United States Geological Survey*, U.S. Geological Society, Washington. 1976.

**McCutcheon, S.C. (1989),** *Water Quality Modeling, Vol. 1, Transport and Surface Exchange in Rivers*, CRC, Boca Raton, FL.

**Martin, J.L. and McCutcheon, S.C. (1999),** *Hydrodynamics and Transport for Water Quality Modeling*, CRC Press, 1999.

**Nielsen, C.F. (2000),** *Finite Element Modelling in a Coastal and Marine Environment*, Master of Engineering Science by Research, Department of Civil Engineering, University of Queensland, 2000.

**Nielsen, C.F. (1990),** *A 2D Hydrodynamic Model of Cleveland Bay*, Bachelor of Engineering Thesis, Civil and Systems Engineering, James Cook University, 1990.

**Rodi, W. (1980),** *Turbulence Models and Their Application in Hydraulics – A State of the Art Review*, International Association for Hydraulic Research, Delft, Netherlands, 1980.

**Secklin, G., Yurtal, R. and Haktanir, T. (1998), "**Contraction and Expansion Losses Through Bridge Constrictions", *Journal of Hydraulic Engineering*, p 546-549, May 1998.

**Smagorinsky, J. (1963),** "General Circulation Experiments with the Primitive Equations", *Monthly Weather Review*, Vol. 91, pp91-164, 1963.

**Stelling, G.S. (1984),** *On the Construction of Computational Methods for Shallow Water Flow Problems*, Rijkswaterstaat Communications, No 35/1984, The Hague, The Netherlands.

**Syme, W.J. (1991),** *Dynamically Linked Two-Dimensional / One-Dimensional Hydrodynamic Modelling Program for Rivers, Estuaries and Coastal Waters*, William Syme, M.Eng.Sc (Research) Thesis, University of Queensland, May 1991.

**Syme, W.J., Nielsen, C.F, Charteris, A.B. (1998),** "Comparison of Two-Dimensional Hydrodynamic Modelling Systems: Part One – Flow Through a Constriction", *Proceedings of HydraStorm '98*, Adelaide, September, 1998.

**Walden, W.J., Syme, W.J., Charteris, A.B., Nielsen, C.F. (1999), "**Integrating Complex Hydraulic Models and GIS – A Powerful Management Tool", *Proceedings Wangaratta Floodplains - Risks and Rewards Conference*, 1999.

**WBM Oceanics Australia (2000),** *TUFLOW Users Manual*, WBM Oceanics Australia, Spring Hill, 2000.

**Wright, N.G. (2001), "**Conveyance implications for 2D and 3D Modelling", *Scoping Study for Reducing Uncertainty in River Flood Conveyance*, H.R. Wallingford and UK Environment Agency, March 2001.

**Yarnell, D.L. (1934a)**, "Pile Trestles as Channel Obstructions", Technical Bulletin 429, U.S. Department of Agriculture, Washington, July 1934.

**Yarnell, D.L. (1934b)**, "Bridge Piers as Channel Obstructions", Technical Bulletin 442, U.S. Department of Agriculture, Washington, November 1934.

# CONTENTS OF APPENDICES

# LIST OF FIGURES



# LIST OF TABLES

# A FRICTIONAL LOSSES

## A.1 Introduction

The total energy loss across the test channel is comprised of frictional losses, contraction losses and expansion losses. Frictional losses occur across the full length of the test channel. These occur due to bed friction and in some cases wall friction. Bed roughness in the test channel has been given a low Manning's value of 0.025 in order to limit the losses due to friction and ensure that other impacts, such as that of eddy viscosity, are evident.

As this study is focussed on the losses due to the contraction and expansion of flow through the constriction, it is beneficial to consider these losses separately. Thus, frictional losses have been estimated so that they may be removed from the total energy loss to give constriction losses.

The advantage of removing friction losses is that it allows comparisons between calculation methods to be made based on constriction losses alone. The disadvantage of removing these losses is that they are only estimates and there is some potential that their removal may result in inaccuracies. Potential inaccuracies and their effect are discussed in the main body of text in relation to each method.

## A.2 Estimation of Friction Losses

Friction losses have been estimated using Manning's equation:

$$v = \frac{R^{2/3} S_f^{1/2}}{n}$$

Where: v = velocity

R = hydraulic radius (A/P)

$S_f$ = friction slope

N = Manning's n (n=0.025 for the test channel)

The head loss due to friction is:

$$\Delta h_f = S_f L$$

Where: $\Delta h_f$ = head loss due to friction

$S_f$ = friction slope

L = length of reach

Thus, the head loss due to friction using the above two equations becomes:

$$\Delta h_f = \frac{v^2 n^2 L}{R^{4/3}}$$

As the friction loss is dependent on the velocity, the test channel has been divided into three sections to provide a better estimation of losses. These three sections are the upstream reach, the constriction, and the downstream reach. In each of these reaches, average velocities for each flow rate for each constriction width were calculated. In the upstream reach the average increase in water level for each flow rate for each constriction width across all calculation methods was used to estimate the average velocity. Estimations of friction losses are provided in Table A-1. The relative magnitude of frictional losses in relation to the total energy loss is provided in Table A-2.

**Table A-1 Friction Loss Estimates**

| b | Flow ($m^3/s$) | $v_c$ | Friction Losses (mm) Upstream Reach | Constriction | Downstream Reach | Total |
|---|---|---|---|---|---|---|
| 15 | 30 | 1 | 0 | 15 | 1 | 16 |
| | 60 | 2 | 0 | 60 | 2 | 62 |
| | 120 | 4 | 1 | 238 | 8 | 247 |
| | 240 | 8 | - | - | - | - |
| | 480 | 16 | - | - | - | - |
| 30 | 30 | 0.5 | 0 | 4 | 1 | 4 |
| | 60 | 1 | 1 | 15 | 2 | 18 |
| | 120 | 2 | 2 | 60 | 8 | 70 |
| | 240 | 4 | 3 | 238 | 33 | 274 |
| | 480 | 8 | - | - | - | - |
| 60 | 30 | 0.25 | 0 | 1 | 1 | 2 |
| | 60 | 0.5 | 1 | 4 | 2 | 6 |
| | 120 | 1 | 2 | 15 | 8 | 26 |
| | 240 | 2 | 7 | 60 | 33 | 100 |
| | 480 | 4 | 12 | 238 | 131 | 381 |

- not calculated

**Table A-2 Frictional Losses Compared to Total Energy Losses**

| b | Flow ($m^3/s$) | $v_c$ | Friction Loss as a % of Total Energy Loss* |
|---|---|---|---|
| 15 | 30 | 1 | 12% to 41% |
| | 60 | 2 | 12% to 41% |
| | 120 | 4 | 15% to 27% |
| | 240 | 8 | - |
| | 480 | 16 | - |
| 30 | 30 | 0.5 | 15% to 32% |
| | 60 | 1 | 14% to 32% |
| | 120 | 2 | 14% to 32% |
| | 240 | 4 | 18% to 28% |
| | 480 | 8 | - |
| 60 | 30 | 0.25 | 22% to 45% |
| | 60 | 0.5 | 25% to 45% |
| | 120 | 1 | 24% to 47% |
| | 240 | 2 | 24% to 48% |
| | 480 | 4 | 28% to 45% |

* The range provided here is based on the minimum and maximum total energy loss computed by the 1D and 2D models used in this study.

## A.3 Discussion

As shown in Table A-1, friction losses through the constriction account for 60% to 97% of the total friction loss. This dominance is due to the dependence of friction loss on velocity which is significantly higher through the constriction. Table A-2 shows that the percentage of the total energy loss attributable to friction ranges from a minimum 12% to a maximum of 48%. This indicates that the results produced by removing the friction loss estimates may be sensitive to the magnitude of these estimates.

# B EDDY VISCOSITY

## B.1 Introduction

Turbulence often contributes a significant proportion of the overall dynamic energy loss in a river, creek or estuary. Turbulent eddies move water from one parcel of water into other parcels which have a different mean velocity, thereby changing the parcel velocity. The transfer of water caused by the turbulent eddies causes a net change in both momentum and mass. This Appendix concentrates on the net change of momentum as it is this aspect of turbulent eddies that is critical to this study.

The impact of turbulent eddies can be described as being analogous to the change caused by viscous shear for momentum transport, $\mu \frac{\partial_u}{\partial_z}$. By including the coefficient for eddy viscosity, the shear stress becomes:

$$\tau = (\mu + \varepsilon)\ \frac{\partial_u}{\partial_z}$$

Where:
- $\tau$ = shear stress
- $\mu$ = coefficient of molecular viscosity (usually significantly smaller than $\varepsilon$ and therefore typically neglected)
- $\varepsilon$ = coefficient of eddy viscosity
- $\frac{\partial_u}{\partial_z}$ = the velocity gradient

Rodi (1980) indicates that the difficulty associated with using the above analogy, is that eddy viscosity is not a property of a fluid but rather is dependent on the state of turbulence. The estimation of its value is what is known in fluid mechanics as the turbulence closure problem. As Reynolds averaging introduces an extra variable into the hydrodynamic equations, a semi-empirical process is needed to produce a closed set of equations (Martin *et al.*, 1999).

The influence of the eddy viscosity is highly dependent on the relative dominance of bed friction. As discussed in Section 2.1 and Appendix A, a low Manning's n of 0.025 has been chosen to limit the bed roughness impacts. A low value such as this will ensure that eddy viscosity impacts are evident.

# B.2 Use of Eddy Viscosity in 2D Models

The use of eddy viscosity in 2D numerical modelling provides an approximate representation of the energy losses due to **turbulent effects at sub-grid scale**.

## B.2.1 RMA2

In RMA2, the depth integrated turbulent viscosity terms in the momentum equation are:

**Momentum Equation X-Direction**

$$D\frac{\partial}{\partial_x}\left(\varepsilon_{xx}\frac{\partial_u}{\partial_x}\right)+D\frac{\partial}{\partial_y}\left(\varepsilon_{xy}\frac{\partial_u}{\partial_y}\right) \qquad \textit{Equation B-1}$$

Where: $\varepsilon_{xx}, \varepsilon_{xy}$ = turbulent exchange coefficients (eddy viscosity)

D = depth

x, y = horizontal Cartesian coordinates

u, v = horizontal velocity components in the x and y direction

RMA2 has three options for specifying the eddy viscosity as discussed in the following sections:

**Fixed Constant**

Values for the eddy viscosity may be input as fixed constants in units of Pa.s.

Care must be taken in utilising this option to ensure that the dimensions of mesh elements assigned a constant value are similar. As the mesh element size controls the resolution of eddies in the system, the use of a constant eddy viscosity across elements of different size will result in differences in the representation of turbulent effects (Nielsen, 2000).

**Scale Factor Based on Element Size and Shape**

The magnitude of the eddy viscosity in each element may be determined by assessment of the size and shape of each element (King, 1997).

**Smagorinsky Turbulence Closure (Smagorinsky, 1963)**

The Smagorinsky closure represents horizontal eddy viscosity in the model. The depth integrated turbulent viscosity terms in the momentum equation are:

*Momentum Equation X-Direction*

$$\frac{\partial}{\partial_x}\left(2A_m D\frac{\partial_u}{\partial_x}\right)+\frac{\partial}{\partial_y}\left(A_m D\frac{\partial_u}{\partial_y}+\frac{\partial_v}{\partial_x}\right)$$

Where: $A_m \quad = \alpha\left(Area\right)\left(\left(\frac{\partial u}{\partial x}\right)^2 + \left(\frac{\partial v}{\partial y}\right)^2 + 0.5\left(\frac{\partial u}{\partial y}+\frac{\partial v}{\partial x}\right)^2\right)^{0.5}$ *Equation B-2*

$\alpha$ = a coefficient (King, 1998 recommends a typical range of 0.01 to 0.5 with 0.2 being the default)

Area = area of current element

## B.2.2 TUFLOW

TUFLOW has three options for determining the eddy viscosity as described in the following sections.

**Fixed Constant**

Values for eddy viscosity may be input as a fixed constant that is used throughout the model. WBM (2000) indicates that this is satisfactory only when the grid size is much greater than the depth. Values of eddy viscosity of between $1m^2/s$ to $5m^2/s$ are recommended for use in TUFLOW (WBM, 2000). An eddy viscosity of 1000 Pa.s (RMA2) is equivalent to $1m^2/s$ multiplied by the density of water ($1000kg/m^3$).

**Empirical Scaling**

Based on empirical tests, the eddy viscosity is scaled by the amplitude of the local velocity vector. WBM (2000) provides no further details on this option.

**Smagorinsky Turbulence Closure (Smagorinsky, 1963)**

TUFLOW uses an approximation to the Smagorinsky formulation (WBM, 2000) as described in the MIKE21 manual (DHI, 1998). Relevant equations are provided below.

*Momentum Equation X-Direction*

$$E_g\left(\frac{\partial^2 p}{\partial x^2} + \frac{\partial^2 p}{\partial y^2}\right)$$

Where: $E_g \quad = C_g\left(Area\right)\left(\left(\frac{\partial u}{\partial x}\right)^2 + \left(\frac{\partial v}{\partial y}\right)^2 + 0.5\left(\frac{\partial u}{\partial y}+\frac{\partial v}{\partial x}\right)^2\right)^{0.5}$

$C_g$ = a coefficient (DHI (1998) recommends a typical range of 0.06 to 1.0)

Area = area of current element (ie grid length x grid length)

p = flux

### B.2.3 Comparison of RMA2 and TUFLOW by Nielsen (2000)

Nielsen (2000) found that a constant eddy viscosity of $1m^2/s$ in TUFLOW was equivalent to a constant eddy viscosity of 1000Pa.s in RMA both in terms of unit dimension and resulting model performance. Simulations undertaken by Nielsen (2000) showed comparable flow distributions, flow separations and eddy currents for both RMA2 and TUFLOW. Sensitivity testing was undertaken by Nielsen (2000) to determine the impact of increasing the eddy viscosity. He found that an increased eddy viscosity can enhance stability in the model, a phenomenon also discussed by DHI (1998). Nielsen (2000) noted that an increase in the eddy viscosity produced visually recognisable differences in the flow patterns of the test model as turbulent effects were dampened. In one simulation, Nielsen (2000) used a constant eddy viscosity and tested the sensitivity of results by increasing the eddy viscosity value tenfold (from 1000Pa.s to 10000Pa.s). In this case, visual inspection of the flow patterns revealed that eddy formation was significantly reduced. In another simulation, Nielsen (2000) used the Smagorinsky formulation and tested the sensitivity of results to a tenfold increase in the $\alpha$ factor (from 0.05 to 0.5). In this case, visible differences in the flow patterns were small with eddy formation still evident. Nielsen (2000) concluded the value of the $\alpha$ factor does not appear to affect the formation of eddies in the simulation to the extent that changing the absolute eddy viscosity values does.

## B.3 The Smagorinsky Formulation

It is believed that the reason for the phenomena identified by Nielsen (2000) (refer to Section B.2.3) may be the buffering capacity offered by the velocity gradient and element area terms in the Smagorinsky equations. That is, when using the Smagorinsky formulation, the eddy viscosity is proportional to the velocity gradient, the area of the element and the $\alpha$ factor. High velocity areas where the velocity gradient is high produce a relatively high eddy viscosity when compared to lower velocity areas where the velocity gradient is lower. Thus, in a numerical model, ignoring other effects, one would expect to see a relatively low eddy viscosity in areas of low velocity when the Smagorinsky formulation is used. A tenfold increase in the $\alpha$ factor, as tested by Nielsen (2000), would be expected to result in a tenfold increase in the eddy viscosity throughout the model. However, as eddies typically form in lower velocity "backwater" areas, a tenfold increase in the relatively low local eddy viscosity may not be visible within the flow patterns.

An additional complication to the above theory arises when the influence of the element area is considered. In finite element models, such as RMA2, element size can vary across the model domain. It is standard practice in developing such models that regions of rapidly varied flow or of particular interest contain an increased mesh density and vice versa. That is, the area of an element in a region of high velocity is typically smaller than the area of an element in a region of low velocity (unless it is a region of particular interest). As the Smagorinsky formulation of eddy viscosity is also proportional to element area, an interesting buffering effect may occur between the velocity gradient and the element area. For a finite difference model with a regular grid, such as TUFLOW, this additional effect would not occur as the element area remains constant across the entire model domain.

# B.4 Sensitivity Testing

All RMA2 model simulations were performed using the Smagorinsky formulation to represent the eddy viscosity. Several references recommend this approach for finite element models if there is significant variation in mesh density across the model domain (Nielsen, 2000; King, 1998). In these simulations a default value of 0.2 for the $\alpha$ factor was used (as recommended in King, 1998). Sensitivity simulations were also undertaken on the full range of RMA2 models using the constant eddy viscosity approach with a eddy viscosity of 1000Pa.s. This is equivalent to an eddy viscosity of $1.0m^2/s$ as used in the TUFLOW sensitivity simulations (refer to Section B.2.3 and Nielsen, 2000).

Similarly, all TUFLOW simulations were performed using the Smagorinsky formulation to represent the eddy viscosity. TUFLOW simulations of floodplain environments are typically undertaken using the constant eddy viscosity approach (verbal communication with developer, Syme (1991)). However, WBM (2000) recommends that the constant eddy approach is only satisfactory when the grid size is much greater than the depth. For the test channel considered here, the grid size (from 1m to 15m) is not consistently much greater than the depth (2m). Thus, the Smagorinsky formulation has been used with $C_g$ set to 0.2 (the TUFLOW $C_g$ is equivalent to $\alpha$ in RMA2). However, a complete set of sensitivity simulations using the constant eddy viscosity approach with the eddy viscosity set to the recommended value of $1.0m^2/s$ have been undertaken. This double simulation set allows the sensitivity of the dynamic head loss coefficient results to the eddy viscosity formulation to be assessed.

## B.4.1 RMA2 Constant Eddy Viscosity Sensitivity Simulations

### *B.4.1.1 Results*

As discussed in the preceding section, sensitivity simulations were undertaken with the full range of RMA2 models using the constant eddy viscosity approach. An eddy viscosity of 1000 Pa.s was used (equivalent to $1m^2/s$). A summary of the simulations is shown in Table B-1.

**Table B-1 RMA2 - Sensitivity Simulations Summary**

| Width of Constriction (m) | Mesh Density | Flow | | | | |
|---|---|---|---|---|---|---|
| | | 30m$^3$/s | 60m$^3$/s | 120m$^3$/s | 240m$^3$/s | 480m$^3$/s |
| 15 | Mesh 5 (Finest) | ✓ | × | × | × | × |
| | Mesh 4 (Fine) | ✓ | ✓ | ✓ | × | × |
| | Mesh 3 (Medium) | ✓ | ✓ | × | × | × |
| | Mesh 2 (Coarse) | ✓ | ✓ | ✓ | × | × |
| | Mesh 1 (Coarsest) | ✓ | ✓ | × | × | × |
| 30 | Mesh 5 (Finest) | ✓ | ✓ | ✓ | × | × |
| | Mesh 4 (Fine) | ✓ | ✓ | ✓ | × | × |
| | Mesh 3 (Medium) | ✓ | ✓ | ✓ | ✓ | × |
| | Mesh 2 (Coarse) | ✓ | ✓ | ✓ | ✓ | × |
| | Mesh 1 (Coarsest) | ✓ | ✓ | ✓ | ✓ | × |
| 60 | Mesh 5 (Finest) | ✓ | ✓ | ✓ | ✓ | × |
| | Mesh 4 (Fine) | ✓ | ✓ | ✓ | ✓ | × |
| | Mesh 3 (Medium) | ✓ | ✓ | ✓ | ✓ | × |
| | Mesh 2 (Coarse) | ✓ | ✓ | ✓ | ✓ | × |
| | Mesh 1 (Coarsest) | ✓ | ✓ | ✓ | ✓ | × |

× Simulation did not run to completion due to instabilities

✓ Simulation ran to completion

Average Velocity in Constriction, $v_c$

| 0.25m/s | 0.5m/s | 1m/s | 2m/s | 4m/s | 8m/s | 16m/s |
|---|---|---|---|---|---|---|

The RMA2 models typically became less stable when using the constant eddy viscosity approach as evident when comparing Table B-1and Table 4-1. The dynamic head loss coefficients without frictional losses are presented in Table B-2 and graphically in Figure B-1. Figure B-2 contains a comparison of results obtained using both the constant eddy viscosity approach (Table B-2) and the Smagorinksy formulation approach (Table 4-3).

**Table B-2 RMA2 - Sensitivity Simulations – Dynamic Head Loss Coefficients**

| Width of Constriction (m) | Mesh Density | Flow | | | | |
|---|---|---|---|---|---|---|
| | | 30m$^3$/s | 60m$^3$/s | 120m$^3$/s | 240m$^3$/s | 480m$^3$/s |
| 15 | Mesh 5 (Finest) | 1.91 | - | - | - | - |
| | Mesh 4 (Fine) | 1.54 | 1.19 | 1.03 | - | - |
| | Mesh 3 (Medium) | 1.35 | 1.10 | - | - | - |
| | Mesh 2 (Coarse) | 0.58 | 0.61 | 1.20 | - | - |
| | Mesh 1 (Coarsest) | 0.58 | 0.60 | - | - | - |
| 30 | Mesh 5 (Finest) | 2.24 | 1.67 | 1.34 | - | - |
| | Mesh 4 (Fine) | 1.97 | 1.48 | 1.22 | - | - |
| | Mesh 3 (Medium) | 1.69 | 1.29 | 1.11 | 1.05 | - |
| | Mesh 2 (Coarse) | 1.23 | 0.91 | 0.82 | 1.05 | - |
| | Mesh 1 (Coarsest) | 0.84 | 0.59 | 0.62 | 1.01 | - |
| 60 | Mesh 5 (Finest) | 2.36 | 1.78 | 1.47 | 1.24 | - |
| | Mesh 4 (Fine) | 2.15 | 1.62 | 1.33 | 1.14 | - |
| | Mesh 3 (Medium) | 1.82 | 1.36 | 1.14 | 1.01 | - |
| | Mesh 2 (Coarse) | 1.61 | 1.21 | 0.99 | 0.88 | - |
| | Mesh 1 (Coarsest) | 1.18 | 0.84 | 0.70 | 0.66 | - |

- no result due to model instability

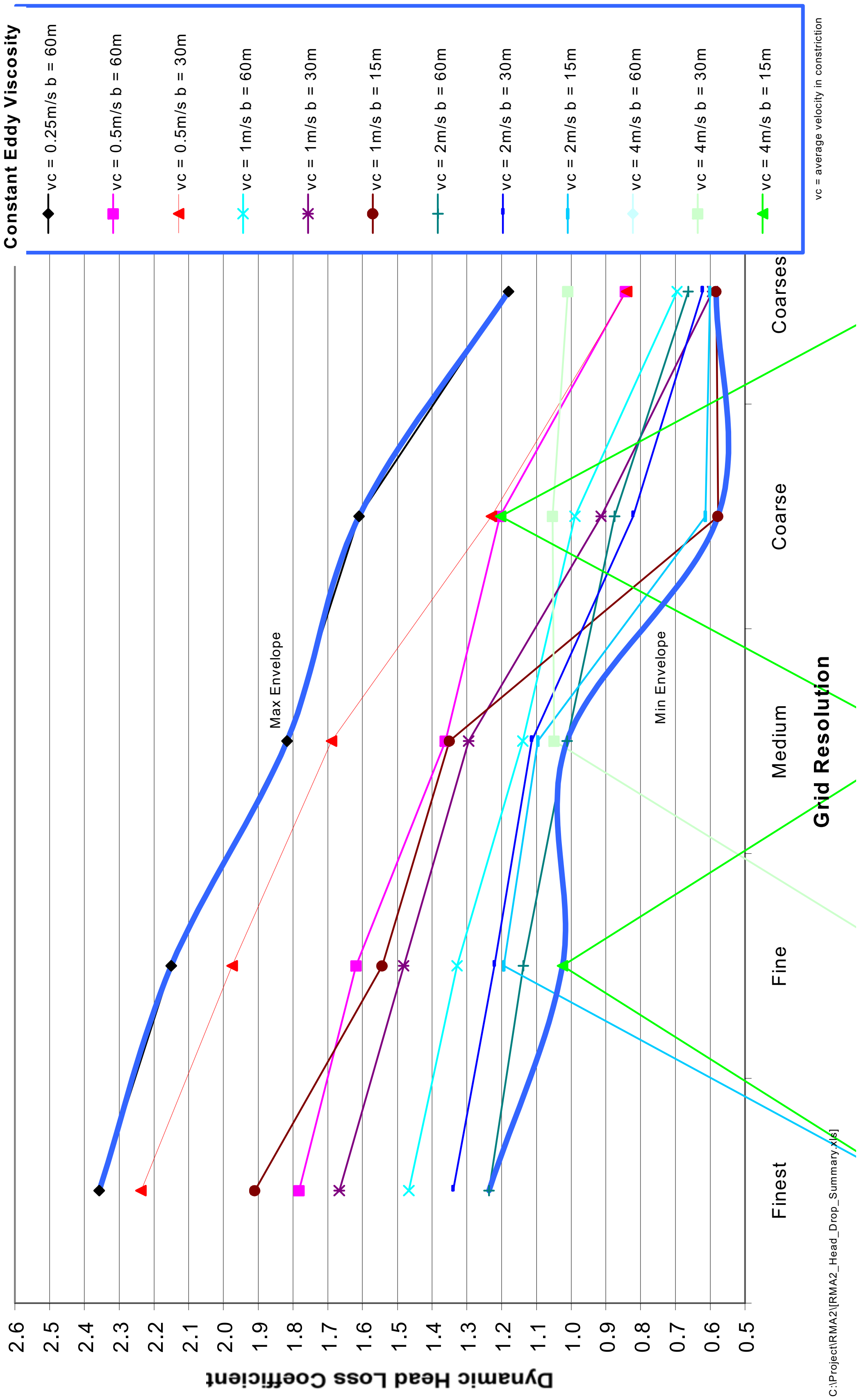


**Figure B-1 RMA2 - Sensitivity Simulations – Dynamic Head Loss Coefficients**

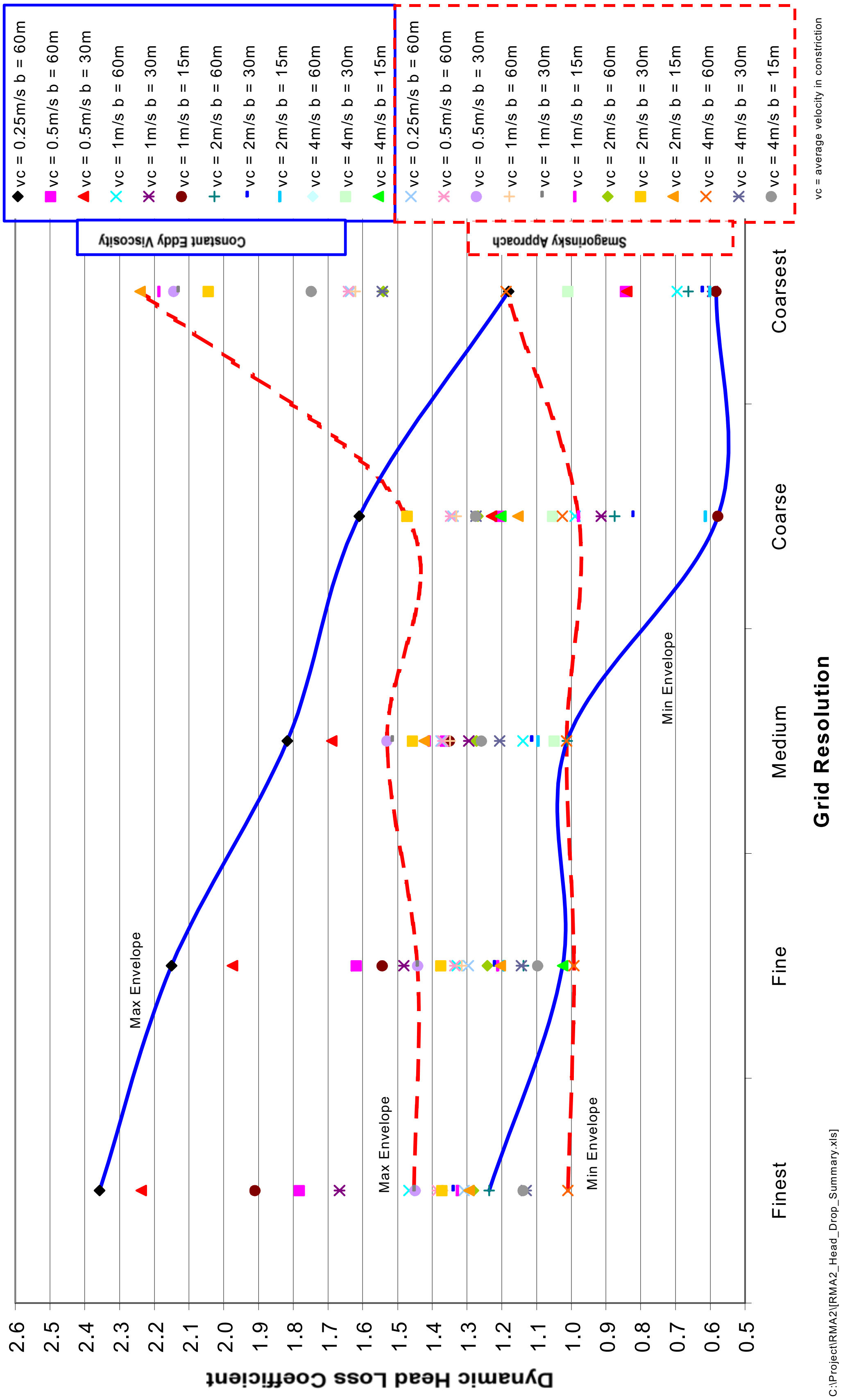


**Figure B-2 RMA2 - Dynamic Head Loss Coefficients - Comparison of Eddy Viscosity Approaches**

## B.4.2 TUFLOW Constant Eddy Viscosity Sensitivity Simulations

### *B.4.2.1 Results*

As discussed in Section B.4, sensitivity simulations were undertaken with the full range of TUFLOW models using the constant eddy viscosity approach. An eddy viscosity of $1m^2/s$ (equivalent to a value in RMA2 of 1000 Pa.s) was used. A summary of the simulations is shown in Table B-3.

**Table B-3 TUFLOW - Sensitivity Simulations Summary**

| Width of Constriction (m) | Grid Dimension | Flow | | | | |
|---|---|---|---|---|---|---|
| | | $30m^3/s$ | $60m^3/s$ | $120m^3/s$ | $240m^3/s$ | $480m^3/s$ |
| 15 | 1m Grid | ✓ | ✓ | ✓ | × | × |
| | 2.5m Grid | ✓ | ✓ | ✓ | × | × |
| | 5m Grid | ✓ | ✓ | ✓ | × | × |
| | 10m Grid | ✓ | ✓ | ✓ | × | × |
| | 15m Grid | ✓ | ✓ | ✓ | × | × |
| 30 | 1m Grid | ✓ | ✓ | ✓ | ✓ | × |
| | 2.5m Grid | ✓ | ✓ | ✓ | ✓ | × |
| | 5m Grid | ✓ | ✓ | ✓ | ✓ | × |
| | 10m Grid | ✓ | ✓ | ✓ | ✓ | × |
| | 15m Grid | ✓ | ✓ | ✓ | ✓ | × |
| 60 | 1m Grid | ✓ | ✓ | ✓ | ✓ | ✓ |
| | 2.5m Grid | ✓ | ✓ | ✓ | ✓ | ✓ |
| | 5m Grid | ✓ | ✓ | ✓ | ✓ | ✓ |
| | 10m Grid | ✓ | ✓ | ✓ | ✓ | ✓ |
| | 15m Grid | ✓ | ✓ | ✓ | ✓ | ✓ |

× Simulation did not run to completion due to instabilities

✓ Simulation ran to completion

Average Velocity in Constriction, $v_c$

| 0.25m/s | 0.5m/s | 1m/s | 2m/s | 4m/s | 8m/s | 16m/s |
|---|---|---|---|---|---|---|

TUFLOW simulations exhibited the same stability in completing model runs regardless of eddy viscosity approach (that is, the same simulations did not run to completion due to instabilities). This is evident by comparing Table B-3 and Table 3-1. The dynamic head loss coefficients without frictional losses are presented in Table B-4 and graphically in Figure B-3. Figure B-4 compares results achieved using the constant eddy viscosity approach with those achieved using the Smagorinsky approach.

**Table B-4 TUFLOW - Sensitivity Simulations – Dynamic Head Loss Coefficients**

| Width of Constriction (m) | Grid Dimension | Flow | | | | |
|---|---|---|---|---|---|---|
| | | $30m^3/s$ | $60m^3/s$ | $120m^3/s$ | $240m^3/s$ | $480m^3/s$ |
| 15 | 1m Grid | 1.79 | 1.36 | 1.27 | - | - |
| | 2.5m Grid | 1.44 | 1.17 | 1.15 | - | - |
| | 5m Grid | 1.19 | 1.05 | 1.13 | - | - |
| | 10m Grid | 0.87 | 0.85 | 1.16 | - | - |
| | 15m Grid | 0.91 | 0.77 | 1.15 | - | - |
| 30 | 1m Grid | 2.09 | 1.60 | 1.31 | 1.40 | - |
| | 2.5m Grid | 1.70 | 1.34 | 1.16 | 1.30 | - |
| | 5m Grid | 1.46 | 1.19 | 1.07 | 1.20 | - |
| | 10m Grid | 1.22 | 1.07 | 1.01 | 1.21 | - |
| | 15m Grid | 1.07 | 1.01 | 0.97 | 1.21 | - |
| 60 | 1m Grid | 2.32 | 1.69 | 1.42 | 1.25 | 1.30 |
| | 2.5m Grid | 2.01 | 1.46 | 1.25 | 1.08 | 1.24 |
| | 5m Grid | 1.69 | 1.30 | 1.13 | 1.01 | 1.19 |
| | 10m Grid | 1.38 | 1.14 | 1.03 | 0.97 | 1.06 |
| | 15m Grid | 1.38 | 1.07 | 0.99 | 0.94 | 1.08 |

- no result due to model instability

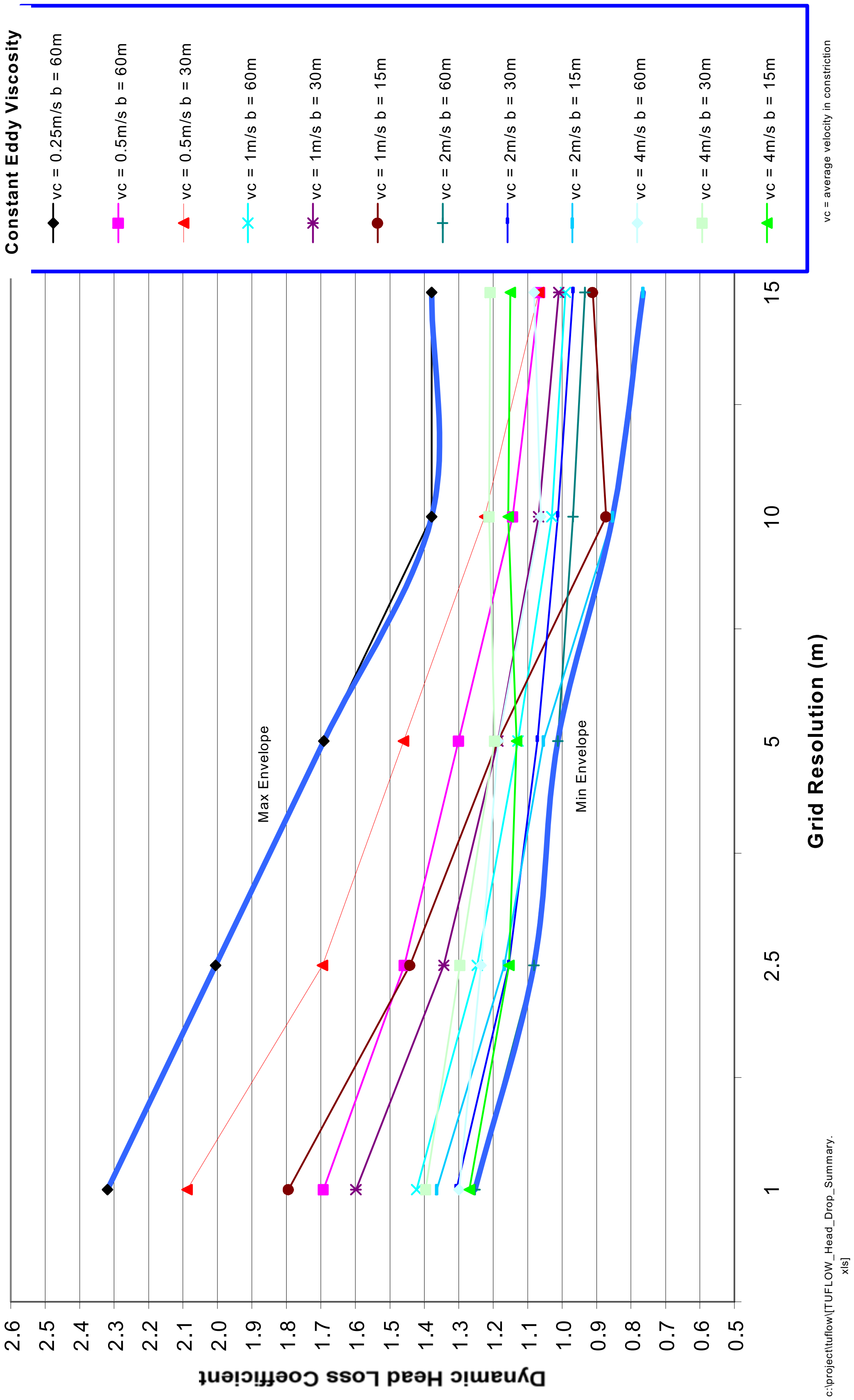


**Figure B-3 TUFLOW - Sensitivity Simulations – Dynamic Head Loss Coefficients**

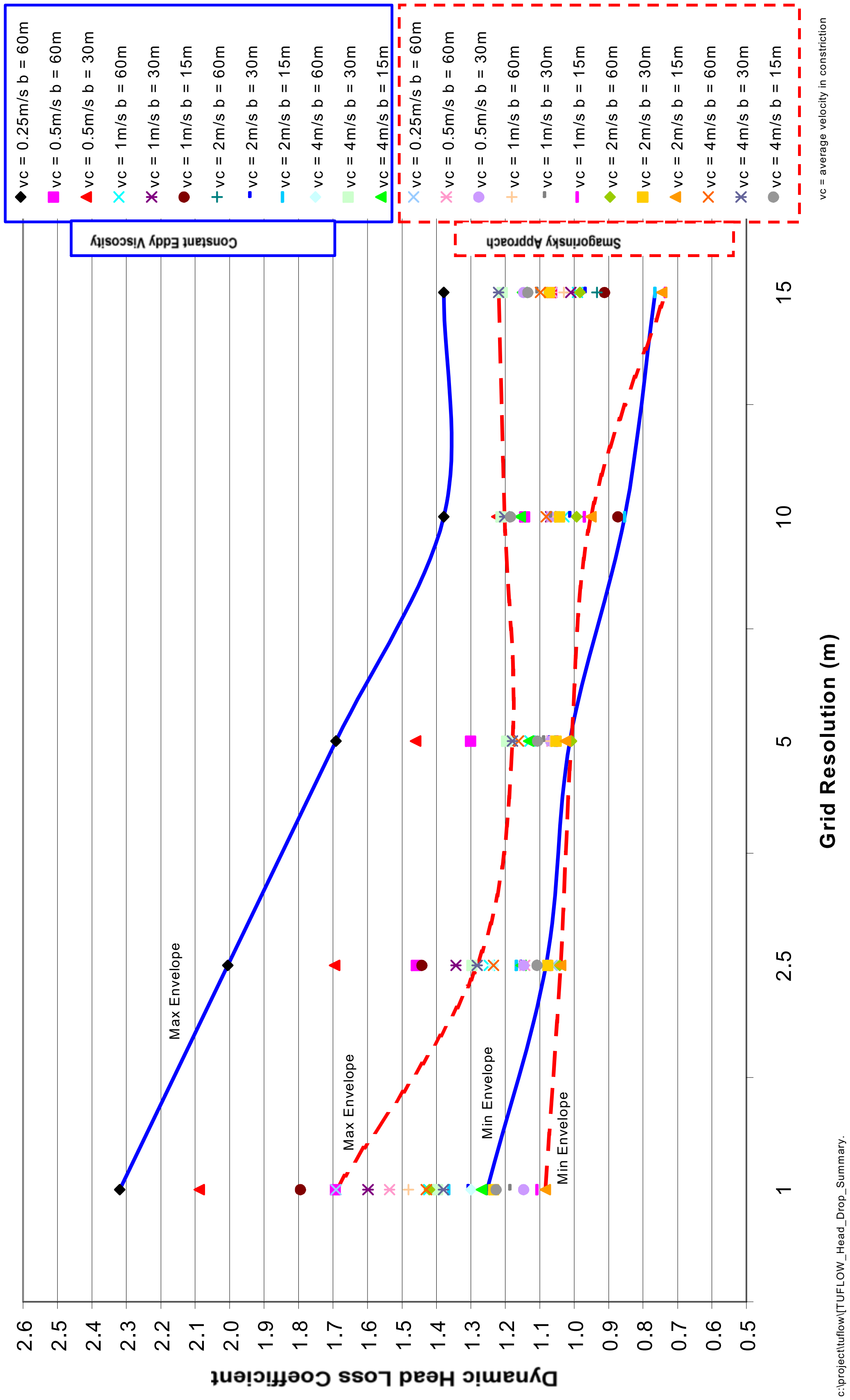


**Figure B-4 TUFLOW - Dynamic Head Loss Coefficients - Comparison of Eddy Viscosity Approaches**

Variations in eddy viscosity calculated according to the Smagorinsky formulation are shown across the model domain in Figure B-5 to Figure B-16. When viewing these figures it is important to be mindful of the difference between the eddy viscosity values across each model domain and the constant eddy viscosity of $1m^2/s$ used in the sensitivity tests.

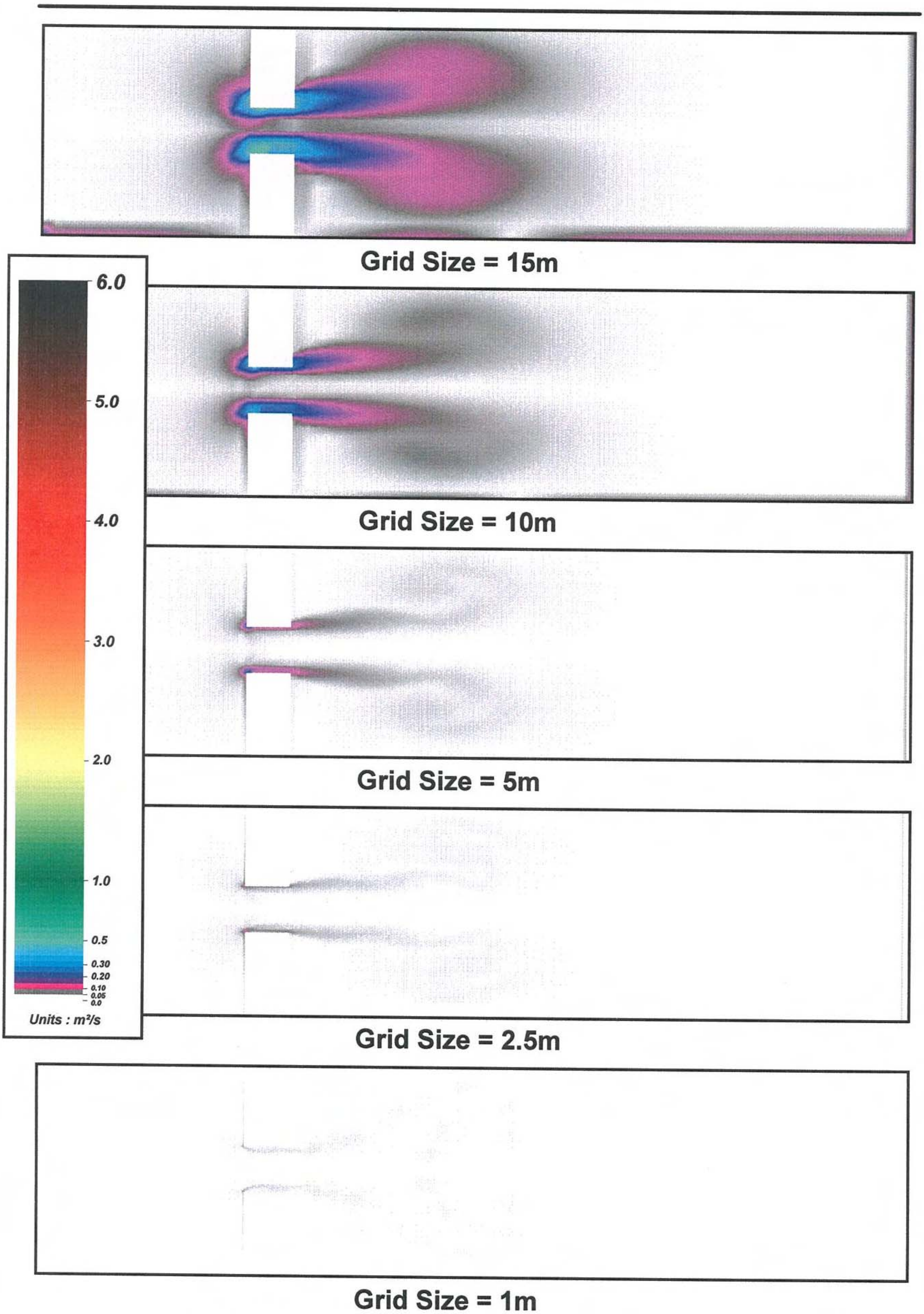


**Tuflow - Variations in Eddy Viscosity:**
**Vc = 0.25m/s ($Q=30m^3/s$ & b=60m)**

**Figure B-5**

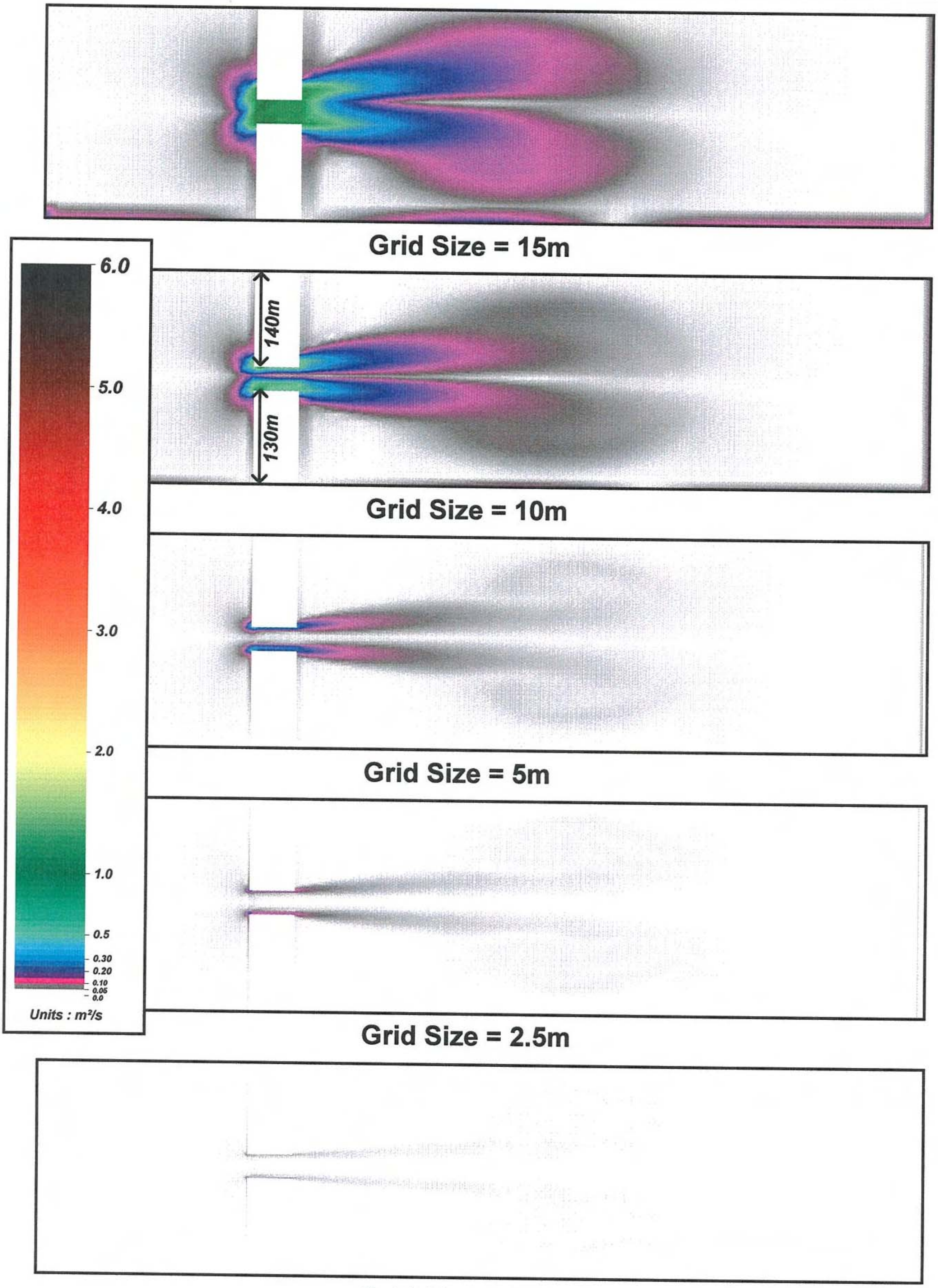


Grid Size = 1m

**TUFLOW- Variations in Eddy Viscosity:**
**Vc = 0.5m/s (Q=30$m^3$/s & b=30m)**

**Figure B-6**

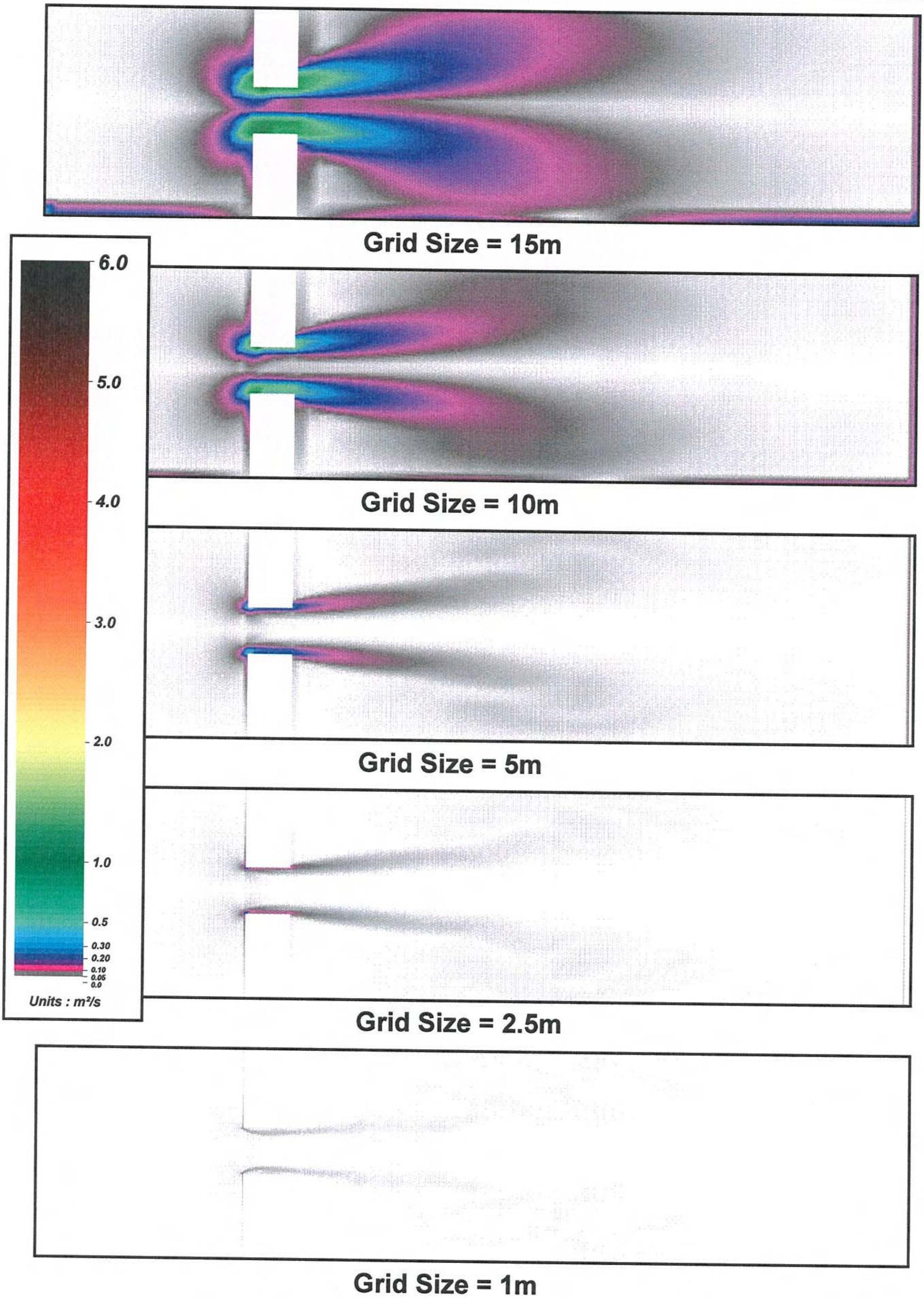


**TUFLOW- Variations in Eddy Viscosity**
**Vc = 0.5m/s (Q=60m$^3$/s & b=60m)**

**Figure B-7**

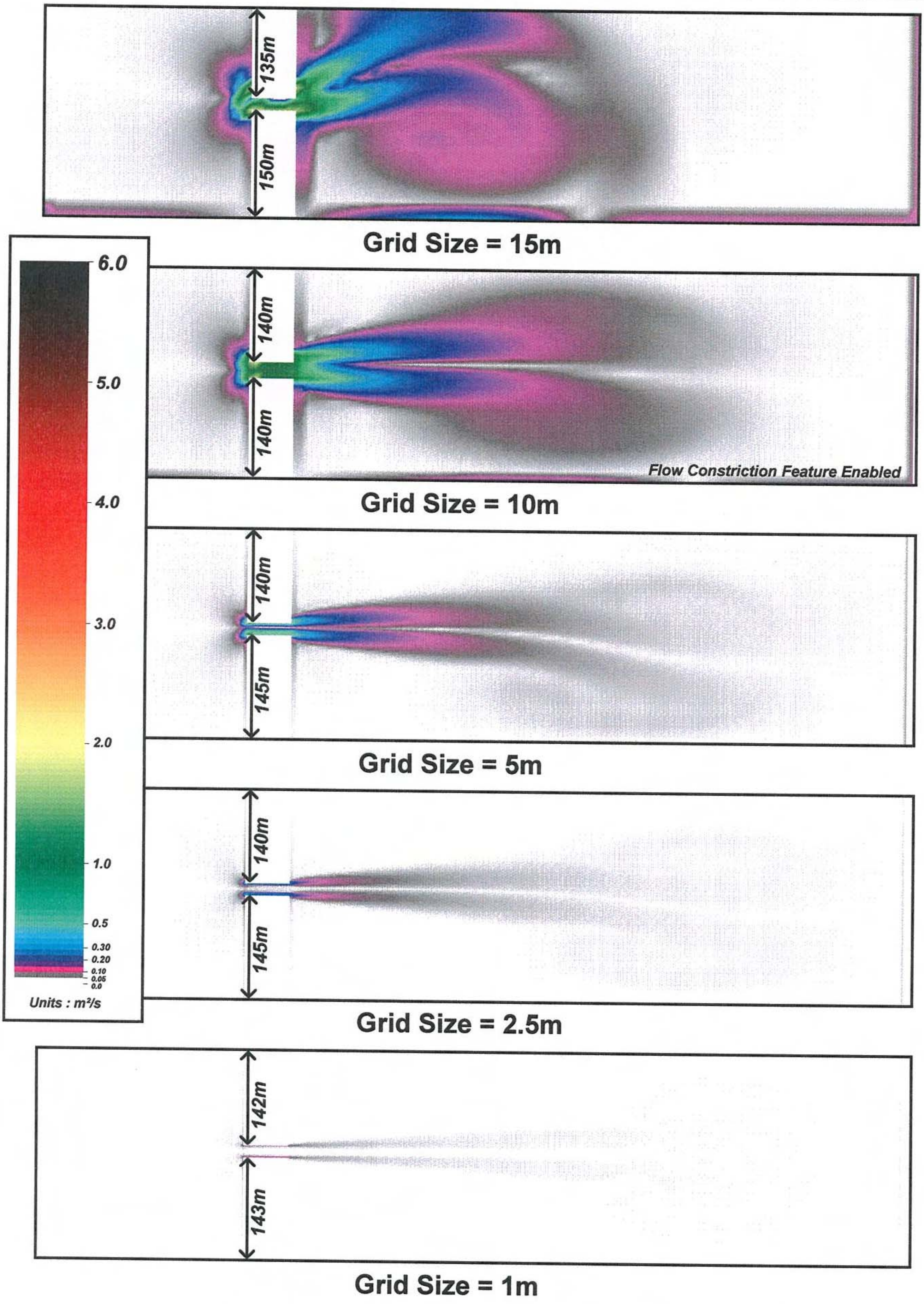


**TUFLOW- Variations in Eddy Viscosity:**
**Vc = 1m/s (Q=30m$^3$/s & b=15m)**

**Figure B-8**

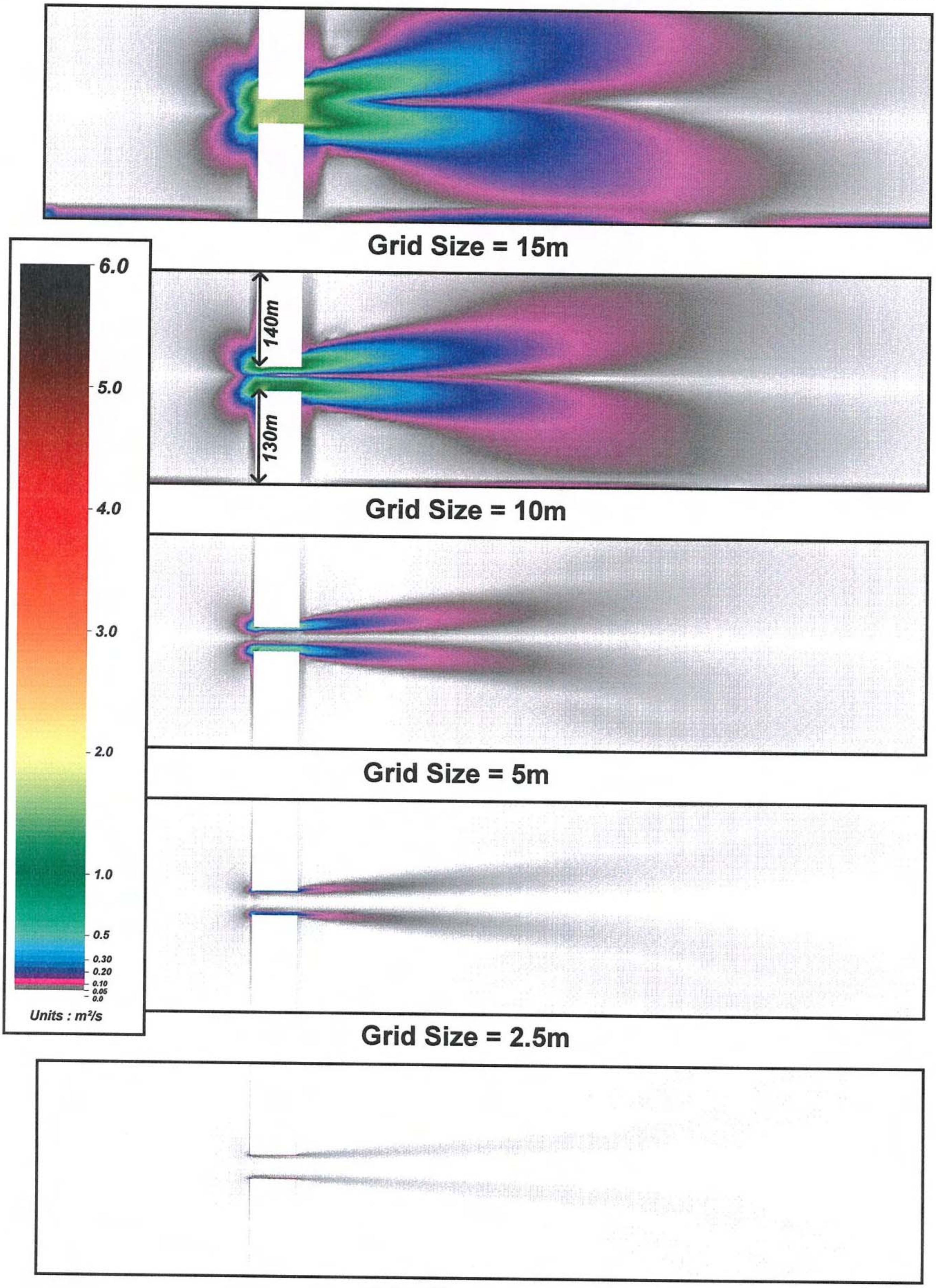


Grid Size = 1m

**TUFLOW- Variations in Eddy Viscosity:**
**Vc = 1m/s (Q=60m$^3$/s & b=30m)**

**Figure B-9**

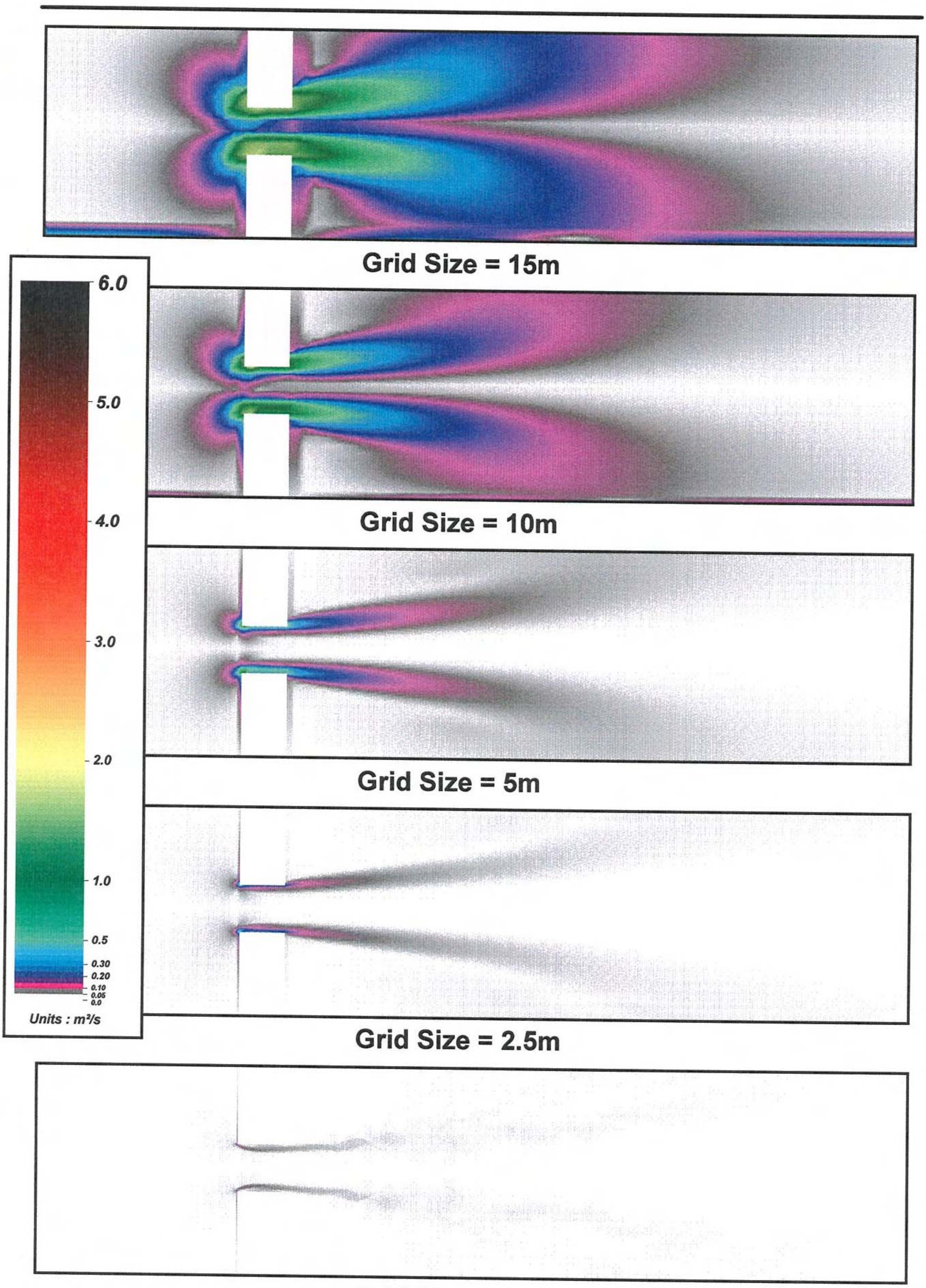


Grid Size = 1m

**TUFLOW- Variations in Eddy Viscosity:**
**Vc = 1m/s (Q=120m$^3$/s & b=60m)**

**Figure B-10**

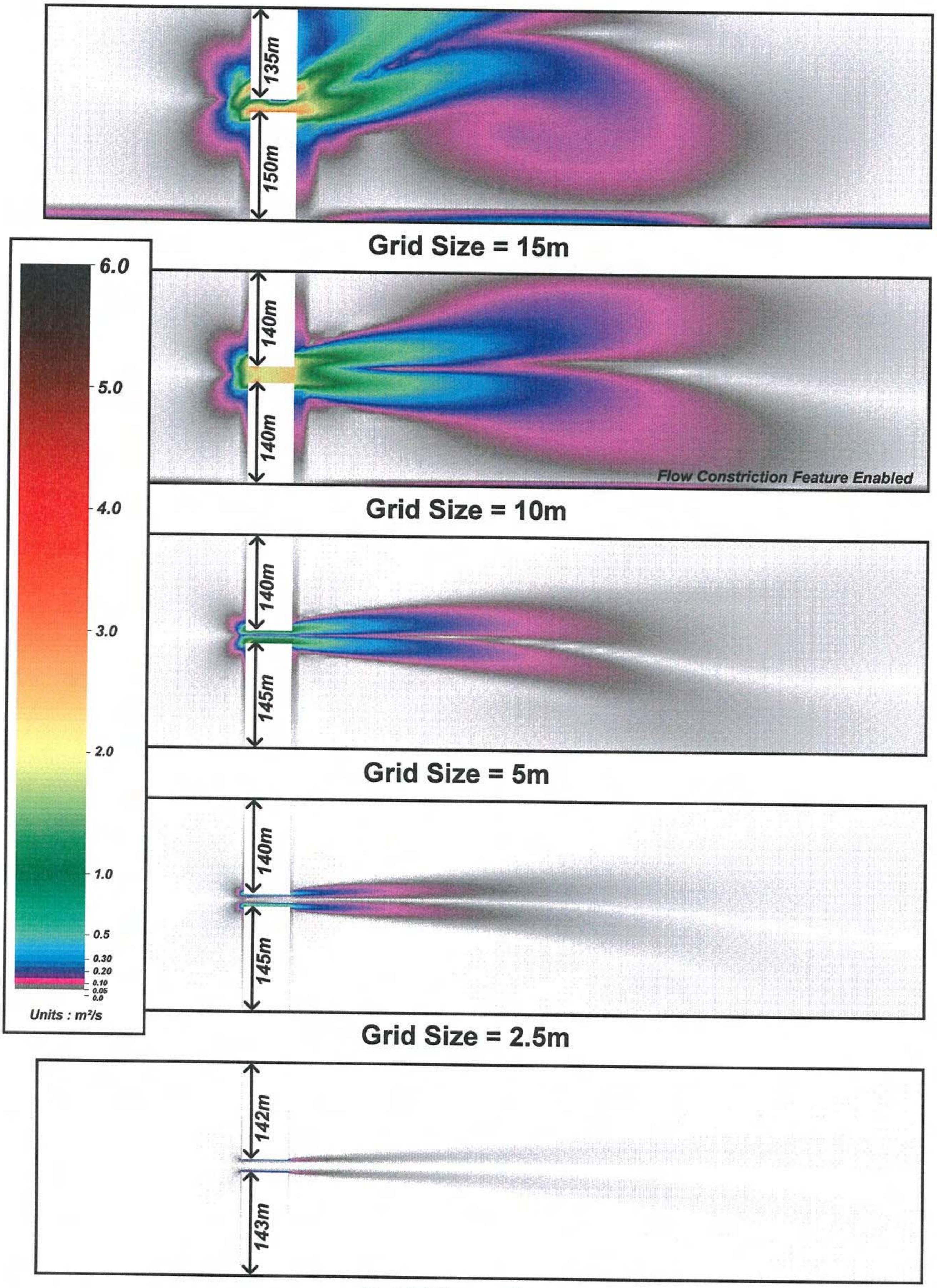


**TUFLOW- Variations in Eddy Viscosity:**
**Vc = 2m/s (Q=60m$^3$/s & b=15m)**

**Figure B-11**

V2_b15.wor

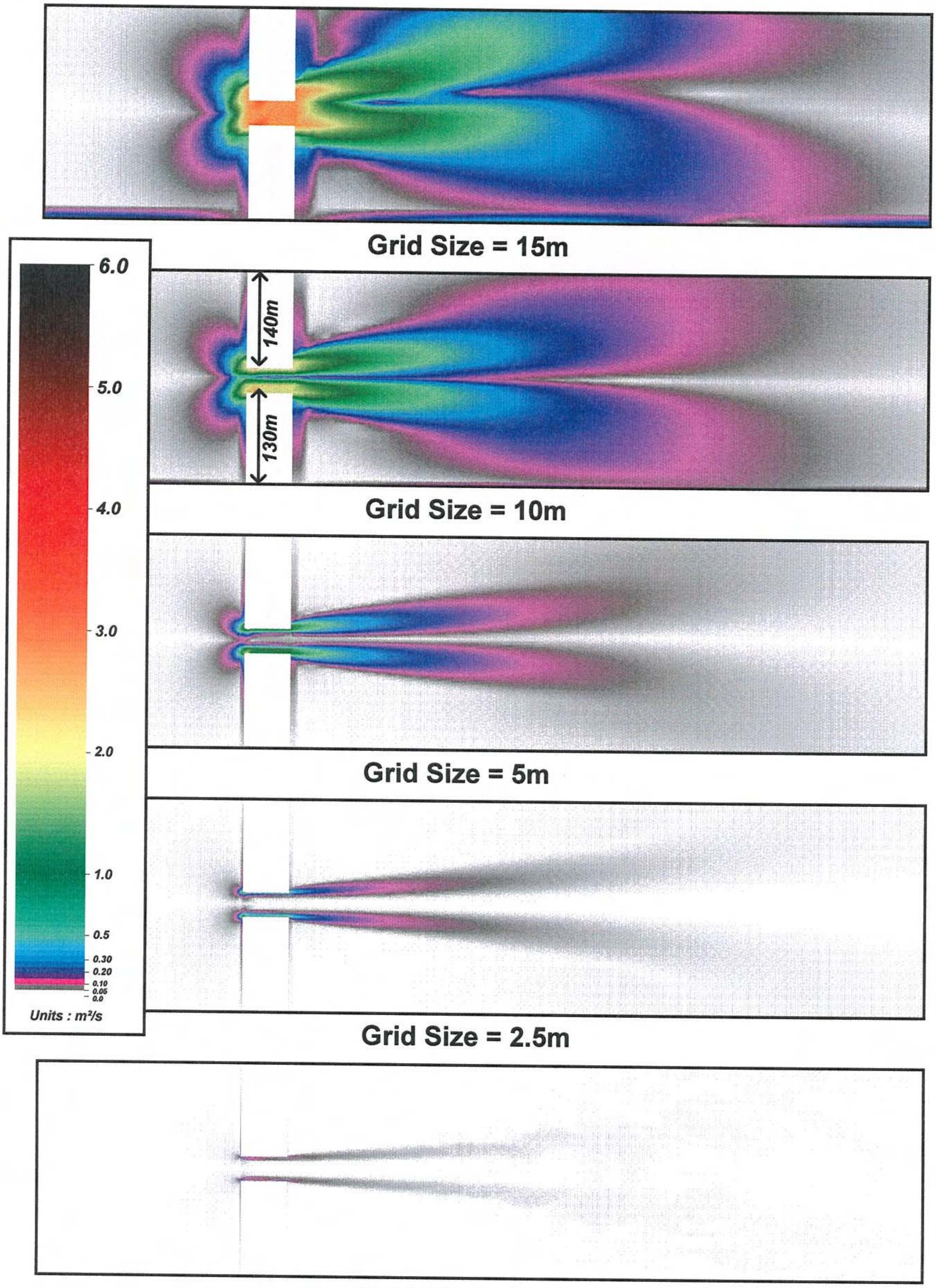


**TUFLOW- Variations in Eddy Viscosity:**
**Vc = 2m/s (Q=120m³/s & b=30m)**

**Figure B-12**

V2_b30.wor

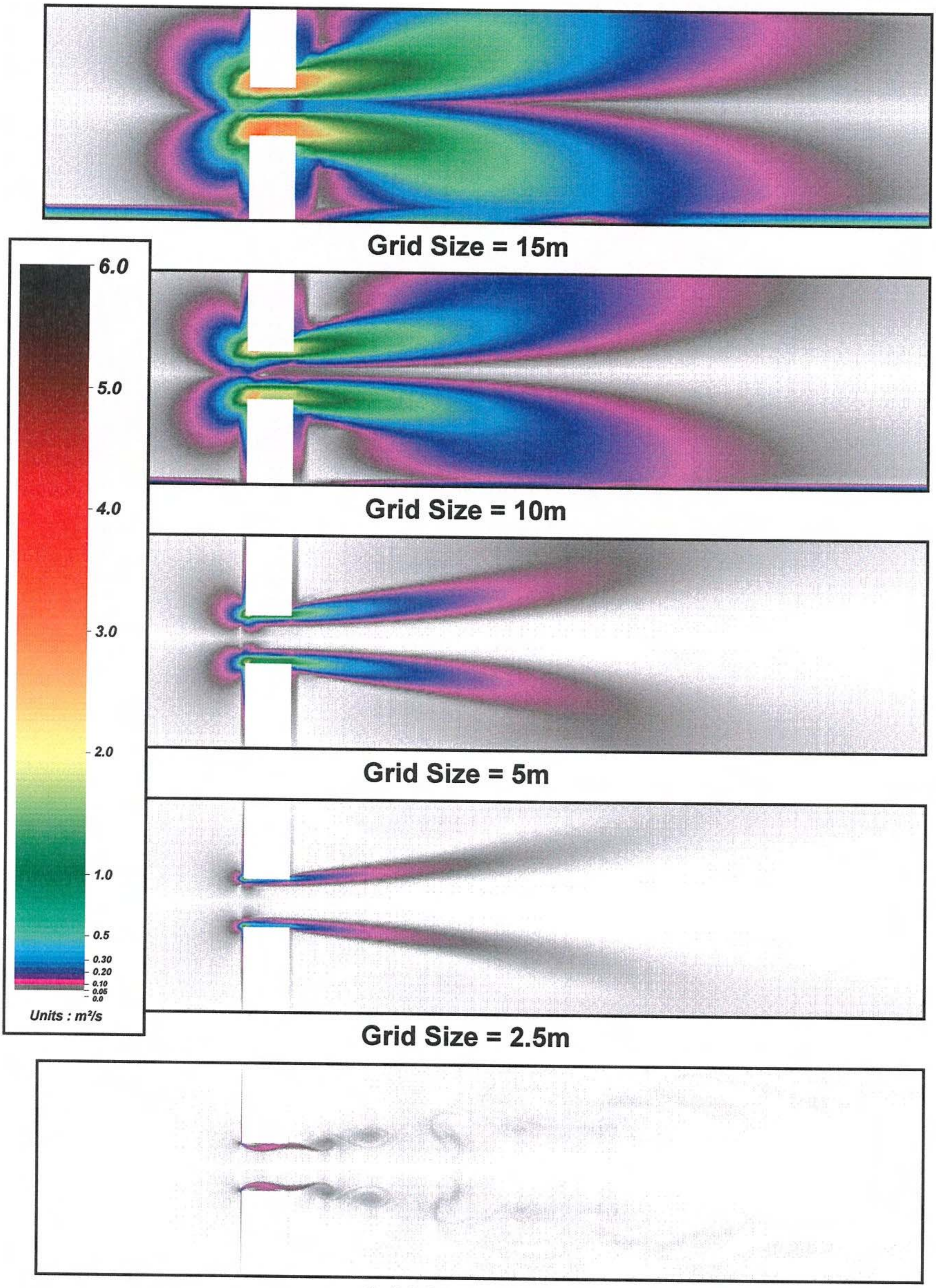


Grid Size = 1m

**TUFLOW- Variations in Eddy Viscosity:**
**Vc = 2m/s (Q=240m³/s & b=60m)**

**Figure B-13**

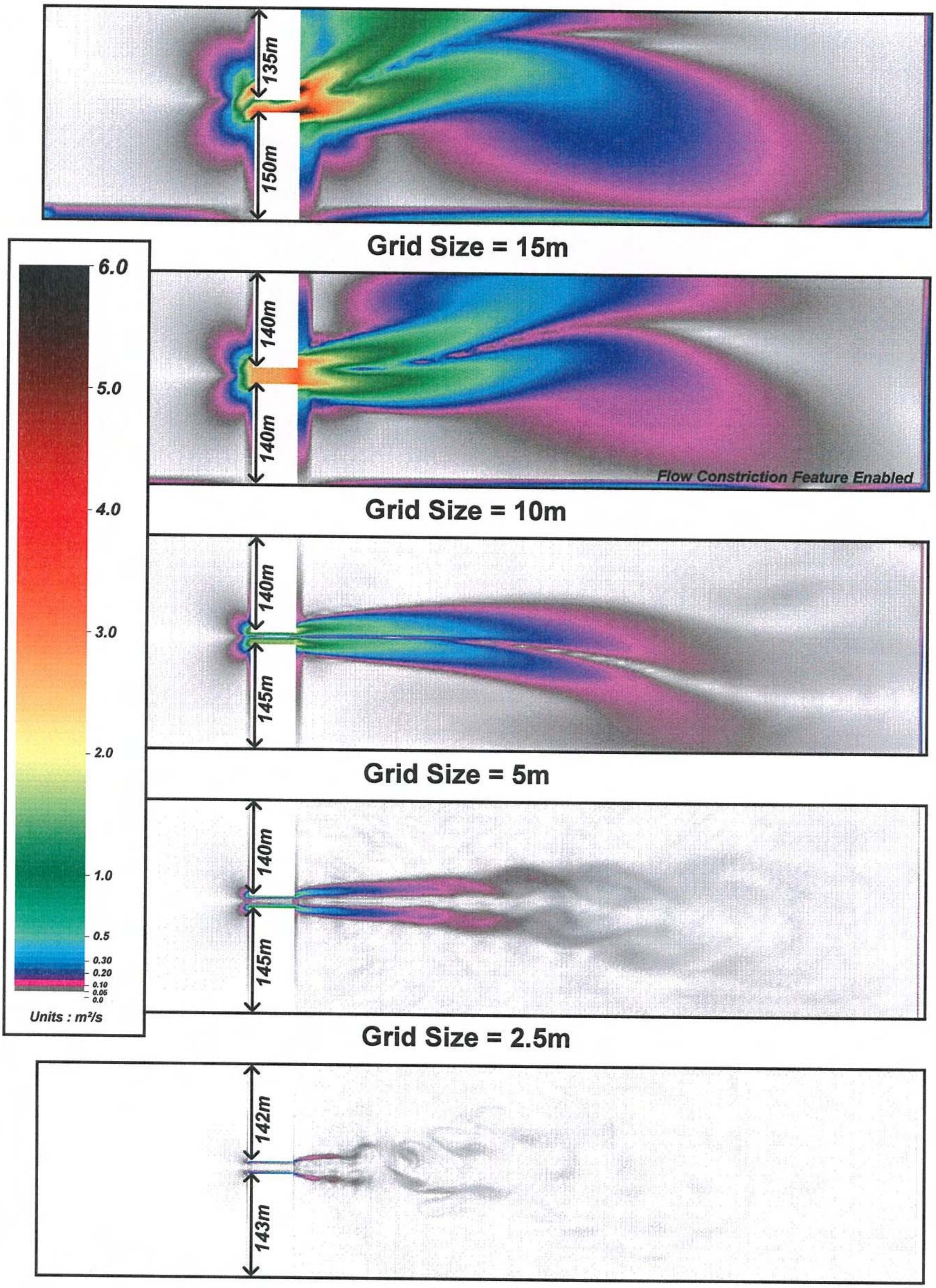


**TUFLOW- Variations in Eddy Viscosity: $V_c$ = 4m/s ($Q=120m^3/s$ b=15m)**

**Figure B-14**

V4_b15.wor

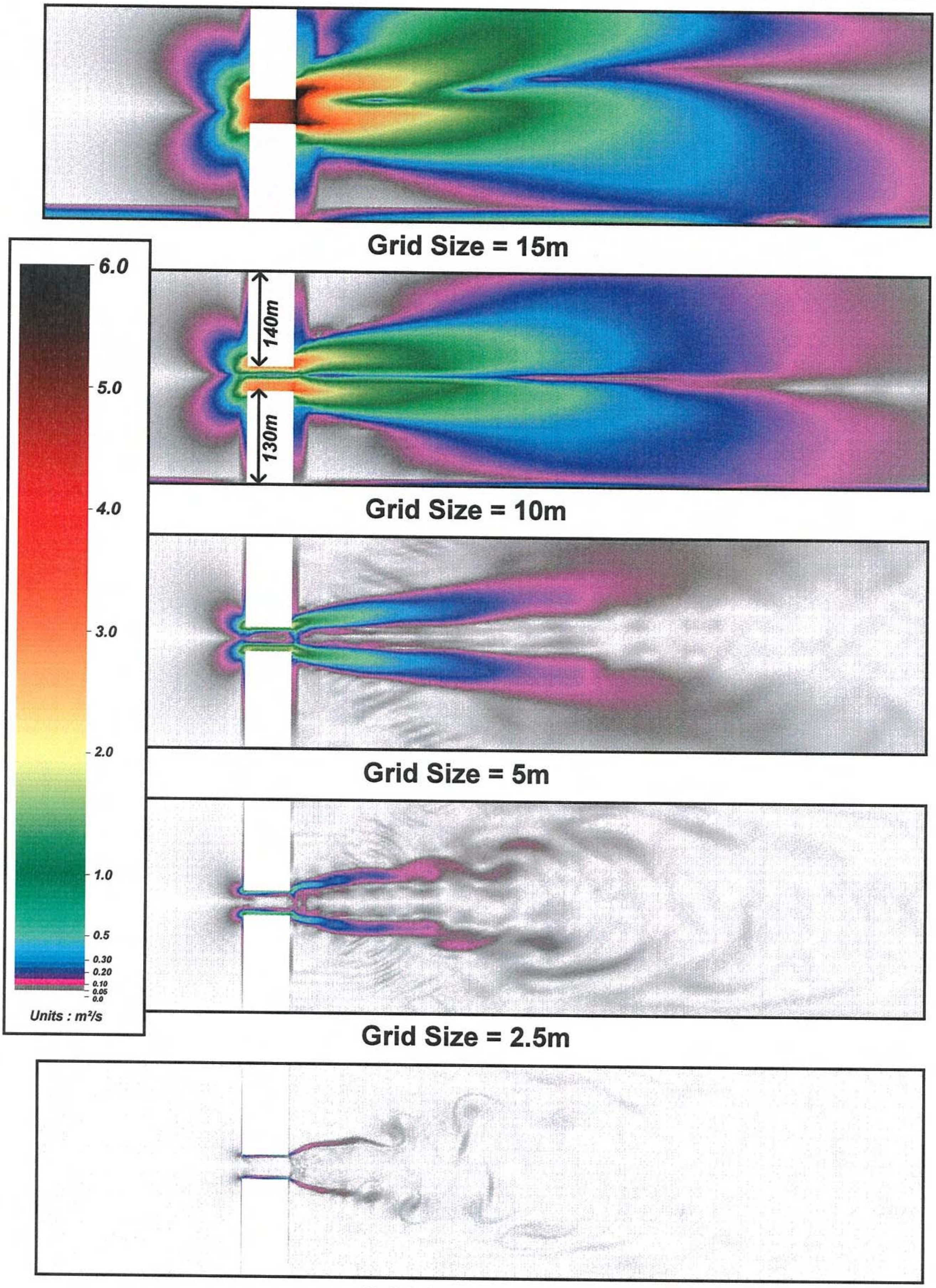


**TUFLOW- Variations in Eddy Viscosity:**
**Vc = 4m/s (Q=240m$^3$/s & b=30m)**

**Figure B-15**

V4_b30.wor

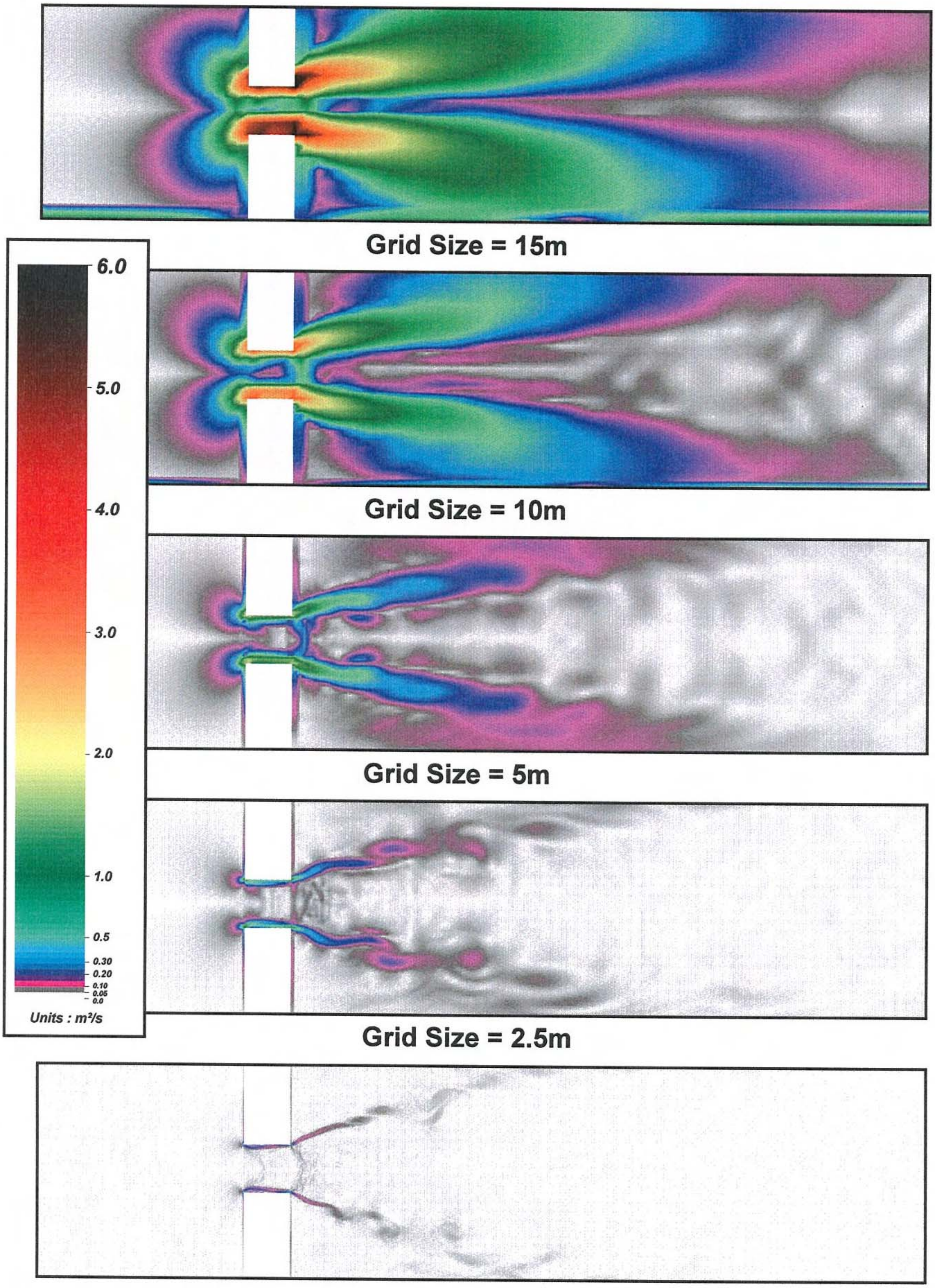


**TUFLOW- Variations in Eddy Viscosity:**
**Vc = 4m/s (Q=480m$^3$/s & b=60m)**

**Figure B-16**

V4_b60.wor

## B.4.3 Discussion

Use of a constant eddy viscosity in both RMA2 and TUFLOW results in a distinct trend that the coarser the mesh resolution, the lower the dynamic head loss coefficient as evident in Figure B-1 and Figure B-3. It is believed that the explanation for this trend lies in the statement made in Section B.2, "the use of eddy viscosity in 2D numerical modelling provides an approximate representation of the energy losses due to **turbulent effects at sub-grid scale**". As the resolution of the mesh increases, the ability of the model to reproduce the energy losses due to turbulent effects also increases. As shown in Equation B-1, the incorporation of eddy viscosity into the momentum equation does have some dependence on mesh size (the $\partial_x$ and $\partial_y$ terms). However, the use of a constant eddy viscosity provides a less accurate representation of sub-grid turbulence compared to the Smagorinsky formulation as the Smagorinksy formulation is far more dependent on mesh size (refer to Equation B-2).

As a finite element model, such as RMA2, is formed by non-uniform mesh elements, the ability of a particular model to reproduce energy losses due to turbulent effects will vary across the model domain depending upon the element size. Hence recommendations from King (1998) and Nielsen (2000) that finite element models utilise the Smagorinsky formulation as it more accurately accounts for the varying element size, amongst other factors, in determining the eddy viscosity. As TUFLOW is a finite difference model developed using a uniform grid, it follows that for each grid size there may be an optimum value for the constant eddy viscosity. As the Smagorinsky formulation accounts for varying grid size in determining the eddy viscosity it appears that this approach produces more consistent results when compared to the constant eddy viscosity results.

It is evident from Figure B-2 and Figure B-4 that the constant eddy viscosity approach produces a broader band of dynamic head loss coefficients across most mesh resolutions than the Smagorinsky approach. In general it appears that the very low average constriction velocities produce the higher dynamic head loss coefficients. From the current investigation it would appear that when the constriction velocities are low, the energy losses due to turbulence are also low so that the use of the constant eddy viscosity may falsely inflate the energy losses. The Smagorinsky formulation appears to partially avoid this problem as it compensates by allowing lower eddy viscosities where the velocity gradient is lower.

Figure B-5 to Figure B-16 provide evidence of the following trends:

- Eddy viscosity values are greater in regions of rapidly varied flow as expected.
- Eddy viscosity values are greater for larger grid sizes as expected.
- Eddy viscosity values are greater for higher average constriction velocities as expected.
- For a grid size of 1m, eddy viscosity ranges from $0m^2/s$ to no more than $0.5m^2/s$ across the model domain.
- For a grid size of 15m, eddy viscosity ranges from $0m^2/s$ to about $6m^2/s$ across the model domain.
- Eddy patterns become evident in the eddy viscosity values as the grid size decreases (refer to Figure B-14 to Figure B-16).

- The impact of a non-centred constriction can be seen in the non-symmetrical patterns produced for those such models (refer to Figure B-8, Figure B-11 and Figure B-14).
- The flow constriction feature utilised to force the 10m grid size to mimic a 15m width of constriction, produces non-symmetrical flow patterns despite the constriction being centred (refer to Figure B-8, Figure B-11and Figure B-14).
- For a grid size of 15m, a non-symmetrical pattern in eddy viscosity values is evident along the edge of the model domain despite the constriction being centred. The reason for this is not known.

## B.5 Recommendations

It is beyond the scope of this research to investigate the inter-relationship between all factors in the Smagorinsky formulation. However, it is recommended that further research be undertaken into this field as the eddy viscosity has to date received little attention in model development and use. The above results and discussion indicate that it is an important variable and further work is necessary.

In utilising the Smagorinsky formulation within RMA2, a minimum eddy viscosity of 0.2 is recommended (King, 1998). One set of simulations was undertaken with this typical minimum value before it was changed to a minimum of zero. The reason for the change was to mirror the Smagorinsky formulation within TUFLOW as TUFLOW does not allow for a minimum eddy viscosity to be set but uses a minimum of 0. In changing the minimum eddy viscosity within the RMA2 simulations it was expected that there would be a noticeable change in the head loss across the model, particularly in the finer meshes. However, the change in head loss was not noticeable. This observation raises the concern as to how the minimum eddy viscosity set within the RMA2 model input files is used. It may be that a zero is interpreted as “use default” rather than the value of zero. Production of eddy viscosity plots from RMA2 in a manner similar to those produced for TUFLOW (Figure B-5 to Figure B-16) will allow the minimum eddy viscosity to be determined. It will also allow a comparison between RMA2 and TUFLOW eddy viscosity across the model domain. It is recommended that this is reviewed in more detail in further work.

# C HEC-RAS COMPUTATIONS

## C.1 Expansion and Contraction Model Details

Key issues associated with the development of the HEC-RAS model for this study are as follows:

- Selection of expansion and contraction coefficients,
- Selection of the expansion and contraction reach lengths,
- Definition of ineffective flow areas and positioning of cross-sections adjacent to the constriction.

The significance of the final point above was discovered after sensitivity tests.

A plan view of the basic cross-section layout for modelling a constriction in HEC-RAS is provided in Figure C-1. Cross-section 1 is located sufficiently downstream from the structure so that the flow is not affected by the structure (that is, the flow has fully expanded). The distance from the constriction to cross-section 1 is called the *expansion reach length*, $L_e$. Similarly, cross-section 4 is located sufficiently upstream of the structure where the flow lines are approximately parallel and the cross-section is fully effective. The distance from the constriction to cross-section 4 is called the *contraction reach length*, $L_c$.

HEC (1998) advises that the distance between cross-section 1 and 2 should not be so great that friction losses are not adequately modelled. As the channel is of uniform nature in this study, this point can be ignored since the area, the conveyance and the friction slope vary linearly between the two cross-sections.

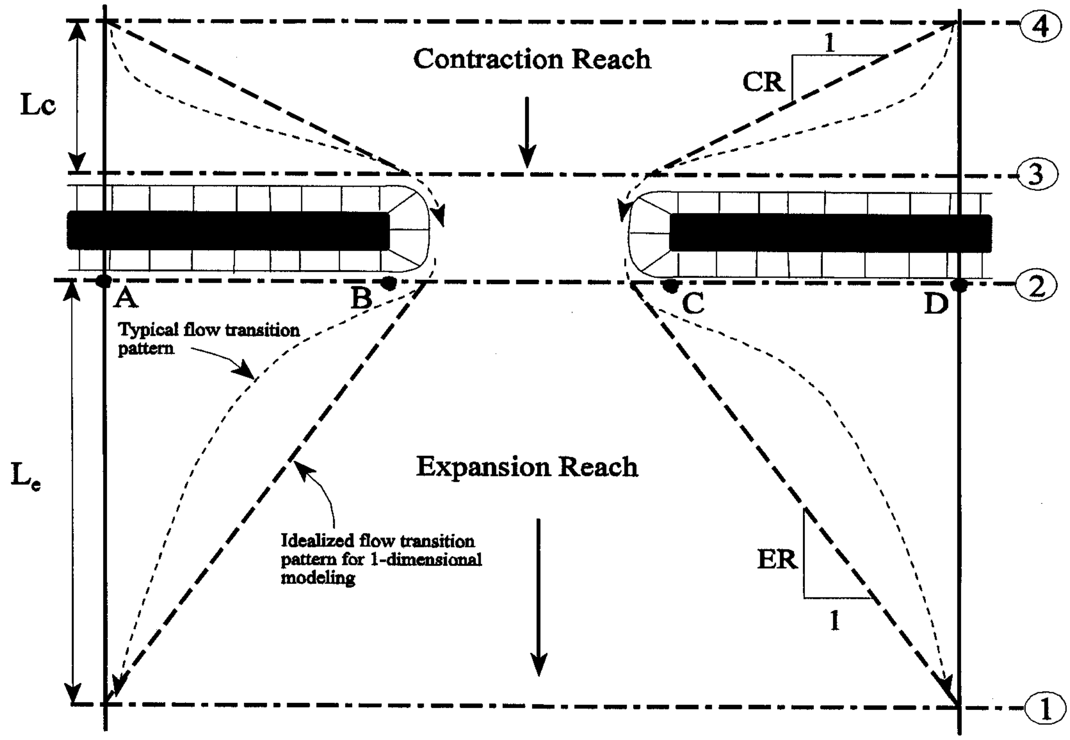


**Figure C-1 Cross-section Locations at a Constriction (from HEC, 1998)**

As indicated by Hunt *et al.* (1999), HEC (1998) and HEC (1995), accurate prediction of energy losses in the contraction reach upstream from the constriction and the expansion reach downstream from the constriction using one-dimensional models is difficult. Accurate evaluation of four key parameters is necessary in order to effectively model these reaches. These parameters are: the expansion reach length, $L_e$, the contraction reach length, $L_c$, the expansion coefficient, $C_e$, and the contraction coefficient, $C_c$. Results of research into these four parameters is presented fully in HEC (1995) and summarised both in HEC (1998) and Hunt *et al.* (1999). It is important within the context of the current study to discuss some details of this research.

The research by HEC (1995) was undertaken using a variety of real and ideal bridge sites and a large number of two-dimensional finite element models (RMA2: King, 1994). The aim was to develop empirical equations by regression analysis of the four key parameters. Ranges of parameters used in determining the empirical equations are contained within Table C-1. Also contained within this table are the ranges of parameters used in the current study.

**Table C-1 Comparison of Parameter Ranges, HEC (1995) vs Current Study**

| Parameter | Value in HEC (1995) | Value in Current Study |
|---|---|---|
| Mannings n | 0.04 to 0.24 | 0.025 |
| Slope, S | 0.02% to 0.2% | 0% |
| Channel Width, B | 305m | 300m |
| Constriction Width, b | 30.5m to 153m | 15m to 60m |
| Discharge, Q | 142m$^3$/s to 849m$^3$/s | 30m$^3$/s to 480m$^3$/s |

## C.1.1 Expansion Reach Lengths

When modelling situations that are similar to those used to develop the HEC (1995) empirical equations, the equation for the expansion reach length is:

$$L_e = -90.85 + 78.35\left(\frac{F_{c2}}{F_{c1}}\right) + 0.918\,\overline{L_{obs}} + 0.0515\,Q \qquad \textit{Equation C.1}$$

Where $L_e$ = Expansion reach length (m)

$F_{c2}$ = main channel Froude number at Section 2

$F_{c1}$ = main channel Froude number at Section 1

$\overline{L_{obs}}$ = average length of obstruction caused by the two bridge approaches (m)

$Q$ = total discharge (m$^3$/s)

When the width of the floodplain and the discharge are smaller than those of the regression data, HEC (1998) indicates that the expansion ratio, ER, can be estimated with the following equation:

$$ER = 0.421 + 0.485\left(\frac{F_{c2}}{F_{c1}}\right) + 6.35 \times 10^{-5}\,Q \qquad \textit{Equation C.2}$$

HEC (1998) recommends that the expansion ratio, ER, should not exceed 4, nor should it be less than 0.5. That is,

$$0.5 \leq ER \leq 4 \qquad \text{Equation C.3}$$

Where: ER $= \text{Expansion Ratio} = \dfrac{2L_e}{(B-b)}$ Equation C.4

Table C-2 contains a summary of the steps involved in calculating the expansion reach length in this study for each width of constriction, b, for each discharge, Q. As shown, the initial values of $L_e$ calculated using Equation C.1, produced expansion ratios outside the bounds indicated by Equation C.3. The expansion ratio was then calculated using Equation C.4. Again, some of the expansion ratios were outside the bounds. The expansion ratios were then altered to lie within the bounds indicated by Equation C.3 and the expansion reach length used was recalculated from the altered expansion ratio. It is believed that the reason why the expansion ratios lie outside the specified bounds is related to the fact that the current study has some parameters outside the ranges used by HEC (1995) in undertaking the regression analysis (refer to Table C-1).

**Table C-2 Expansion Reach Length Calculation Summary**

| **b (m)** | **Q ($m^3/s$)** | **$L_e$ Calculated using Eqn C.1 (m)** | **Expansion Ratio Calculated $\frac{2L_e}{(B-b)}$** | **Expansion Ratio Calculated Using Eqn C.2** | **Expansion Ratio Used** (within bounds of Eqn C.3) | **$L_e$ Used (m)** |
|---|---|---|---|---|---|---|
| 15 | 30 | 1610 | 11.3 | 10.1 | 4.0 | 570 |
| | 60 | 1610 | 11.3 | 10.2 | 4.0 | 570 |
| | 120 | 1610 | 11.3 | 10.2 | 4.0 | 570 |
| 30 | 30 | 820 | 6.1 | 5.3 | 4.0 | 540 |
| | 60 | 820 | 6.1 | 5.3 | 4.0 | 540 |
| | 120 | 820 | 6.1 | 5.3 | 4.0 | 540 |
| | 240 | 830 | 6.1 | 5.4 | 4.0 | 540 |
| 60 | 30 | 410 | 3.4 | 2.9 | 3.0 | 360 |
| | 60 | 410 | 3.4 | 2.9 | 3.0 | 360 |
| | 120 | 420 | 3.5 | 2.9 | 3.0 | 360 |
| | 240 | 420 | 3.5 | 3.0 | 3.0 | 360 |
| | 480 | 440 | 3.7 | 3.2 | 3.0 | 360 |

## C.1.2 Contraction Reach Lengths

Again, when modelling situations similar to that used in developing the equations, the contraction reach length in metres is:

$$L_c = 80.18 + 11.83\frac{F_c2}{F_c1} + 78.35\left(\frac{Q_{ob}}{Q}\right)^2 - 17.9\left(\frac{n_{ob}}{n_c}\right)^{0.5} + 0.161\,\overline{L_{obs}} \qquad \textit{Equation C.5}$$

Where: $\overline{L_{obs}}$ = average length of obstruction caused by the two bridge approaches (m)

$Q_{ob}$ = the discharge conveyed by the two overbanks (in this case $Q_{ob} = Q$)

$Q$ = total discharge ($m^3/s$)

$n_{ob}$ = the Manning n value for the overbanks (in this case $n_{ob} = n_c$)

$n_c$ = the Manning n value for the main channel (in this case $n_c = n_{ob}$)

When the floodplain scale and discharge are significantly larger or smaller than those that were used in the regression analysis, the following equation should be used to estimate the contraction ratio, CR:

$$CR = 1.4 - 0.333\left(\frac{F_c2}{F_c1}\right) + 1.86\left(\frac{Q_{ob}}{Q}\right)^2 - 0.19\left(\frac{n_{ob}}{n_c}\right)^{0.5} \qquad \textit{Equation C.6}$$

HEC (1998) recommends that the contraction ratio should not exceed 2.5, nor should it be less than 0.3. That is,

$$0.3 \le \frac{2L_c}{(B-b)} \le 2.5 \qquad \textit{Equation C.7}$$

Table C-3 contains a summary of the steps involved in calculating the contraction reach length in this study for each width of constriction, b, for each discharge, Q. As shown, the initial values of $L_c$ calculated using Equation C.5, produced contraction ratios outside the bounds indicated by Equation C.7. The contraction ratios were then altered to lie within the bounds indicated by Equation C.7 and the contraction reach length actually used was recalculated from the altered contraction ratio. It is believed that the reason why the contraction ratios lie outside the specified bounds is related to the fact that the current study has some parameters outside the ranges used by HEC (1995) in undertaking the regression analysis (refer to Table C-1).

**Table C-3 Contraction Reach Length Calculation Summary**

| b (m) | Q ($m^3/s$) | $L_c$ Calculated using Eqn C.5 (m) | Contraction Ratio Calculated $\frac{2L_c}{(B-b)}$ | Contraction Ratio Calculated Using Eqn C.7 | Contraction Ratio Used (within bounds of Eqn C.7) | $L_c$ Used (m) |
|---|---|---|---|---|---|---|
| 15 | 30 | 400 | 2.8 | -3.6 | 2.3 | 265# |
| | 60 | 400 | 2.8 | -3.6 | 2.3 | 265# |
| | 120 | 400 | 2.8 | -3.6 | 2.3 | 265# |
| 30 | 30 | 280 | 2.1 | -0.3 | 2.3 | 265# |
| | 60 | 280 | 2.1 | -0.3 | 2.3 | 265# |
| | 120 | 280 | 2.1 | -0.3 | 2.3 | 265# |
| | 240 | 280 | 2.1 | -0.3 | 2.3 | 265# |
| 60 | 30 | 220 | 1.8 | 1.4 | 1.4 | 170 |
| | 60 | 220 | 1.8 | 1.4 | 1.4 | 170 |
| | 120 | 220 | 1.8 | 1.4 | 1.4 | 170 |
| | 240 | 220 | 1.8 | 1.4 | 1.4 | 170 |
| | 480 | 220 | 1.8 | 1.4 | 1.4 | 170 |

# The value of Lc calculated is 320. However, the model is limited by the proximity of the upstream boundary, which is 270m from the face of the constriction. Thus, 265m is the maximum available contraction length. This may lead to an underestimation of the true head loss through the constriction. However, all models assessed in this study have identical lengths and all should produce similar head losses regardless.

### C.1.3 Expansion and Contraction Losses

For the flow through an abrupt constriction, the expansion and contraction losses are higher than the losses due to friction. For this reason, the selection of the correct expansion and contraction loss coefficients is vital in achieving the most accurate result. HEC (1998) provides a table indicating appropriate contraction and expansion loss coefficients to use in sub-critical flow situations. This table is reproduced as Table C-4.

**Table C-4 Subcritical Flow Contraction and Expansion Coefficients (HEC, 1998)**

| | Contraction, $C_c$ | Expansion, $C_e$ |
|---|---|---|
| No transition loss computed | 0 | 0 |
| Gradual transitions | 0.1 | 0.3 |
| Typical bridge sections | 0.3 | 0.5 |
| Abrupt transitions | 0.6 | 0.8 |

HEC (1998) advises that the maximum value for the contraction and expansion coefficient is 1. Lower coefficient values are recommended for **supercritical** flow as in supercritical flow the velocity heads are much higher. An overestimation of energy losses can result from using contraction and expansion coefficients that are typical for sub-critical flow. Oscillations in the computed water surface profile can also occur. Typical values for gradual transitions in supercritical flow would be around 0.1 for both the contraction and expansion coefficient (HEC, 1998). This will increase as the transition becomes more abrupt. For abrupt bridge transitions, HEC (1998) suggests the higher values of 0.3 and 0.5 for the contraction and expansion coefficients respectively.

### *C.1.3.1 Expansion Coefficient*

The regression analysis undertaken by HEC (1995) with regard to expansion coefficients, $C_e$, did not yield a regression equation that fits the data well. HEC (1995) found that the best equation for predicting the expansion coefficient is:

$$C_e = -0.09 + 0.57\left(\frac{D_{ob}}{D_c}\right) + 0.075\left(\frac{F_{c2}}{F_{c1}}\right) \qquad \textit{Equation C.8}$$

Where: $D_{ob}$ = hydraulic depth for the overbank at the fully-expanded flow section

$D_c$ = hydraulic depth for the main channel at the fully-expanded flow section

HEC (1998) advises that the expansion coefficient should not be higher than 0.80.

**Table C-5 Expansion Coefficients Used**

| b (m) | Q ($m^3$/s) | $C_e$ from Eqn C.8 | $C_e$ Used* |
|---|---|---|---|
| 15 | 30 | 1.98 | 0.8 |
| | 60 | 1.98 | 0.8 |
| | 120 | 1.98 | 0.8 |
| 30 | 30 | 1.23 | 0.7 |
| | 60 | 1.23 | 0.7 |
| | 120 | 1.23 | 0.7 |
| | 240 | 1.23 | 0.7 |
| 60 | 30 | 0.86 | 0.4 |
| | 60 | 0.86 | 0.4 |
| | 120 | 0.86 | 0.4 |
| | 240 | 0.86 | 0.4 |
| | 480 | 0.86 | 0.4 |

* based on limitations provided by HEC (1998)

### *C.1.3.2 Contraction Coefficient*

HEC (1995) were not able to carry out regression analysis to determine the contraction coefficient. Table C-6 is provided in HEC (1998) as an indication of the recommended contraction coefficient values according to the degree of constriction. The contraction coefficients used in this study are shown in Table C-7.

**Table C-6 Recommended Contraction Coefficient Values (HEC, 1998)**

| Degree of Constriction | Recommended Contraction Coefficient |
|---|---|
| $0.0 < b/B < 0.25$ | 0.3 – 0.5 |
| $0.25 < b/B < 0.5$ | 0.1 – 0.3 |
| $0.50 < b/B < 1.0$ | 0.1 |

**Table C-7 Contraction Coefficients Used**

| b | Q | b/B | $C_e$ Used |
|---|---|---|---|
| 15 | 30 | 0.05 | 0.5 |
| | 60 | 0.05 | 0.5 |
| | 120 | 0.05 | 0.5 |
| 30 | 30 | 0.1 | 0.5 |
| | 60 | 0.1 | 0.5 |
| | 120 | 0.1 | 0.5 |
| | 240 | 0.1 | 0.5 |
| 60 | 30 | 0.2 | 0.4 |
| | 60 | 0.2 | 0.4 |
| | 120 | 0.2 | 0.4 |
| | 240 | 0.2 | 0.4 |
| | 480 | 0.2 | 0.4 |

## C.1.4 Ineffective Flow Areas

The ineffective flow option is used on cross-sections 2 and 3 (xs2 and xs3) shown in Figure C-1 to keep all the active flow in the area of the bridge opening. HEC (1998) advises that on the upstream side of the bridge where the flow is contracting rapidly, the ineffective flow station should be assumed to be a distance equal to the distance of xs3 from the bridge. That is, if xs3 is a distance of 5m upstream from the bridge, then the ineffective flow stations should be placed 5m away from each side of the bridge opening. On the downstream side of the bridge at xs2, the positioning of the ineffective flow stations can be difficult as the active flow area may be less than, equal to, or greater than the width of the bridge opening (HEC, 1998). HEC (1998) suggests that in general, the user should make the active flow area equal to the width of the bridge opening at the downstream xs2.

Results presented for HEC-RAS have been computed following the above recommendations. However, sensitivity tests performed showed that for some situations, results were extremely sensitive to the placement of xs2 and xs3 and the ineffective flow areas assigned to each (refer to Table C-8). The most sensitive condition appeared to be when the average velocity through the constriction was 4m/s or more. For example, widening the ineffective flow area at xs2 by about 3m (1% of the total channel width), produced a decrease in head loss of up to 25% for average constriction velocities of 4m/s and more. Sensitivity of the results to changes in the position of xs2 and xs3 were also tested. By moving xs2 and xs3 closer to the constriction, differences in head losses of up to 40% were found for average constriction velocities of 4m/s and more. It is not within the scope of this study to determine the reasons for these sensitivities although it is thought that they are related to the transition to supercritical flow. However, it is important to be cognisant of the sensitivities for the 4m/s average velocity situations when comparing the results with that of other models.

**Table C-8 HEC-RAS Sensitivity Results**

| Description of Sensitivity Test | Change in Total Head Loss Across Model (mm) |
|---|---|
| Set ineffective flow areas equal to constriction width | 0 to 140 (10% rise)[a] |
| Widen ineffective flow areas | 0 to -330 (25% drop)[a] |
| Move cross-sections adjacent to constriction closer to constriction (only 1m away) with widened ineffective flow areas | 0 to -570 (40% drop)[a] |
| Increase number of cross-sections with cross-sections close to constriction only 1m away | 0 to –200 (15% drop)[a] |

[a] Change evident for $v_c$ of 4m/s only